CONTROL METHODS FOR AIDING A PILOT DURING STOL ENGINE FAILURE TRANSIENTS

by

Ernest R. Nelson
Daniel B. DeBra, Principal Investigator

Department of Aeronautics and Astronautics
Guidance & Control Laboratory
Stanford University
Stanford, California 94305

research sponsored by

NASA Ames Research Center
Dr. James Franklin, Scientific Monitor
Grant NSG 2100

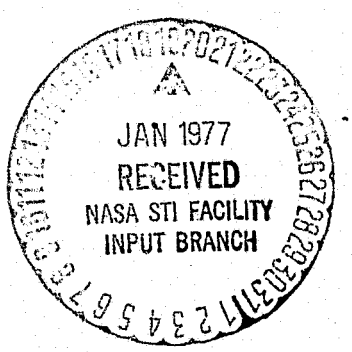

December 1976

ABSTRACT

Advanced S.T.O.L. aircraft are critically sensitive to loss of engine thrust during landing, with the problem of encountering unacceptably high sink rates. The problem is aggravated by the high degree of stability augmentation common to this class of aircraft which denies the pilot the immediate motion cues required to manually arrest large transient sink rates. Automatic control is required to arrest the immediate transients, allowing the pilot time to recognize the situation and decide upon appropriate action.

Modern optimal control theory, which determines state variable feedback controllers for multivariable systems, is especially tailored for application to this S.T.O.L. control problem. System performance can be specified in terms of the desired response characterized in the system state variables. The resulting performance is typically better than that obtained from classical design procedures.

The purpose of this research is to define candidate autopilot control laws that control the engine failure transient sink rates, by demonstrating the engineering application of modern state variable control theory.

This work provides a comparison of the results of approximate modal analysis to those derived from full state analyses provided from computer design solutions. The aircraft is described and a state variable model of its longitudinal dynamic motion due to engine and control

variations is defined. The classical fast and slow modes are assumed to be sufficiently different to define reduced order approximations of the aircraft motion amendable to hand analysis control definition methods. The original state equations of motion are also applied to a large scale state variable control design program, in particular OPTSYS. The resulting control laws are compared with respect to their relative responses, ease of application, and meeting the desired performance objectives. The limitations of minimizing feedback paths is investigated with the objective of utilizing those currently in use by the classical autopilot control law. The performance of each resulting control law is demonstrated by digital computer simulation. The sink rate transients are shown to be controlled within 5-10 sec after an engine failure and the peak sink rates are shown to be less than 19 ft/sec.

CONTENTS

ILLUSTRATIONS

TABLES

LIST OF SYMBOLS

a	first order system time constant
A	state cost function weight matrix
Ah	altitude state cost function weight coefficient
Aq,Aqq	pitch rate state cost function weight
AREF	aerodynamic coefficient reference area
A_{Tail}	horizontal tail area
Au,Auu	longitudinal velocity state cost function weight coefficient
Aw,Aww	vertical velocity state cost function weight coefficient
$A_{w\theta}$	product of vertical velocity and pitch angle state cost function weight coefficient
A_{θ} ,$A_{\theta\theta}$	pitch angle state cost function weight coefficient
B	cost function control weight matrix
Bcj	thrust control cost function weight coefficient
Bde	elevator control cost function weight coefficient
Bdf	aft flap control cost function weight coefficient
Bdsp	spoiler control cost function weight coefficient
cj	thrust coefficient
C	state feedback gain matrix
C_{cj}	thrust control feedback gain row matrix
C_D	drag aeordynamic coefficient
C_L	lift aerodynamic coefficient
C_M	pitch moment aerodynamic coefficient
C_q	pitch rate feedback gain coefficient
CREF	aerodynamic coefficient reference length

C_u	longitudinal velocity feedback gain coefficient
C_θ	pitch angle feedback gain coefficient
dcj	thrust variation
de	elevator deflection
df	aft flap deflection
dsp	spoiler deflection
D	total drag force
F	state dynamics matrix
g	gravitational acceleration
G, G_1	control influence matrix
G_2	disturbance influence matrix
G_h	altitude perturbation control influence row matrix
G_w	vertical velocity perturbation control influence row matrix
h	altitude state perturbation
H Ch X	total altitude
H Ch XI	measurement matrix
H_o	nominal altitude
Iyy	pitch moment of inertia
j	imaginary coefficient
J	optimal quadratic cost function
K	filter gain matrix
L	total lift force
m	aircraft mass
M	rotational dimensional derivative about body pitch axis
M.A.C.	mean aerodynamic chord

q	pitch rate perturbation
$\bar{q}$	dynamic pressure
Q ch IV	volume flow rate
Q ch VII	modal matrix
s	laplace domain variable
t	time
T	thrust
T_c	commanded thrust
u	longitudinal velocity perturbation in the body axes
$\underline{u}, \underline{u}_1$	control state vector
$\underline{u}_2$	disturbance input vector
U	total longitudinal velocity in the body axes
U_o	nominal longitudinal velocity in the body axes
$\underline{v}$	measurement noise vector
V	total aircraft velocity
$V_{aircraft}$	aircraft forward velocity
$V_{exhaust}$	velocity of engine efflux
w	vertical velocity perturbation in the body axes
$\underline{w}$	random disturbance vector
W, W_o	nominal vertical velocity in the body axes
x	longitudinal body axis
$\underline{x}$	state vector
$\bar{\underline{x}}$	intermediate state vector, before measurement application
$\hat{\underline{x}}$	estimated state vector
X	longitudinal dimension derivative

X	see Figure II-1
y	lateral body axis
$\underline{y}$	measurement vector
Y	see Figure II-1
z	vertical body axis
Z	vertical dimensional derivative
Z_t	see Figure II-1

Greek Symbols

α	angle of attack
γ	flight path angle
Γ	disturbance input state transition matrix
Δf	complete flap deflection
θ	pitch angle perturbation
θ_o	nominal pitch angle
Λ	eigensystem transition matrix
ρ	atmospheric density
τ	system characteristic time constant
ϕ	state transition matrix
ω	frequency component of laplace variable - s

Subscripts

dcj	indicates a derivative with respect to thrust variation
de	indicates a derivative with respect to elevator deflection

df	indicates a derivative with respect to aft flap deflection
dsp	indicates a derivative with respect to spoiler deflection
q	indicates a derivative with respect to pitch rate
u	indicates a derivative with respect to longitudinal velocity
w	indicates a derivative with respect to vertical velocity

Superscripts

$( )^*$	indicates a special form of ( ) defined in the text
$( )^T$	denotes matrix transpose

Abbreviations

deg	degrees
ft	feet
kt	knots
OPTSYS	Optimal System Design Program
rad	radians
sec	seconds

Math Symbols

$\dot{( )}$	time derivative
$\underline{( )}$	vector quantity
$\partial( )$	partial differentiation of ( )
$\lvert( )\rvert$	absolute value of ( )
$<<$	much less than

ACKNOWLEDGEMENTS

A am deeply grateful to my adviser, Dr. Daniel B. DeBra, for introducing this research opportunity to me and for his advice and guidance throughout the course of this research.

I wish to extend my appreciation to Dr. James A. Franklin of the N.A.S.A. Ames Flight Systems Branch, whose suggestions, questions, and criticisms so capably guided the practical emphasis of this research.

Particular gratitude is expressed to the National Aeronautics and Space Administration for the opportunity to perform this research under Grant NSG 2100, and to Lockheed Missiles and Space Company for their support and for providing flexible work schedules that allowed me the time to accomplish this research.

Special thanks go to my wife, Diane, for her patience, understanding, and her excellent secretarial skills which she applied to typing and editing this document.

I. INTRODUCTION

1.1 STATEMENT OF THE PROBLEM

The critical phases of aircraft flight are landing and takeoff. This is especially true of short distance takeoff and landing (S.T.O.L.) transports because they fly slowly during these phases depending upon powered lift augmentation to maintain the desired flight path. In this thesis, the landing phase is studied of S.T.O.L. flight of aircraft using lift augmentation from the primary engines, typified by the YC-14 and YC-15 transports currently being flight tested. It is the purpose of this study to minimize the effects of loss of one engine during the final phases of approach (less than 500 feet altitude). The problem has been defined in the similar research of Messrs. Franklin and Nieuwnhuisse at NASA-Ames (N-1), wherein several simple solutions were attempted without the desired results.

The approach to this problem is to utilize the integrated analysis feature of modern state variable control theory to define several candidate feedback control laws that minimize the buildup of sink rate when an engine fails. The relative performance of these control laws is compared by linear simulation. The effectiveness of the control laws is demonstrated.

Preliminary familiarization efforts with the study aircraft and engine performance brings about the conclusion that the engine response is significantly faster than the expected closed loop airframe response

that is required to control major sink rate disturbances. Therefore, the approach used in development of a workable control law is to perform design analyses without considering the engine response constraints. Engine influence is evaluated with the control law to determine the validity of this assumption by simulation studies. Two control analyses methods are researched to identify the relationship between standard aircraft modes and the dynamic modes of the study aircraft configuration. A byproduct of this approach is the comparison of approximate analyses methods (valid when significant mode separation exists; such as is the case in convention aircraft) to optimal control algorithms which account for full state interactions. Second order effects as well as resolving resulting engine influence problems were not included. Topics for further research associated with these issues have been identified.

1.2 ENGINE FAILURE DURING APPROACH

When an engine fails during the landing approach of a S.T.O.L. aircraft, excessive sink rates may occur before the pilot becomes aware of the failure.

The aircraft of interest in this study obtains lift augmentation through directing the engine flow over the extended flaps. Loss of one engine immediately reduces the lift by 10% with an increase in drag due to the engine nacelle and the asymetric trimmed flight condition. The aircraft is control augmented with pitch and roll/yaw stability augmentation and a yaw trim control. These systems respond so as to main-

tain the aircraft heading and minimize transients. The aircraft drag is increased due to the control deflection and asymetric flight attitude required to maintain the proper heading.

All of these actions, on the part of the automatic controls, virtually eliminate any immediate cues to the pilot that an engine has failed. The only remaining cue is the resultant sink rate due to loss of an engine without a compensating increase in power setting. Separate engine failure indicators provided to the pilot (researched in Reference N-2) do not alleviate the sink rate because the pilot's workload keeps him too busy to notice the indications, especially during turbulent approaches. Therefore, an additional automatic control loop is required, either internal to the S.A.S. or specially triggered by an engine failure.

1.3 CONTROL STUDIES OVERVIEW

The control studies are directed to determine state feedback control laws that arrest the sink rate due to the loss of one engine. The feedback control is defined using the five state plant model as a basis for development. Once a particular control law is defined, it is tested in simulation with the engine model adjoined to the plant model. This approach is employed because the engine performance model provided for this study responds slightly faster than the fast airframe dynamics (this is expanded in a subsequent section). Two analytical approaches are employed to contrast the results and gain understanding of the "roles" of each of the controls in relation to the states.

Three control concepts are investigated to determine their relative effectiveness in controlling sink rate and maintaining acceptable aircraft response. The bulk of the work utilizes the three controls (which seem to be sufficient in the proper mixture) of thrust, elevator and aft flap. The spoilers, nominally deflected 30 degrees, are added to the control list to determine if fast direct lift control significantly increases the response in arresting sink rate. These control options are employed using full state feedback which includes the altitude state. The third concept studied removes the altitude state feedback to determine if sufficient damping is available to eliminate excessive sink rates.

The first control concept is analyzed using reduced order approximations to define feedback control laws. The standard approach of separating the short period and phugoid/altitude modal equations of motion is attempted. Such methods work well if these modes are widely separated. The separation of modes in this case is marginal making it an interesting attempt to obtain workable solutions where the poles are situated so they may interact severely. Two solutions are generated from this approach.

The value of the approximate study is not wholly in determining working control laws. The analysis provides experience with the relationshipment of airframe response eigenvalues and the controls. The Root Square Locus method (Reference B-3) of defining optimal approximate solutions provides a format to observe the relative power of controls in providing

desired responses and also observe the root interactions that may cause trouble.

The second analytical approach employs the full five state plant model and the power of automated optimal solutions provided by the Stanford OPTSYS Computer Program (Reference B-1). Each control concept is analyzed with this method, obtaining control law results for simulation. This method has one drawback, however, it assumes full state feedback, since it is common that some states are not available for feedback. The standard solution to this is to define an estimator to provide the necessary states. Another approach is to eliminate the unmeasured state feedback from the control law without recomputing the remaining feedback gains. Since this latter scheme is economical it is investigated as part of the control analysis.

1.4 ENGINE MODEL ANALYSES

Engine throttle response curves of the study aircraft's power plant are provided. These are studied to define a first order response model for simulation analyses. The previous work included three characteristic engine models that had thrust transient responses ranging from slow to fast. (Reference N-2). The preliminary results from the engine performance provided herein show this engine to be about equally responsive as the medium response engine model from that previous study. (Reference N-2).

A closer look using identification analyses to define higher order models to determine their effects (slower roots perhaps) is identified as a suggested topic for continuation of this work.

1.5 SIMULATION MODEL WORK

A linear simulation model is provided in FORTRAN IV to facilitate demonstration of the control law results and comparison of state deviations and control deflections resulting from the control laws. Several of the control law results are simulated and their relative performance is compared.

1.6 CONTROL LAW APPLICATION

The feedback control laws developed in this study are perturbation control laws, whereas the full state values are measured. The conversion of these control laws into an aircraft application is discussed, with specific attention to the need of unmeasured state feedback. The study aircraft is defined to have speed, pitch, and pitch rate readily measured. Altitude is also available as either a direct measure or an open loop observer that is said to work as well as a direct measure. Angle of attack is not measured.

II. COORDINATE SYSTEM

The coordinate system employed is a right handed orthogonal basis presented in Etkin and Seckel (References E-1 and S-1) modified to provide positive parameters defining sink rate. The positive pitch angle, theta (θ) is down and sink rate $\dot{h}$ is also positive down, allowing the sink rate equation to be made up of a sum of positive quantities. This requires theta rate ($\dot{\theta}$) to be opposite in sign to q (the latter being defined in the standard convention of positive nose up). This coordinate system is shown on Figure II-1 indicating positive quantities of the states and forces on the aircraft. The intertial and body fixed axes are shown with the pitch axis directed out of the page. The system equations of motion are derived in these coordinates in Appendix A. Where results are shown (such as the simulation state histories in Chapter X, the axes of the modified states are inverted making the visual association of downwards orientations being below the axes origin.

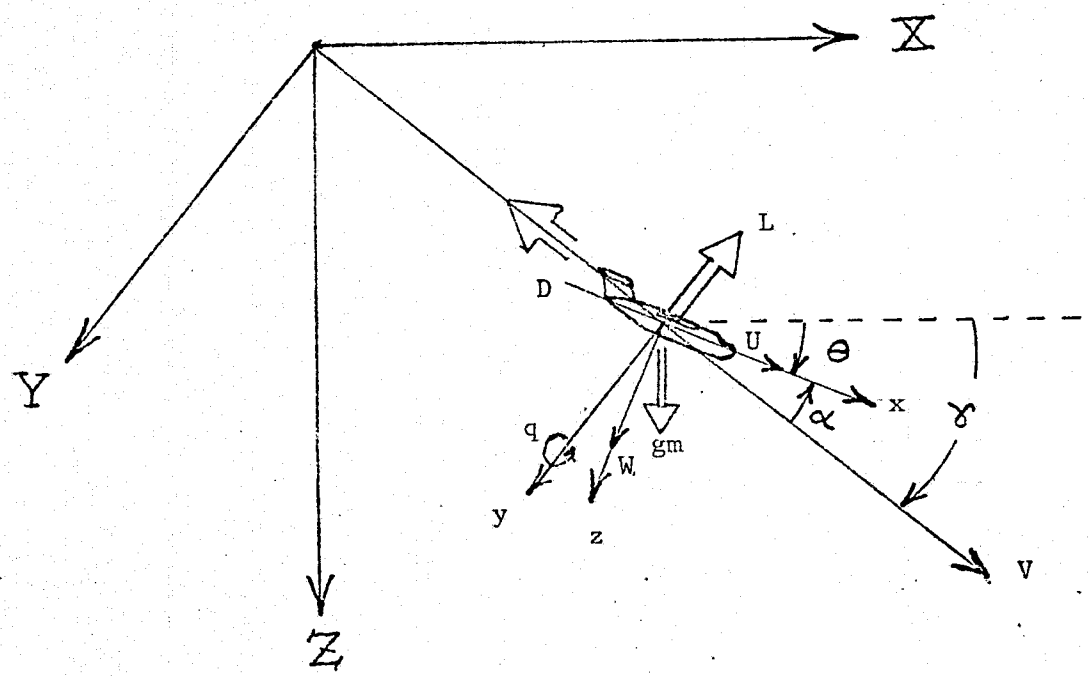

FIGURE II-1 COORDINATE SYSTEM

III. AIRCRAFT CONFIGURATION

3.1 SUMMARY

The particular S.T.O.L. aircraft chosen for this study is a four engine high wing transport which uses an externally blown flap system for lift augmentation. The characteristics of the study aircraft are described in Reference N-2 and N-3. The particular details pertaining to this research (longitudinal dynamics) are repeated here. The aircraft is a study model currently in use at NASA Ames in moving base simulator studies.

3.2 STUDY AIRCRAFT DESCRIPTION

The study aircraft configuration is displayed on Figure III-1, and its longitudinal physical characteristics are summarized on Table III-1. It is a 150,000 lb transport similar to the McDonnell-Douglas YC-14 currently being flight tested. The lift augmentation is provided during takeoff and landing approach by externally blown flaps, as shown on Figure III-1. Unlike conventional aircraft, the flaps extend into the engine efflux. The high speed flow is diverted by the flap structure, increasing the circulation over the wing and increasing the lift provided by the wing.

The nominal approach configuration is used in this research. The nominal approach is trimmed for equilibrium flight with the flaps extended to the 60 deg position.

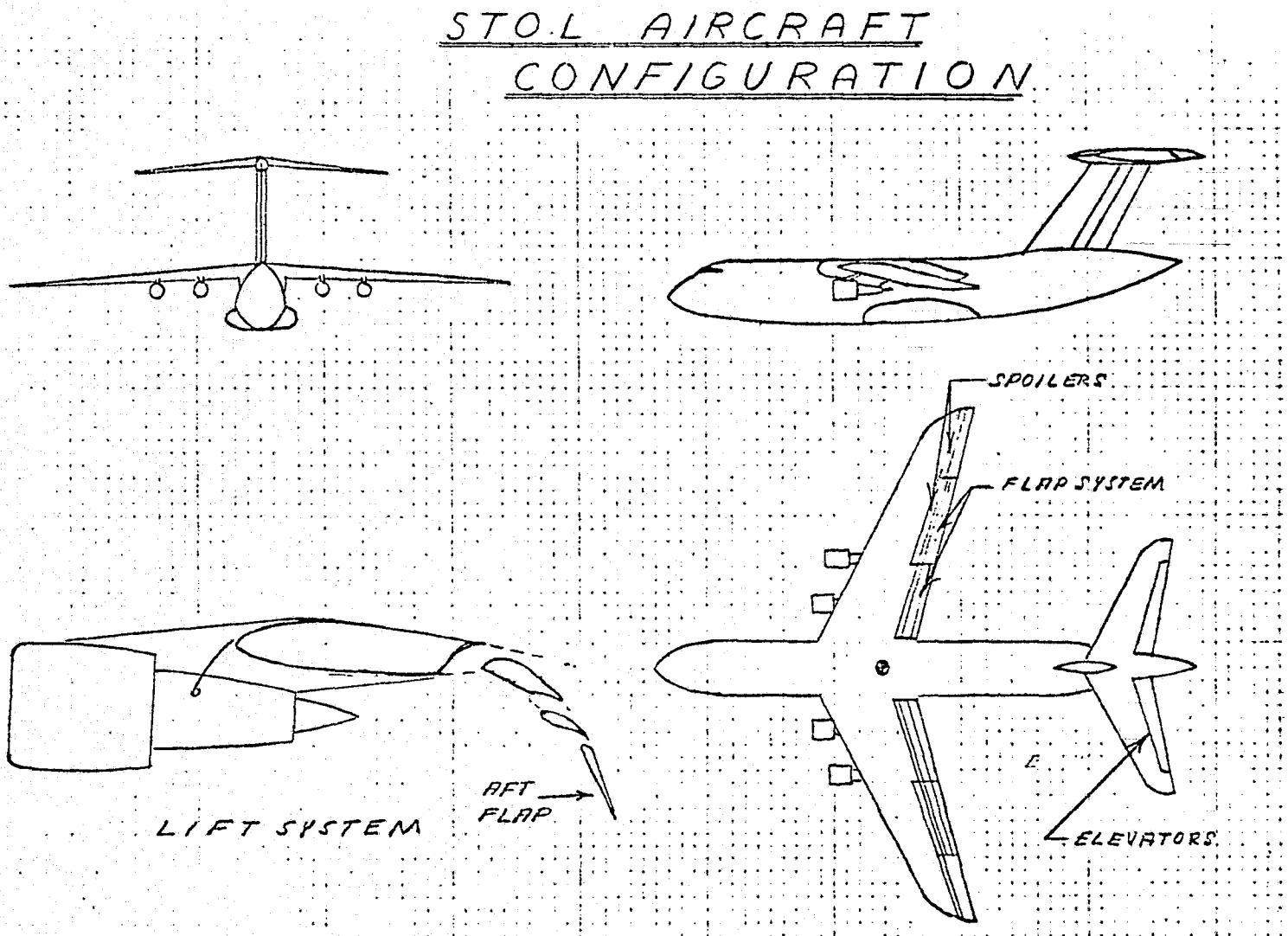

FIGURE III-1 AIRCRAFT CONFIGURATION AND LIFT SYSTEM

The study aircraft in the approach configuration has four longitudinal controls available. These longitudinal controls are: elevator, engine thrust, spoilers, and aft flap. The elevator operates the same as conventional aircraft; the elevator controls pitch attitude and rate. (The thrust or throttle modulates lift and drag.) The spoilers are usually operated differentially for lateral control. However, with the spoilers initially deployed and operated together they can provide direct lift control, with response faster than the typical engine throttle response. The aft flap control consists of the last element of the flap structure, which is geared to move rapidly like the elevator or spoiler surfaces (shown on Figure III-1). Whereas the main portion of the flap is slow moving and considered to be a variable configuration device deployed to varying degrees when low speed and high lift is required. The aft flap is principally a drag modulation control.

TABLE III-1

S.T.O.L. TRANSPORT PHYSICAL CHARACTERISTICS

Weight	150,000 lb
Pitch Moment of Inertia (Iyy)	2,105,000 slug ft^2
Wing Area (AREF)	1,667 ft^2
Mean Aerodynamic Chord (CREF)	16.3 ft
Horizontal Tail Area	570 ft^2
Maximum Engine Thrust (Sea Level Static)	84,000 lb

IV. AIRCRAFT AERODYNAMICS

4.1 SOURCE OF AERODYNAMIC DATA

The aerodynamic coefficients for this study are provided in raw form. The data, given in Reference N-3, requires modification before computing the numerical derivatives in the equations of motion. Most of the longitudinal coefficients are given in standard form referenced to the wing area (AREF) and mean aerodynamic chord (M.A.C.). However, two coefficients, the lift and drag due to elevator deflection are given referenced to the horizontal tail area in Reference N-3.

4.2 AERODYNAMIC DATA MODIFICATION

The raw form aerodynamic data must be modified for use in this study. The raw data is not in a consistent form, two aerodynamic coefficients must be modified to be consistent with the reference area (AREF). The data is digitized for use in this study to allow computer solution of the dynamics matrices in state variable form.

The coefficients $C_{L_{de}}$ and $C_{D_{de}}$ must be normalized to the wing referenced area:

$$C_{L_{de}} = C_{L^*_{de}} \frac{A_{Tail}}{AREF}$$

$$C_{D_{de}} = C_{D^*_{de}} \frac{A_{Tail}}{AREF}$$

The aerodynamic coefficients of powered lift aircraft include the thrust effects on lift, drag, and moments, and it is nearly so in this case. The ram drag component due to the air entering the engine nacelles is not included in the coefficients of drag (CD) and must be added separately. Ram drag is part of the forward thrust contribution of the engines, where the thrust is due to the air mass accelerated through the engine (Reference D-1).

$$T = \rho Q \, (V_{exhaust} - V_{aircraft})$$

$$T = \rho Q \, V_{exhaust} - \rho Q \, V_{aircraft}$$

$$T = \rho Q \, V_{exhaust} - \rho Q \, U_o$$

The latter quantity is ram drag $\rho Q \, U_o$ where ρQ is mass flow rate. Dividing by reference area (AREF) and dynamic pressure ($\bar{q}$) provides the drag coefficient contribution due to ram drag.

$$D_{CD} = \frac{\rho Q \, U_o}{\bar{q} \, AREF}$$

4.3 STUDY AERODYNAMIC COEFFICIENTS

The raw data for the 60 deg flap deflection configuration (given in Reference N-3) is digitized into a consistent form referenced to the wing geometry. These data are shown in tabular form in Appendix C from the data in Reference N-3. The following coefficients are provided in graphic form as a function of angle of attach (α) and thrust coefficient (cj) in Reference N-3.

CL	CD	CM
$C_{L_{de}}$	$C_{D_{de}}$	$C_{M_{de}}$
$C_{L_{df}}$	$C_{D_{df}}$	$C_{M_{df}}$

The apparent plotted data points are read to provide the digitized data to minimize the introduction of significant interpolation errors. However, the spoiler data is provided in table form. The coefficients CL_{dsp} and CD_{dsp} are given over a range different from the plotted data. CM_{dsp} is not given, so it is assumed the spoiler deflection does not affect the aircraft moments. These table data are interpolated to provide digital points at the same conditions the plotted data are taken for presentation in appendix C and use in this study.

The aerodynamics are not modified for ground effects. The study is done without ground effects, leaving their contribution for evaluation by simulation, as the resulting control must work out of ground effect as well. Ground effects increase the lift near touchdown so their elimination is a conservative choice.

V. EQUATIONS OF MOTION

5.1 FORM OF THE EQUATIONS OF MOTION

The plant dynamic equations are derived in state variable form, in Appendix A as linear dynamic equations about unperturbed (equilibrium) steady approach condition. The resulting linear state variable model is of the form:

$$\dot{\underline{x}} = F\underline{x} + G\underline{u}$$

In particular the equations are:

$$\begin{bmatrix} \dot{u} \\ \dot{w} \\ \dot{q} \\ \dot{\theta} \\ \dot{h} \end{bmatrix} = \begin{bmatrix} X_u & X_w & X_q & -W & q & 0 \\ Z_u & Z_w & Z_q & -U & 0 & 0 \\ M_u & M_w & M_q & & 0 & 0 \\ 0 & 0 & -1 & & 0 & 0 \\ 0 & 1 & 0 & & U & 0 \end{bmatrix} \begin{bmatrix} u \\ w \\ q \\ \theta \\ h \end{bmatrix} + \begin{bmatrix} X_{cj} & X_{de} & X_{df} & X_{dsp} \\ Z_{cj} & Z_{de} & Z_{df} & Z_{dsp} \\ M_{cj} & M_{de} & M_{df} & M_{dsp} \\ 0 & 0 & 0 & 0 \\ 0 & 0 & 0 & 0 \end{bmatrix} \begin{bmatrix} dcj \\ de \\ df \\ dsp \\ \end{bmatrix}$$

The derivatives are defined in terms of the nominal states and the airframe aerodynamic coefficients in Appendix B.

The plant model consists of the equations of motion with the dimensional derivatives computed about the nominal approach condition for the particular configuration of the plant model requires the equilibrium trimmed approach conditions be first determined, from which, the dimen-

sional derivatives are computed. The approach employed is to generate an equilibrium performance map for each configuration of interest; select the desired approach condition; and compute the dimensional derivatives.

Two computer programs are built to facilitate computation of the derivatives, one which computes a map of equilibrium flight conditions for a specified configuration, and another that computes a particular equilibrium flight condition and the corresponding perturbation derivatives in the above dynamic equations. These assist the designer in providing numerical forms of the equations of motion, directly in the form for analysis and/or simulation, for any equilibrium approach condition and configuration of interest. The latter of these two programs is used in conjunction with a linear simulation model to demonstrate the resulting control performance, providing the capability to evaluate control laws at off design conditions by specifying the appropriate equilibrium conditions without recomputing the dynamics matrices.

5.2 EQUILIBRIUM PERFORMANCE MAP

The equilibrium performance map is derived for the range of angles of attack from -8 deg to 20 deg, and over the thrust range of the study aircraft. The configuration is defined by selecting the nominal position of the aft flap and spoiler controls (with the main flap deflection 60 deg). The force equations are solved by iteration using the digitized aerodynamics tables. The particular equations are:

$$CM = 0 \text{ (eg trimmed condition)}$$

$$\bar{q} = \tfrac{1}{2} \rho V^2$$

$$cj = T/(\bar{q}.AREF)$$

$$\gamma = TAN^{-1}(-CD/CL)$$

$$g \cdot m \cdot COS(\gamma) = CL \cdot \bar{q} \cdot AREF$$

Where the aerodynamic coefficients represent the sum of aerodynamic derivatives in the form:

$$CL = CL(\alpha, cj) + CL_{de}(\alpha, cj)\, de + CL_{df}(\alpha, cj)\, df + CL_{dsp}(\alpha, cj)\, dsp.$$

An iterative algorithm is programmed in FORTRAN IV to provide the desired performance maps. This program is included in Appendix D.

Equilibrium performance maps are generated for the two configurations considered in this study to indicate the magnitude of the problem of engine failure during approach. The nominal approach configuration is with the flaps deflected 60 deg and the spoilers retracted. The nominal approach condition of approximately 80 kt provides a 5.6 deg flight path angle with the elevators trimmed at -3.2 deg deflection trimming the aircraft at 2.2 deg angle of attack (Figure V-1). The nominal approach sink rate is 13.2 ft/sec. The nominal approach thrust is 50400 lb at 60 percent of the maximum thrust of 84000 lb. A loss of one engine provides a thrust of 37800 lb. The equilibrium flight condition at 80 kt with one engine out is trimmed at 6 deg angle of attack providing a flight path angle of 8 deg (a sink rate of 19 ft/sec. If the initial trim angle of attack of 2 deg is maintained, the flight

conditions are 87 kt at a flight path of 7 deg (an 18 ft/sec sink rate). The constant thrust curves show the aircraft to be operating on the back side of the power curve where increased angle of attack results in increased sink rate. It is also interesting to notice that the full throttle capability of this aircraft in the approach configuration with one engine failed (63000 lb of thrust) does not provide level flight, but does provide a significant margin to maintain the approach conditions (Figure V-1). Therefore, the configuration must change, by retracting the flaps, to perform a go-around (e.g. abort the landing).

The possibility of approaching at a slightly higher speed with the spoilers deflected is considered in this study. A 6 deg approach is possible at 84 kt with the spoilers deflected 30 deg at the nominal approach thrust and angle of attack (Figure V-2). In this condition, it is expected that the control response upon engine failure be to retract the flaps. Viewing the equilibrium conditions with flaps retracted at 84 kt and one engine failed shows the flight path to be 7.5 deg which has a sink rate of 18.5 ft/sec (Figure V-1) at two degrees angle of attack (requiring an additional 4 percent of the maximum total thrust to maintain the flight). The flight path is 6.5 degrees and a sink rate of 16 fps. The spoilers may alleviate the sink rate somewhat but additional control and throttle response is required to maintain a nominal approach flight path.

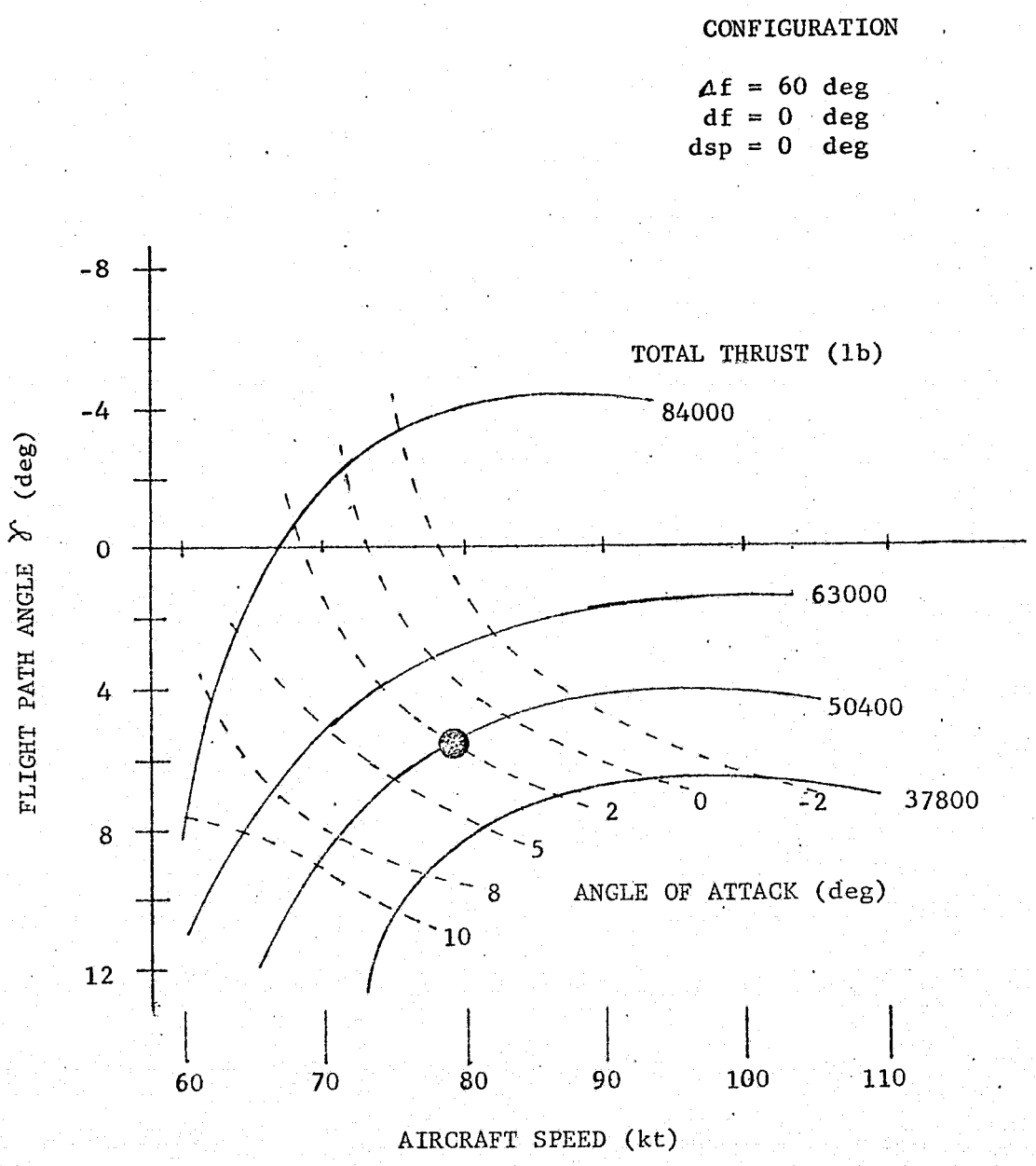

FIGURE V-1 NOMINAL CONFIGURATION
EQUILIBRIUM PERFORMANCE

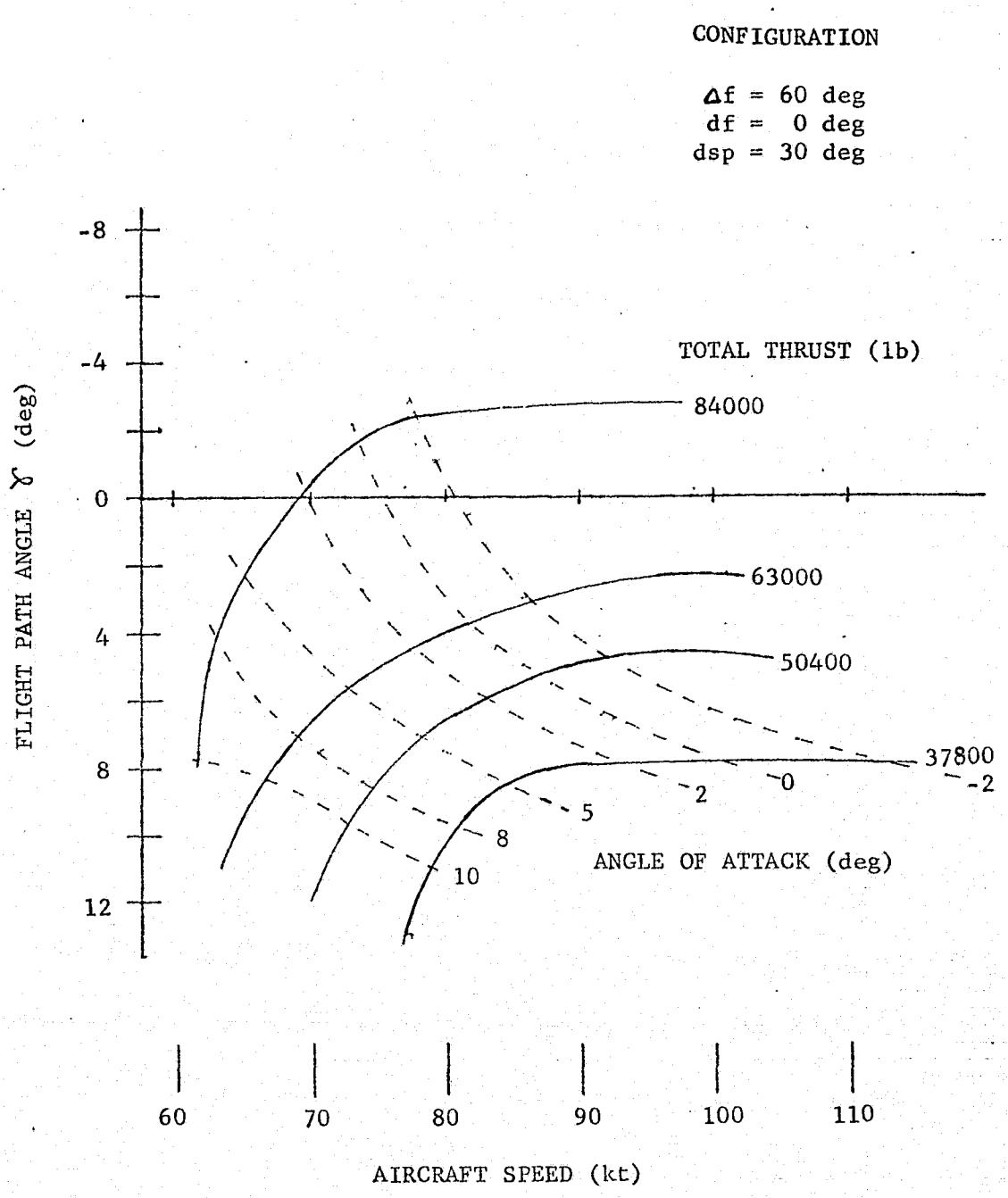

FIGURE V-2 SPOILER CONFIGURATION
EQUILIBRIUM PERFORMANCE

5.3 COMPUTATION OF DIMENSION DERIVATIVES

The dimensional derivatives that comprise the F and G matrices in the equations of motion are computed about an equilibrium approach condition. The method is to first determine the angle of attack of equilibrium for specified thrust, control settings, approach speed and flight path which are approximately determined from the performance maps. The equilibrium solution here serves to determine the angle of attack condition to more accuracy than is apparent from visual interpolation of the equilibrium approach performance curves, when a particular velocity and flight path is desired for study.

Once the appropriate trim equilibrium conditions are determined, the dimensional derivatives are computed from the aerodynamic coefficients and the equilibrium flight conditions . The computational details for the dimensional derivatives in the coordinates of this study in Appendix B and the FORTRAN V computer program is presented in Appendix D.

The dynamics matrices are computed for the two configurations described in the previous section (Section 5.2). The nominal approach conditions are: (Where units are consistently in ft, rad, sec with the control deflections in deg)

F MATRIX

$$\begin{bmatrix} -.0372 & .0766 & -5.2114 & 32.2000 & .0000 \\ -.4769 & -.4424 & 135.2396 & .0000 & .0000 \\ -.0000 & -.0046 & -.7457 & .0000 & .0000 \\ .0000 & .0000 & -1.0000 & .0000 & .0000 \\ .0000 & 1.0000 & .0000 & 135.2396 & .0000 \\ .0000 & .0000 & .0000 & .0000 & .0000 \end{bmatrix}$$

G MATRIX

$$\begin{bmatrix} .9102 & -.0269 & -.2230 & .0002 \\ -9.6367 & -.0899 & -.2631 & .0547 \\ -.0393 & -.0261 & .0133 & .0000 \\ .0000 & .0000 & .0000 & .0000 \\ .0000 & .0000 & .0000 & .0000 \end{bmatrix}$$

Which are of the form described in Section 5.2.

The dynamics matrices at the approach condition with 30 deg of spoiler deflection are:

F MATRIX

$$\begin{bmatrix} -.0393 & .0730 & -5.2933 & 32.2000 & .0000 \\ -.4564 & -.4222 & 140.4003 & .0000 & .0000 \\ -.0000 & -.0051 & -.7647 & .0000 & .0000 \\ .0000 & .0000 & -1.0000 & .0000 & .0000 \\ .0000 & 1.0000 & .0000 & 140.4003 & .0000 \end{bmatrix}$$

G MATRIX

$$\begin{bmatrix} .9652 & -.0279 & -.2295 & .0001 \\ -10.9655 & -.0952 & -.2678 & .0579 \\ -.0422 & -.0279 & .0146 & .0000 \\ .0000 & .0000 & .0000 & .0000 \\ .0000 & .0000 & .0000 & .0000 \end{bmatrix}$$

The two nominal approach conditions have nearly the same dynamics matrices. This similarity provides the basis for an expediate assumption applied to the spoiler analyses (discussed later in this report).

VI. APPROXIMATE MODEL ANALYSIS

6.1 THE METHOD OF MODAL ANALYSIS

The standard aircraft approach of separating the analysis of short period and phugoid modes is investigated. This results in reduced order equations that are amendable to hand analysis techniques such as successive loop closure. The practice of analyzing the two basic aircraft modes independently is based upon spectral decomposition concepts. When the characteristic roots are widely separated, then their characteristic eigenvectors, which are composed of combinations of the states that are disturbed by each mode (set of characteristic roots), exclude the states of other modes. Therefore, any particular mode is composed of a small subset of the aircraft's states, allowing analysis of that mode with the other modes undisturbed (i.e. perturbations remain zero). The open loop characteristic roots are moderately separated in the case of the study aircraft (Figure VI-1). If feedback control can move these roots further into the left half plane, while maintaining separation of the modal state responses, the approximate solutions will be valid.

6.2 SHORT PERIOD MODE

The approximate analysis first proceeds in the same manner as for conventional aircraft: beginning with the short period (fast) mode to obtain increased damping; then approximate phugoid-altitude mode equations are defined to develop stable responses. The short period (made up of $\dot{w}$ and $\dot{q}$) has very little feedback of other states

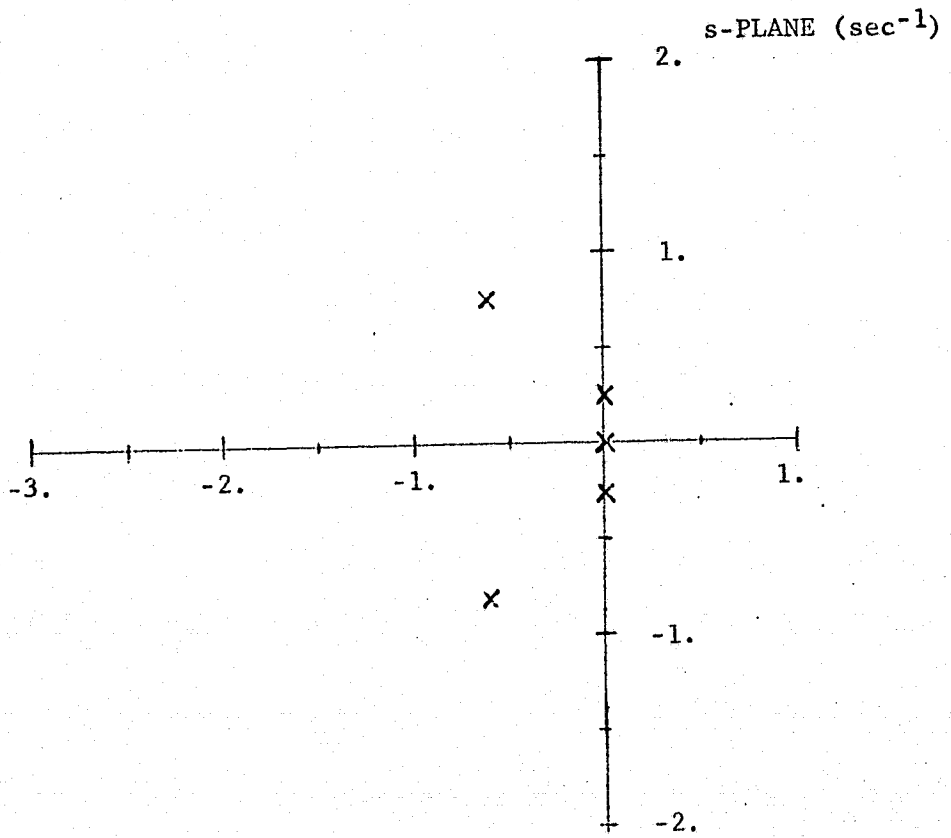

FIGURE VI-1 AIRCRAFT OPEN LOOP POLES

(u, Θ, and h) and feeds those states derivatives. The partioned short period equations are:

$$\begin{bmatrix} \dot{w} \\ \dot{q} \end{bmatrix} = \begin{bmatrix} -.4420 & 135.2 \\ -.0046 & -.7461 \end{bmatrix} \begin{bmatrix} w \\ q \end{bmatrix} + \begin{bmatrix} -.090 \\ -.026 \end{bmatrix} \quad de$$

choosing the elevator control for moment damping.

Assume a feedback control of the form

$$\dot{\underline{x}} = F\underline{x} + Gde$$

$$de = (0, Cq)\ \underline{x}$$

to increase the system damping. The resulting characteristic equation is determined from:

$$F - GC = \begin{bmatrix} -.442 & 135.2 + .09\ Cq \\ -.0046 & -.7461 + .026\ Cq \end{bmatrix}$$

which provides the characteristic equation from the determinant of the dynamics matrix:

$$s - (F - GC) = 0.$$

Resulting in the characteristic equation:

$$s^2 + (1.188 - .026\ Cq)\ s + .9517 - .0111\ Cq = 0$$

The root locus for this system is sketched as a function of Cq on Figure VI-2. A gain of -47.4 deg sec/rad provides roots on the real axis. The study by Franklin shows that the existing gain selection is -40 deg sec/rad which provides poles at $s = 1.116 \pm j\ .389\ sec^{-1}$. This

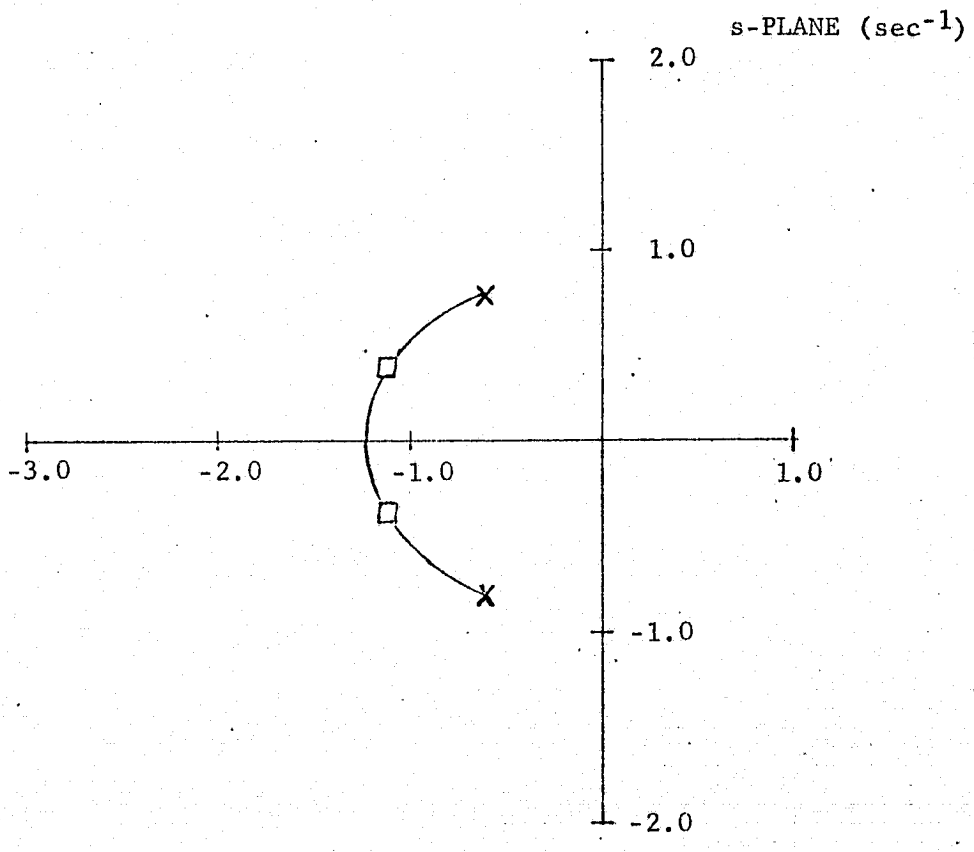

FIGURE VI-2 SHORT PERIOD ROOT LOCUS
VERSUS DAMPING FEEDBACK (Cq)

latter gain is selected since it provides acceptable damping and is currently in use in other studies of this aircraft. The approximate phugoid equations are defined with the short period feedback loop closed.

6.3 PHUGOID AND ALTITUDE CONTROL

The approximate phugoid equations are determined by making the quasi-steady assumption that $\dot{w}$ and $\dot{q}$ are zero. Then, solving for w and q in terms of the other states (u, Θ, and h) and the controls (dcj, de, and df), so that w and q can be replaced in the other state equations. The relationship between w and q to the other states is determined from the $\dot{w}$ and $\dot{q}$ rows of the full state dynamical equations:

$$0 = \begin{pmatrix} -0.4772 \\ 0 \end{pmatrix} \begin{bmatrix} u \end{bmatrix} + \begin{pmatrix} -0.442 & 131.6 \\ -0.0046 & -1.1790 \end{pmatrix} \begin{bmatrix} w \\ q \end{bmatrix} + \begin{pmatrix} -9.641 & -0.2632 & 0.0569 \\ -0.0391 & 0.0133 & 0 \end{pmatrix} \begin{bmatrix} dcj \\ df \\ dsp \end{bmatrix}$$

which results in the following relationship for w and q:

$$\begin{bmatrix} w \\ q \end{bmatrix} = \begin{bmatrix} -0.6117 \\ 0.0015 \end{bmatrix} \begin{bmatrix} u \end{bmatrix} + \begin{pmatrix} -16.04 & 0.9159 & 0.073 \\ 0.0194 & 0.0051 & -0.0002 \end{pmatrix} \begin{bmatrix} dcj \\ df \\ dsp \end{bmatrix}$$

replacing w and q in the equations for $\dot{u}$, $\dot{\Theta}$, and $\dot{h}$ results in the approximate phugoid equations with the short period loop closed:

$$\begin{bmatrix} \dot{u} \\ \dot{\Theta} \\ \dot{h} \end{bmatrix} = \begin{bmatrix} -0.0919 & 32.20 & 0 \\ -0.0047 & 0 & 0 \\ -0.6117 & 135.2 & 0 \end{bmatrix} \begin{bmatrix} u \\ \Theta \\ h \end{bmatrix}$$

$$+ \begin{bmatrix} -0.4233 & -0.1793 & 0.0072 \\ -0.0194 & -0.0051 & 0.0002 \\ -16.04 & 0.9159 & 0.073 \end{bmatrix} \begin{bmatrix} dcj \\ df \\ dsp \end{bmatrix}$$

These approximate equations are used with the two remaining controls dcj and df (dsp is investigated later).

The remaining states u, Θ, and h are to be controlled by dcj and df. The two controls allow only two states to be directly addressed, depending upon the resulting system interactions to provide acceptable response of the remaining state. The method applied to determinine control laws for dcj and df is successive application of the root square locus technique, which is described in Reference H-1.

The speed and altitude states are chosen for control by df and dcj respectively. The Θ state is chosen to be implicitly controlled because it has the smallest coefficients in the dynamical equation and it is a state that contributes in a small way to the problem at hand. The choice of df to control u is due to the large impact of dcj on $\dot{h}$ ($\partial \dot{h} / \partial dcj$ is 38 times $\partial \dot{u} / \partial dcj$ while $\partial \dot{h} / \partial df$ is only 5 times more than $\partial \dot{u} / \partial df$). At this point it appears natural to connect dcj with h.

The speed control loop is determined from the u/df transfer function in the s plane, which is:

$$\frac{u}{df}(s) = \frac{-0.1793\ s\ (s + 0.9159)}{s\ (s^2 + 0.0919\ s + 0.1513)}$$

The root square locus is formed about the optimal weight ratio A_u/B_{df}

$$\left| \frac{u}{df}(s) \quad \frac{A_u}{B_{df}} \quad \frac{u}{df}(-s) + 1 \right| = 0$$

The locus is sketched on Figure VI-3. The closed boxes on Figure VI-3 indicate the location selected for closed loop roots which correspond to $\frac{A_u}{B_{df}}$ of 14.25 deg^2 sec^2/ft^2. The roots are located at $s = -.6 \pm j\ .525$ sec^{-1}, to provide approximately 0.6 - 0.7 damping ratio. The feedback gains are determined from an assumed feedback configuration by matching the like coefficients of the transfer function and solving for the undetermined feedback coefficients. In this case two feedback gains are sufficient to define the quadratic root location. A feedback law of the form:

$$\dot{x} = (F + GC)\ x$$

is assumed, where the feedback coefficient matrix is assumed to be:

$$C = (Cu,\ C_\theta\ ,\ 0).$$

Entering this form of feedback into the approximate phugoid equations provides the following characteristic equation:

$$s^3 + s^2 + (0.0919 + 0.0051\ C_\theta + 0.1793\ Cu)\ s$$
$$+ 0.15134 - 0.00037\ C_\theta + 0.1642\ Cu = 0.$$

which is to look like the following as determined from the root locus diagram:

$$s\ (s^2 + 1.2\ s + .636) = 0.$$

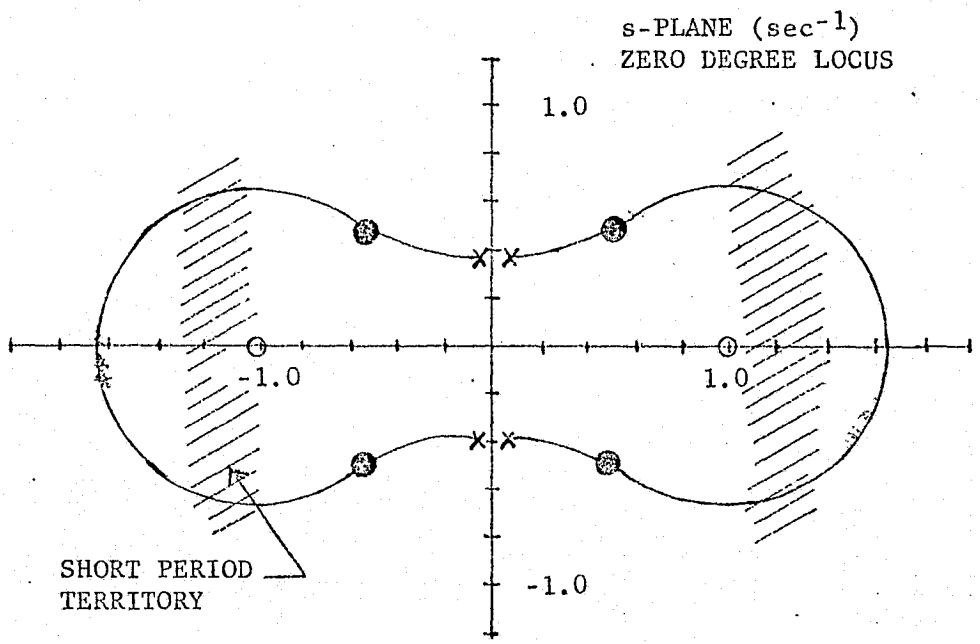

FIGURE VI-3 ROOT SQUARE LOCUS $\frac{u}{df}(s)$

Solving for the feedback gains results in:

$$C = (Cu,\ C_{\theta}\ ,\ 0) = (3.19,\ 105.26,\ 0.)$$

in consistent units of deg per ft, sec and rad. The equations for the next control determination are:

$$\dot{x} = (F + GC)\ x + Gu$$

where the F + GC matrix includes the feedback computed above. The analysis is repeated for the next successive control, in this case dcj which is chosen to control h. The new dynamical equations are:

$$\begin{bmatrix} \dot{u} \\ \dot{\theta} \\ \dot{h} \end{bmatrix} = \begin{bmatrix} -0.663 & 13.327 & 0 \\ -3.196 & 0.5368 & 0 \\ 2.306 & 231.646 & 0 \end{bmatrix} \begin{bmatrix} u \\ \theta \\ h \end{bmatrix} + \begin{bmatrix} -0.423 \\ -0.0194 \\ -16.04 \end{bmatrix} \begin{bmatrix} dcj \end{bmatrix}.$$

Again, determine the transfer function:

$$\frac{h}{dcj}(s) = -\frac{16.04\ (s^2 + .4676\ X + 22.889)}{s\ (s^2 + 1.2\ x + .636)}\ (ft)$$

which is put into root square locus form:

$$\left| \frac{h}{dcj}(s)\ \frac{A_h}{B_{cj}}\ \frac{h}{dcj}(-s) + 1 \right| = 0.,$$

The resulting root locus is sketched on Figure VI-4. The locus is sketched as a zero degree locus which provides a stable path along the real axis for the root at the origin (the h root). Notice that the path of the real root is unbounded. However, this approximate analysis is

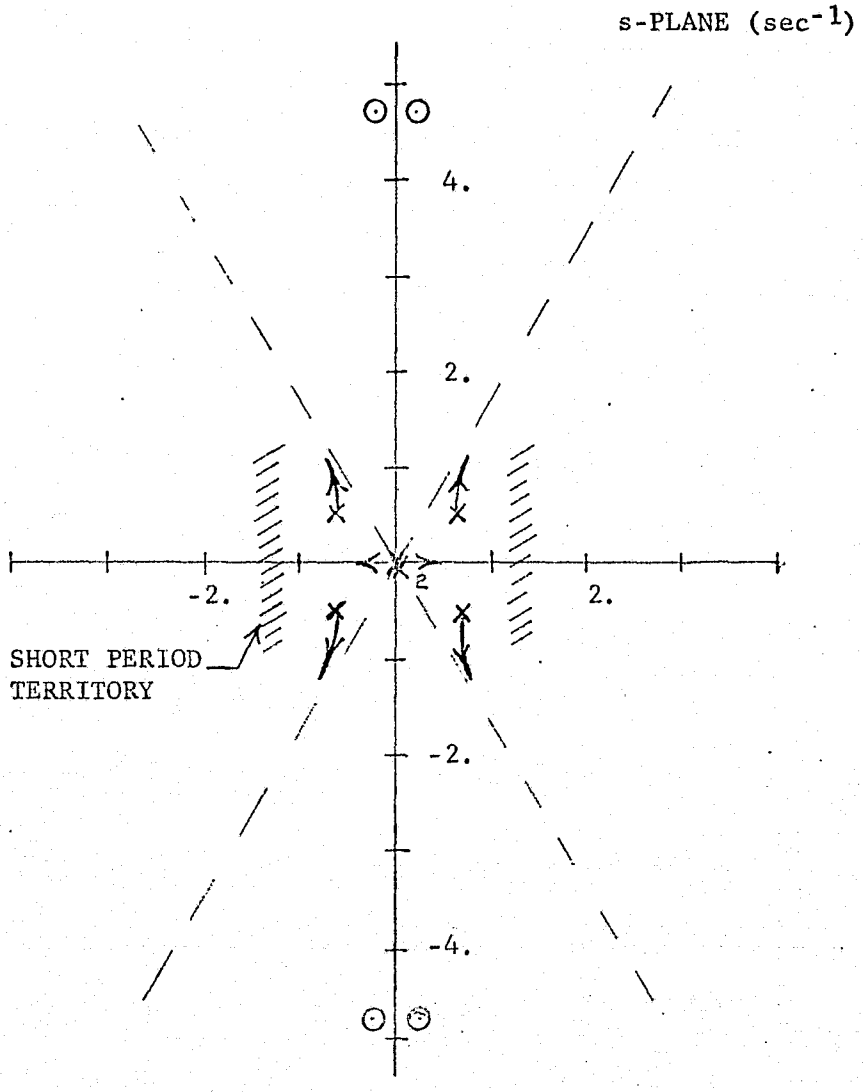

FIGURE VI-4 ROOT SQUARE LOCUS $\frac{h}{dcj}(s)$

predicated upon the separation of modes and the short period mode roots lie about the $s = -1.0\ sec^{-1}$ region. The pole selection of the previous part (u/df) is half way between the origin and the short period territory and possibly interacting. The selection of root locations here, is made to just make h stable and not move the other roots to far out. Additionally, the asymptotes of the oscillatory roots are at less damping than the initial root location, so the less they're moved the better the damping of the phugoid, barring major interactions. Selecting the real root location to be $s = -0.2\ sec^{-1}$ meets the criteria. This location is obtained with a weight ratio of $\frac{A_h}{B_{cj}} = 0.0003\ (ft^{-2})$, where upon the oscillatory roots move imperceptibly. The approximate characteristic equation is:

$$(s + .2)\ (s^2 + 0.467\ X + 22.89) = 0.$$

The cubic requires three feedback coefficients of the form:

$$C = (Cu,\ C_\theta\ ,\ Ch).$$

Proceding as in the previous control case (equating coefficients of the closed loop characteristic equations) provides the following control gains defining dcj:

$$C = (0.175,\ 13.762,\ 0.0125).$$

in consistent units of ft, sec and rad.

6.4 EVALUATION OF THE CONTROL LAW

The approximate modal analysis, just described, provides a set of control laws, obtained by ignoring any interaction between the traditional aircraft modes. The resulting expected root locations are

indicated by X's on Figure VI-5. The dotted lines indicate the expected travel of the unaugmented poles to the closed loop positions. The phugoid poles are moved out into the region occupied by the short period poles before augmentation and also close to their closed loop location. It is possible that significant root interaction has taken place, changing these results. This is tested by computing the closed loop poles of the full five state model with the control law just determined (with the aid of the OPTSYS Program).

The closed loop pole locations of the five state model demonstrate that significant mode interaction does occur. The open boxes shown on Figure VI-5 are the actual closed loop pole locations provided by the control law.

The true results compared with those of the approximate solution appear very different. The true poles are much slower than expected and the real pole is much faster; their relative real locations are switched about. The approximation assumption (which assumes no interaction) is violated severely; there being great apparent interaction between the w, q, u, and h states. The poor association of results provided by the approximate mode analysis occurs because the original slow mode is driven into the region of the fast modes. Therefore, if this fast and slow separation can be maintained, the validity of the approximation shall be also. This hypothesis is tested by arbitrarily locating the phugoid roots closer to the origin.

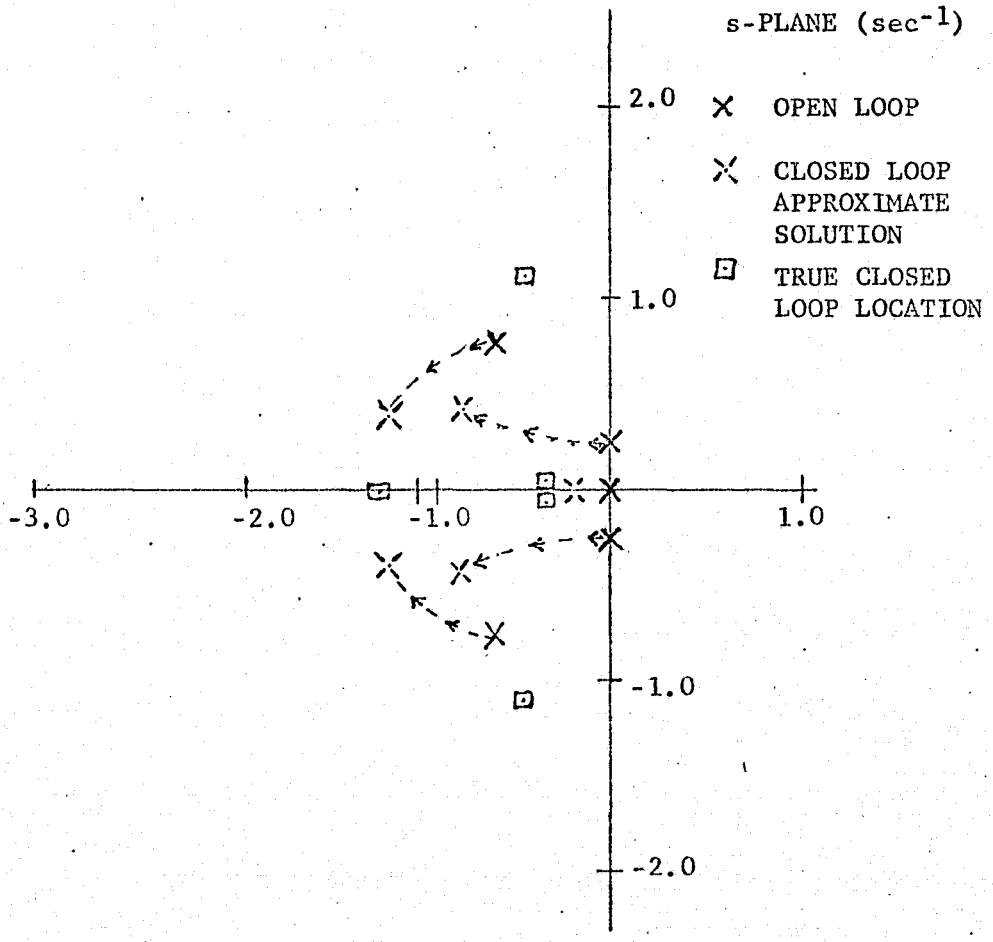

FIGURE VI-5 CLOSED LOOP POLES
APPROXIMATE OPTIMAL SOLUTION

6.5 REVISED APPROXIMATE PHUGOID ANALYSIS

The approximate analysis is revised to maintain the validity of the spectral mode separation assumption. Stepping back to the first loop closure (u/df) of the previous analysis, it is observed that the two oscillatory poles can be placed arbitrarily with the two feedback coefficients C_u and C_θ. The trouble is caused by the oscillatory poles being moved out two far to the left, into short period territory on the s plane. The objective here is to increase the damping of these two poles without moving them into short period territory, as did the root square locus technique. The following choice of feedback gains meets the criterion by placing the oscillatory poles at $s = -0.39 \pm j\ 0.176\ (sec^{-1})$:

$$C_u = 0.4946 \text{ (deg sec/ft)}$$

$$C_\theta = 119.9 \text{ (deg/rad)}.$$

The phugoid poles are now about half way between the origin and the closed loop short period poles (which at at $s = -1.116 \pm j\ 0.389\ sec^{-1}$) as indicated on Figure VI-6. The damping factor of this location is 0.9 whereas the optimal selection provides only 0.7 damping factor.

The thrust feedback dcj is determined as previously using the revised closed loop (on u/df) approximate dynamics matrix. Applying the same weight ratio for $\frac{A_u}{B_{cj}}$ of 0.0003 sec^2/ft^2 causes the h pole at the origin to move out to $s = -0.179\ sec^{-1}$ without moving the oscillatory poles into short period territory, as indicated on Figure VI-7. The resulting feedback gains are (in u, θ, and h in consistent units of ft, sec, and rad):

$$C_{cj} = (-.058,\ 3.895,\ .0173).$$

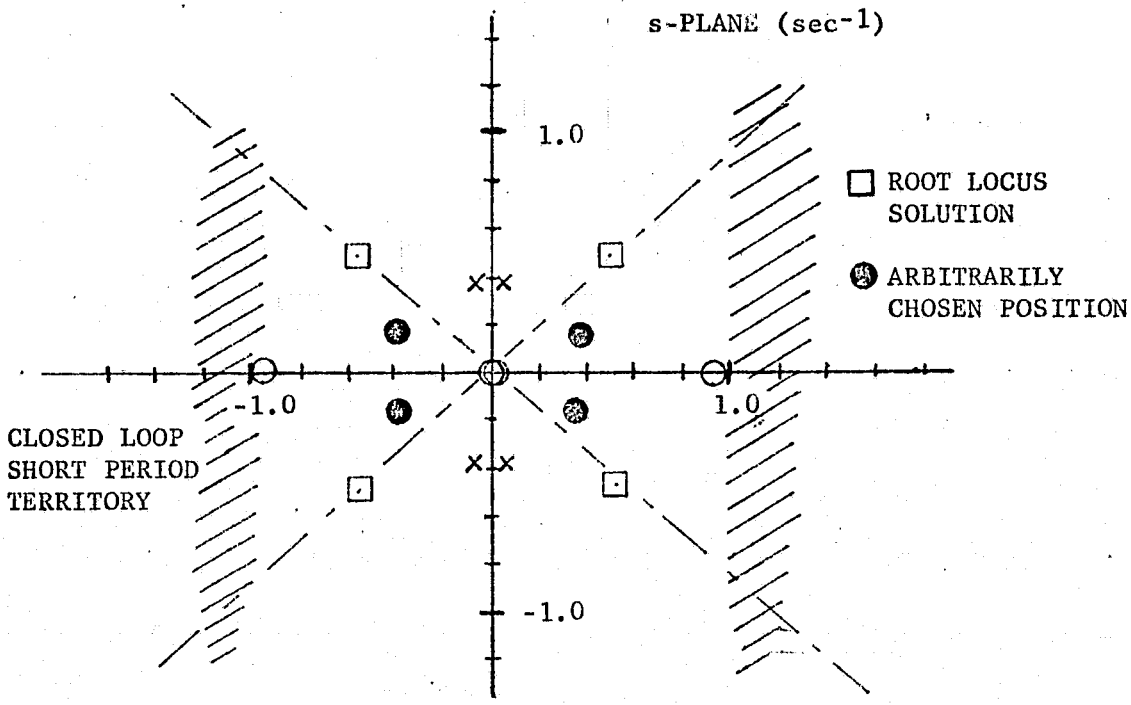

FIGURE VI-6 ROOT SQUARE LOCUS $\frac{u}{df}(s)$

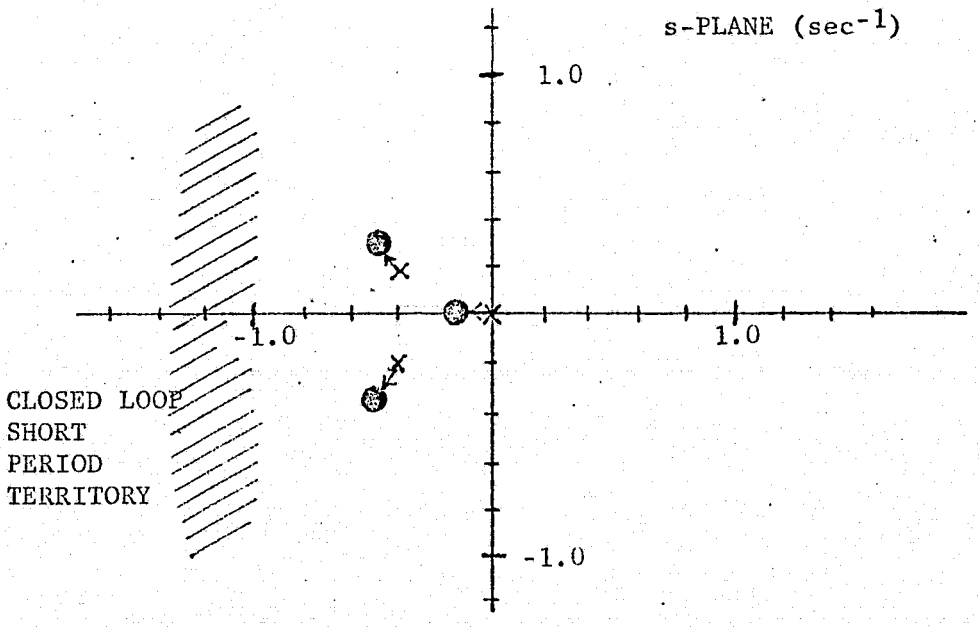

FIGURE VI-7 LOCATION OF CHARACTERISTIC POLES AFTER CLOSING $\frac{u}{dcj}(s)$ FEEDBACK LOOP

These results are tested, as before, in the five state model to observe the resulting true pole locations. The revised approximate solution is tested using OPTSYS to determine if the mode interaction is decreased through judicious choice of pole placement by approximate modal analysis. The resulting true pole location is contrasted with the expected location on Figure VI-8. The apparent mode interaction is manifested in a decrease in damping of the oscillatory modes. However, no reversal of mode (pole) relations is indicated and the altitude (h) pole remains at the chosen position. The two modes remain separated, demonstrating the spectral separation assumption is not violated. The approximate solution can provide a rough estimate of the closed loop response and a readily useable tool to determine feedback control gains without the aid of sophisticated computer programs; even when modes are separated by as little as a factor of two (as are the resulting closed loop poles in this case).

6.6 FURTHER APPROXIMATE ANALYSES

The following discussion presents excursions into several violations of the separation assumption. The two mode (fast and slow) reduction is assumed to be valid while applying controls that are coupled to the fast mode onto the slow mode approximation. The first selection involves the elevator control. Second, the spoiler is applied to enhance the slow root configuration. In each case, the approximate solution is tested by applying its control laws to the five state model and evaluating the resulting closed loop characteristic poles. The analysis is carried out in the same manner as described in detail in the previous section; therefore, only the results are summarized in this discussion.

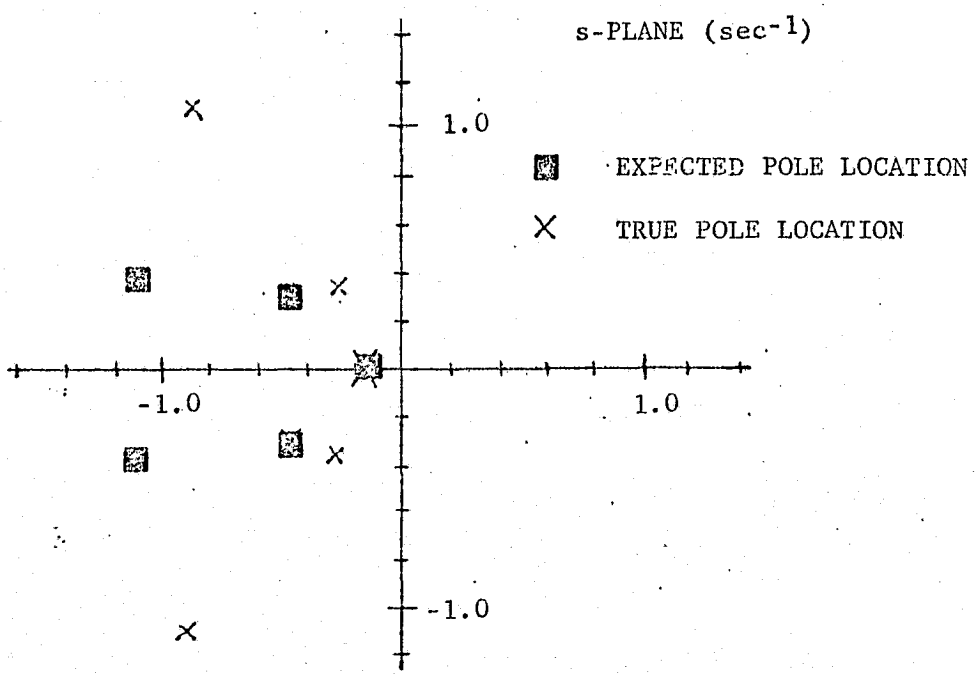

FIGURE VI-8 CLOSED LOOP POLE CONFIGURATION
(REVISED APPROXIMATE SOLUTION)

The inclusion of the elevator as a phugoid damping mechanism is stimulated by its presence in the NASA work of Messrs. Franklin and Koening (Reference N-2). The elevator feedback included a pitch angle term in the stability augmentation used in that study. Although the application of elevator control to the approximate phugoid mode violates the concept of separation, since the elevator is included in the short period closed loop embodied within the approximate phugoid equations.

The elevator is applied to the approximate phugoid mode to provide damping to the oscillatory poles. This is the role of the aft flap in the first control definition, leaving it free to be applied to the altitude transfer function. One attraction of this approach is the throttle (cj) control may not be required to arrest transient sink rates (assuming of course that pilot intervention would shortly include the rapid addition of throttle). The control definition includes both approaches, with and without throttle (cj) included in the feedback control.

The phugoid oscillations are damped utilizing pitch angle (θ) feedback to the elevator. The transfer function associated with this control is:

$$\frac{\theta(s)}{de} = \frac{.008\ s\ (s + 0.199)}{s\ (s + 0.0919\ s + 0.151)} \quad \text{(rad/deg)}.$$

Applying root square locus techniques provides a root locus as sketched on Figure VI-9. Pole locations of $s = -0.45 \pm j\ 0.2\ sec^{-1}$ are selected which produce the following feedback gains:

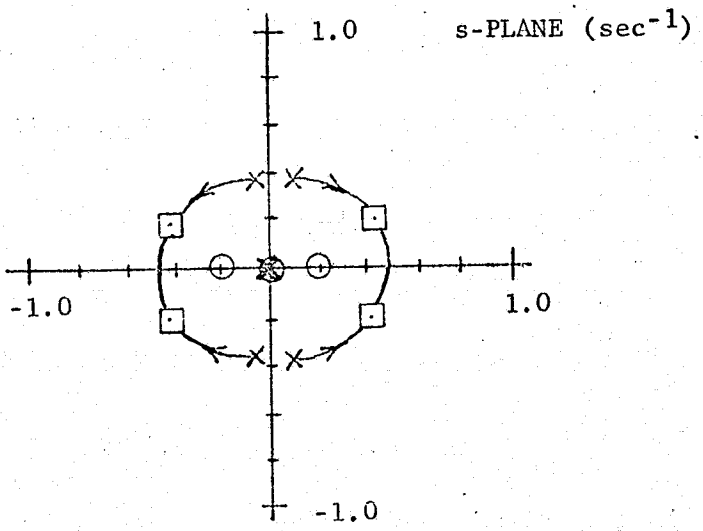

FIGURE VI-9 ROOT SQUARE LOCUS $\frac{\Theta(s)}{de}$

$$C_u = 0.239 \text{ (deg sec/ft)}$$

$$C_\theta = -95.526 \text{ (deg/rad)}.$$

Dropping the Cu term moves the poles to $s = -0.43 \pm j\ 0.35\ sec^{-1}$ changing the damping factor from 0.9 to 0.8 while economizing on feedback terms.

Two control approaches utilize the elevator damped phugoid to develop control of altitude; first with the aft flap (df) alone, and second with the thrust (dcj) included. The aft flap alone control is determined by applying the control to the altitude state (e.g. $\frac{h}{df}(s)$). The results of this approach are contrasted with the full state interaction on Figure VI-10. Application of both aft flap (df) and throttle (dcj) is taken in the same manner as done initially, the aft flap (df) is associated with speed (u) and the throttle (dcj) with the altitude state. These results are shown in contrast with the full state poles on Figure VI-11. The approximate solution poles are shown as closed boxes and the resulting full state (true) poles are denoted by X's on both figures. The results indicate that interaction is significant but not overwhelming. The approximation, though violated, provides an indication of the control response and in performing the root square locus a weighting ratio of desired state to control is obtained. The relation of these weight ratios is an indication of the control influence that is being applied.

Application of the spoiler as an altitude or sink rate control is investigated, utilizing the last result as a starting point. The spoiler control influence is investigated with the non-spoiler dynamics equations since these equations do not change significantly between the two equi-

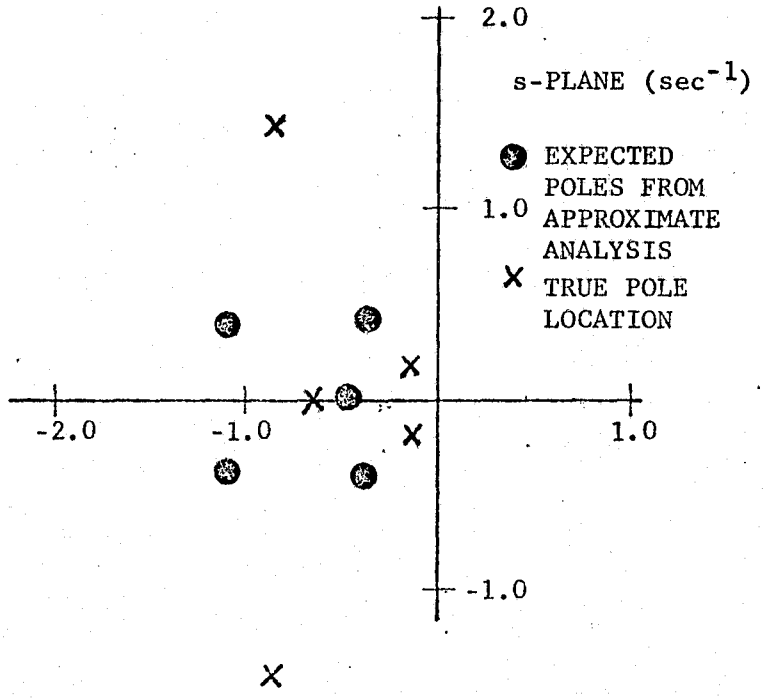

FIGURE VI-10 CLOSED LOOP POLES
WITH df, de CONTROL

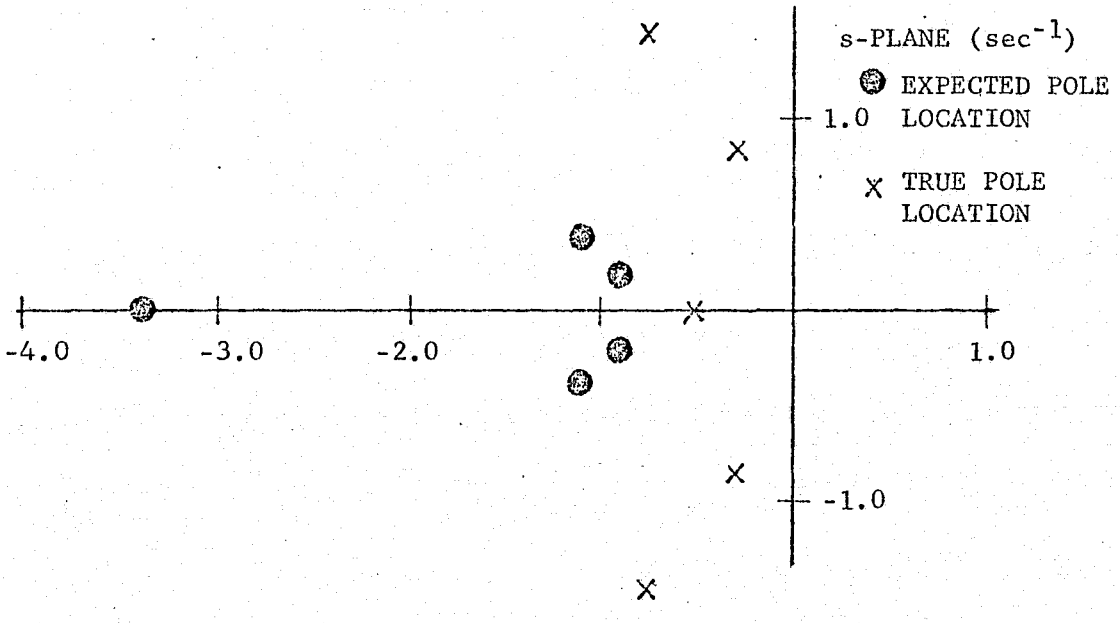

FIGURE VI-11 CLOSED LOOP POLES
WITH dcj, df, AND de CONTROL

librium condition (see the equations in Section 5.3). The approximations of separation are further stretched since the spoiler is principally a w control as is evident from the full state equations. The spoiler is viewed as an adjunct to the previous loop closures of de, df , and dcj assisting the dcj in h control. The results are presented on Figure VI-12.

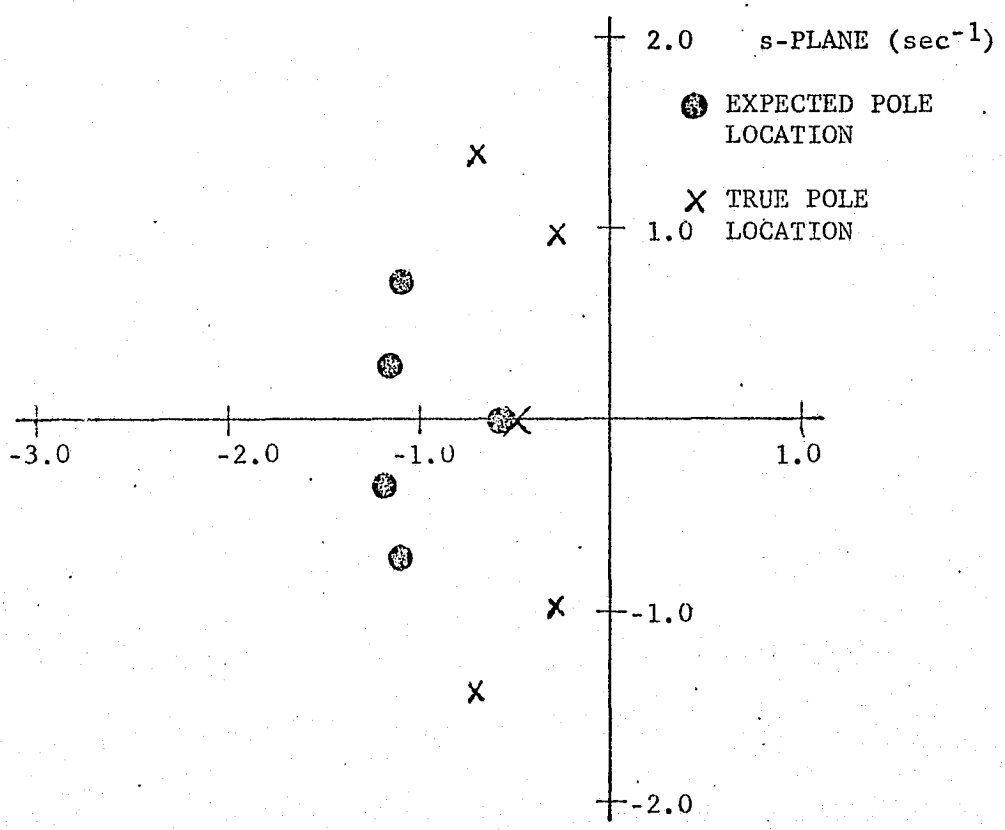

FIGURE VI-12 CLOSED LOOP POLES OF APPROXIMATE SOLUTION WITH SPOILER CONTROL

VII. FIVE STATE MODEL ANALYSIS

7.1 AUTOMATED ANALYSIS USING THE FIVE STATE MODEL

The control problem of determining state feedback control laws to arrest excessive sink rates due to engine failure is addressed using the full five state plant model and an automated control computing algorithm. The Stanford OPTSYS computer program computes the optimal regulator control solution subject to the system dynamic constraints by minimizing the weighted squares of selected states and controls. The program's capability is described in detail in Reference (B-1). OPTSYS computes the feedback control gains with their closed loop eigenvalues and eigenvectors. The closed loop dynamics matrix is provided as output also, making successive loop analysis possible without the associated computational tasks. The feedback control includes all the states which can be a drawback if all the states aren't measured. Therefore, OPTSYS control solutions usually require an estimator to determine the unmeasured states; which the program can define (in steady state) given the appropriate input definition of measurements, measurement noise, and disturbance noise (see Reference B-1). Another approach (an engineering expediant as opposed to scholastic or scientific) to the problem of unmeasured states is to delete them. Perhaps the particular state feedback that is not measured is also not providing the major portion of the desired stabilization. If this is so, then that state's feedback, though required to provide an "optimal solution" is not necessary for acceptable control response. The scholastic approach

would be redefine the initial weights until the feedback in the undesired channel was rendered negligible. However, this would be very time consuming since the current approach to minimize a state component in a particular eigenvalve mode is by trial and error. There is no readily available algorithm that can provide the desired eigenvalves with specified eigenvectors.

7.2 THE ROLE OF EIGENVECTORS IN COST WEIGHT SELECTION

Automated control solutions change the control problem from the computational task of choosing eigenvalves by determining the required coefficients in characteristic equations to selection (or guessing) the weights in the cost function that will provide the desired response. The presence of a ready computer and a control problem to be solved, often in a short time, provides a strong desire to obtain foolproof weights with negligible effort; which on occasion may be a guess at some values. No foolproof weight selection exists to this author's knowledge. One rapid method to initially estimate the cost function weights is suggested by Bryson (Reference B-2).

Bryson suggests that the designer identify the maximum expected value desired for each state of interest and each control. The tendency of the optimal solution is to spread the control so each part of the cost is treated equally in minimization. Therefore, weighting the squares of the states so they are normalized relative to their importance will provide the desired result. The suggested weights are the inverse of the square of the expected value of each state.

Another method is demonstrated by the analysis of the previous section. That is first analyze by approximate methods using successive root locus to identify weight ratios then define consistent state and control weights for the automated solution which includes the ignored interactions. Both weight selection methods are applied to this problem.

Once an initial set of weights are determined the computer computes the control and closed loop response characteristics that may not be entirely satisfactory. If the solution is unsatisfactory the weights must be changed and a new solution computed. The question of which weights to choose and by how much must be determined by trial. In cases, such as the one considered here, where the number of states is large, the search for good weights can be a major task. The uncertainty of which weights to attack can be reduced by utilizing the eigenvectors.

The eigenvectors associated with particular eigenvalues identify the relative amount of each state that is included in the mode of that eigenvalue. Any good text on state variable system theory shows the eigenvectors make up the modal matrix which, in turn is the transformation of the system (in its state variable form) to modal form (Reference D-2, C-1):

$$\underline{x} = Q\underline{x}^*$$

where: $\underline{x}^*$ is the modal state vector. The dynamics matrix can be transformed into modal form (diagonal in the case of distinct eigenvalues) and solution determined by transition matrix of the form:

$$\underline{x}(t) = \phi(t, t_o)\, \underline{x}(o).$$

The modal form of the transition matrix solution is:

$$\underline{x}^*(t) = \Lambda\, \underline{x}^*(o)$$

where

$$= Q^{-1}\, \phi\, Q .$$

Minor algebraic manipulation provides the state response in terms of its modal components:

$$\underline{x}(t) = Q \Lambda Q^{-1}\, \underline{x}(o)$$

$$\underline{x}(t) = Q \Lambda Q^{-1} Q \underline{x}^*(o)$$

$$\underline{x}(t) = Q \Lambda\, x^*(o).$$

The term $\Lambda\, x^*(o)$ is the modal response to the system. Q is the modal matrix made up of columns of the eigenvectors associated with the particular eigenvalues of the system. Each column provides the state component multiplier to the modal response which transforms the normalized characteristic response into state units. The eigenvectors provided by the OPTSYS program, therefore, identify the state make up of each mode (eigenvalue or characteristic root).

Selecting a weight to change, once an unacceptable closed loop response is determined from an initial selection of weights, is aided by considering the resulting closed loop eigenvectors. Since the eigenvectors show the state makeup of each mode, it is expected that the largest coefficients represent the dominant states of that mode.

Increasing the state weight in the cost matrix associated with a dominant state in an undesirable mode should result in increasing the stability of that mode (moving its poles to the left in the s - plane). However, the desired result is not guaranteed. If several states are dominant, then it is possible that increasing a weight on one of those state results, not in an increase in mode stability, but in a decrease of amount of tnat state presence in the mode! Such action indicates that the weights not only determine the characteristic location of closed loop poles, but also the relative state orientation of the modal responses.

The present approach of increasing state weights is a trial and error scheme which may either increase the associated mode pole response stability or decrease the amount of state presence in the particular mode. If the dependance of eigenvector orientation upon the relative weight selection could be identified then a new design approach to control could be obtained. Often control problems are associated with specifying a fast response of a few states while allowing others to be much slower. Inevitably, it seems, the fast and slow states are combined in a common mode making the control specifications difficult if not impossible to meet. If feedback control could be defined so as to eliminate, for example, the fast state presence in a slow mode through a proper selection of cost weights the control problem would, in cases such as is described, be simplified and possibly more efficient.

7.3 INITIAL COST WEIGHT SELECTION

The choice of cost function weights for application to the optimal control solution process is made in three different manners. The first is to apply directly the weight ratios from the initial approximate analysis (Section 6.1-6.2). The next choice involves reviewing the various approximate solution attempts and defining a set of average cost weights. The last method is the application of Bryson's rule (Section 7.2).

The first example of cost function weights are chosen from the initial approximate analysis. The ratios of state cost weight to control cost weight arise from the root square locus gain required to provide the expected pole locations. In order to apply these ratios one set of costs are chosen arbitrarily since no unique solution exists to determine both state and control weights. The root locus analysis only provides one ratio per state explicitly analyzed, so there are twice as many weights to define. The control weights are chosen arbitrarily to be:

$$B_{cj} = 25.0$$

$$B_{de} = B_{df} = 0.001 \ (\text{deg}^{-2}).$$

The state weights are determined from the root square locus ratios as follows:

$$\frac{A_q}{B_{de}} = 3500. \qquad A_q = 3.5 \quad (\text{rad}^{-2})$$

$$\frac{A_u}{B_{df}} = 14.25 \qquad A_u = 0.01425 \ (\text{sec}^2/\text{ft}^2)$$

$$\frac{A_h}{B_{cj}} = 0.0003 \qquad A_h = 0.0075 \ (\text{ft}^{-2}).$$

The successive root square locus technique doesn't explicitly identify the weights of the states that are not chosen to be controlled explicitly; therefore the state weights of A_w and A_θ are made zero.

Several approximate solution analyses were made which provides an overall background of state to control weight ratios. These are reviewed with engineering intuition applied to obtain a set of state weights. No interaction between states is considered in the cost function so the chosen weights are diagonal terms in the cost function matrices A and B as listed below:

$$A_u = 0.001 \quad B_{cj} = 0.1$$

$$A_w = 0.005 \quad B_{de} = 0.01$$

$$A_q = 75.0 \quad B_{df} = 0.01$$

$$A_\theta = 500.0$$

$$A_h = 0.0005$$

(Where the units of each term are the inverse of the state unit, to which they apply, squared.)

Another set of cost function weights are determined by applying Bryson's rule. A reasonable choice of control and state excursions is estimated to define the independent state and control weights. For example, select a speed variation (Δu) of 10 ft/sec as reasonable, then the weight associated to it is:

$$A_u = \frac{1}{u^2} = \frac{1}{10^2} = 0.01 \ (sec^2/ft^2)$$

The following table relates the reasonable variations and their resulting cost weights:

WEIGHT	STATE-CONTROL	VARIATION	WEIGHT VALUE
A_u	u	10 ft/sec	0.01 sec^2/ft^2
A_w	w	10 ft/sec	0.01 sec^2/ft^2
A_q	q	0.1 rad/sec	100.0 sec^2/rad^2
A_θ	θ	0.1 rad	100.0 rad^{-2}
A_h	h	10 ft	0.01 ft^{-2}
B_{cj}	dcj	0.2 (approx 15% of nominal thrust)	25.0
B_{de}	de	10 deg	0.01 deg^{-2}
B_{df}	df	10 deg	0.01 deg^{-2}

7.4 OPTIMAL CONTROL SOLUTIONS

The three sets of initial cost weights as they are defined are input with the five state model to OPTSYS to obtain the optimal control laws. The resulting feedback control laws are shown on Table VII-1 and the respective closed loop pole locations are presented on Figures VII-1,VII-2, and VII-3. The characteristic response as indicated for each weight set comparing the results to the approximate work.

The first chosen weight set results in the pole configuration shown on Figure VII-1. Also shown, are the expected pole locations derived from the approximate analysis (Section 6.3). Recalling the results of that solution, the feedback gains that were determined in that analysis had true pole locations totally different from their expected locations. Indeed they had no apparent relationship with the analysis beyond being stable (e.g. located in the left half s-plane). Now, the weights from

TABLE VII-1

OPTIMAL CONTROL LAWS

$$\dot{\underline{x}} = F\underline{x} + Gu$$

$$\underline{u} = C\underline{x}$$

In each case units are consistently ft, sec, rad and deg.

1) Weights directly from approximate analysis

$$C = \begin{bmatrix} -0.012 & 0.0079 & -0.0641 & 1.292 & 0.0068 \\ 4.523 & -3.244 & 85.241 & -581.32 & -2.101 \\ 3.262 & 1.262 & -45.091 & 263.35 & 1.385 \end{bmatrix}$$

2) Weights determined by review of the approximate analyses

$$C = \begin{bmatrix} -0.058 & 0.210 & 8.479 & -1.384 & 0.063 \\ 0.062 & -0.178 & 106.58 & -205.56 & -0.083 \\ 0.125 & 0.167 & -56.25 & 115.13 & 0.057 \end{bmatrix}$$

3) Weights determined by Bryson's rule

$$C = \begin{bmatrix} -0.039 & 0.024 & -0.080 & 4.128 & 0.017 \\ 1.073 & -0.519 & 109.51 & -218.71 & -0.483 \\ 1.607 & 0.272 & -54.47 & 109.77 & 0.274 \end{bmatrix}$$

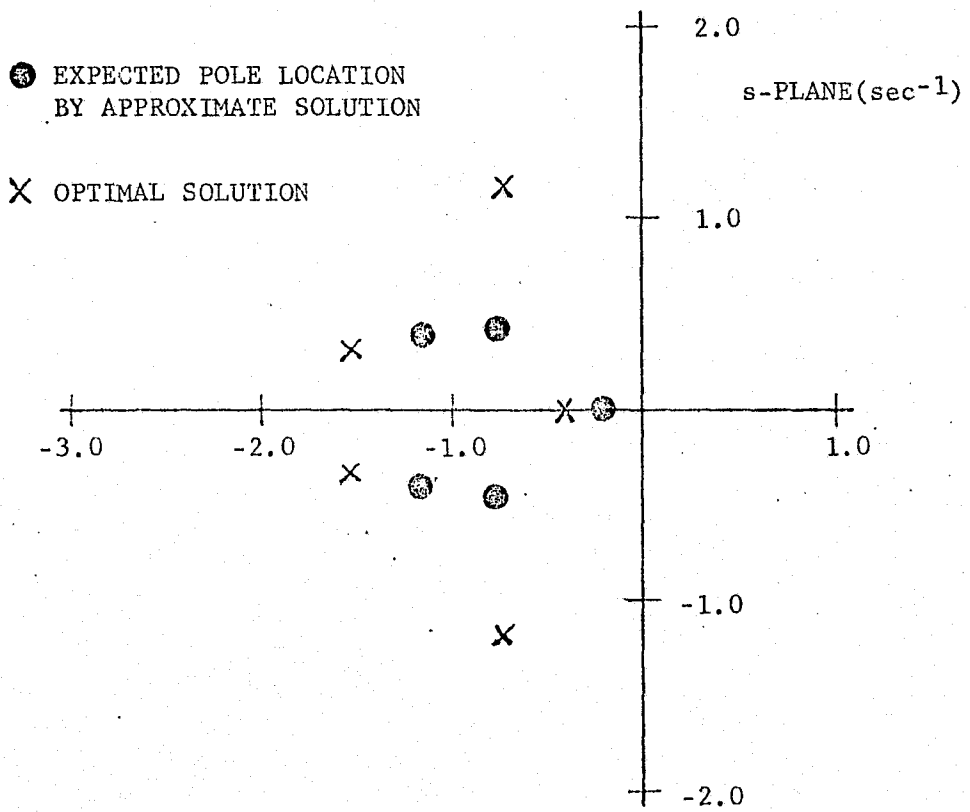

FIGURE VII-1 CLOSED LOOP POLES DUE TO INITIAL APPROXIMATE SOLUTION COST WEIGHTS

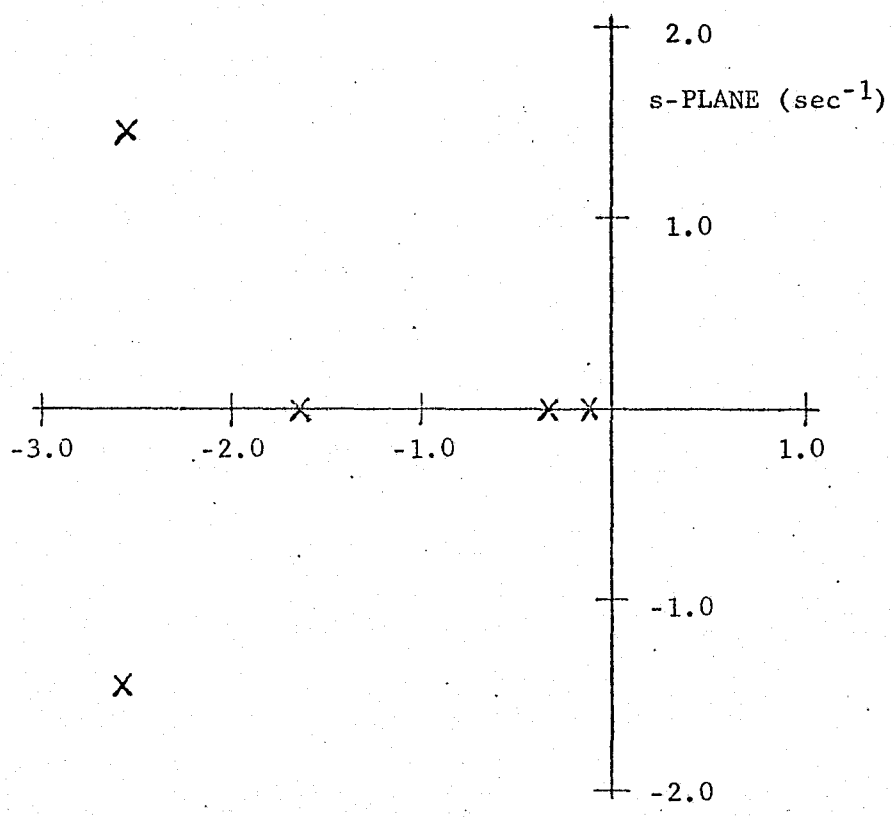

FIGURE VII-2 CLOSED LOOP POLES DUE TO AVERAGE APPROXIMATE SOLUTIONS COST WEIGHTS

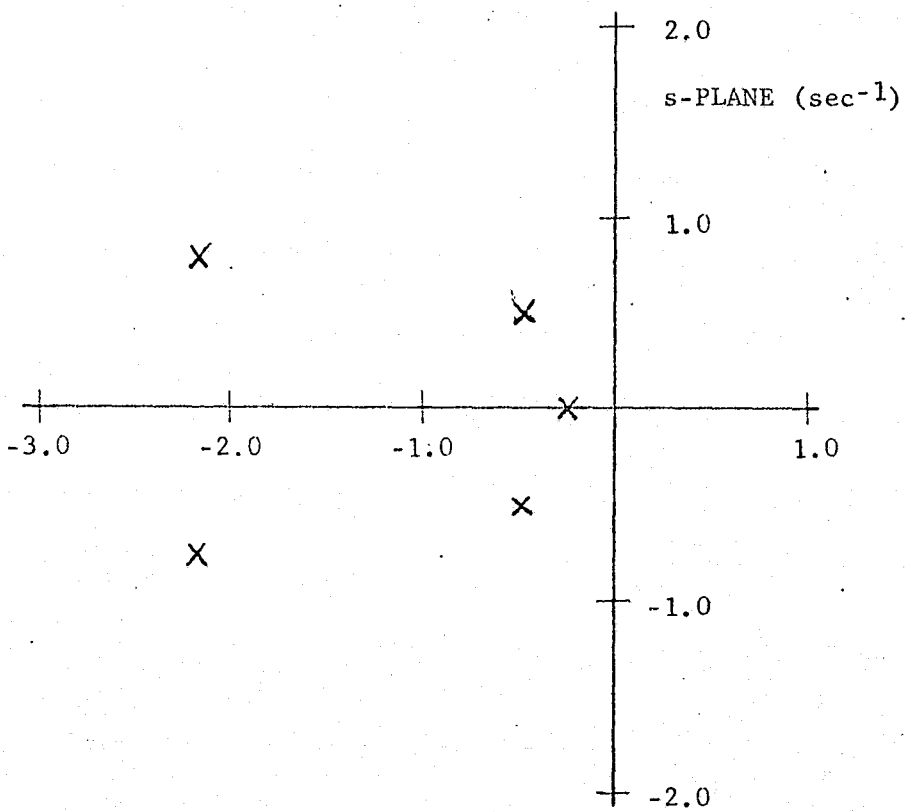

FIGURE VII-3 CLOSED LOOP POLES DUE TO BRYSON'S RULE DERIVED COST WEIGHTS

that analysis provide reasonable pole constellations with the resemblance to the expected pole locations (Figure VII-1). The mode separation is about that which was expected but with changes in response frequency and damping. This demonstrates that the mode interaction that was ignored in the approximate analysis was the major factor in providing results totally unlike those that were expected.

The next example utilizes the intuitively averaged cost weights obtained from the approximate analysis experience. The major issue in the approximate work was mode interaction and the inability to avoid it. One might expect the resulting weights to be conservative, in that they ask for tight control. Indeed, such a result is apparent from the closed loop pole constellation on Figure VII-2. The short period is driven far out into the left half plane and the slow roots are pushed onto the real axis. One might conclude this is overpowering control in view of the mild movement of roots of the first case. Viewing the control laws, though, contradict such a conclusion (Table VII-1). The feedback matrices for the first and second cases have coefficients of the same order of magnitude. Indeed, most of the second case coefficients are of lower magnitude than the first. The significant difference from this trend is in the thrust control channel, where the second case feedback gains are larger than the first case. The difference in the resulting pole constellation in this second case is due to a fortunate choice of weights causing tighter control without significantly larger feedback gains.

The application of Bryson's rule results in the closed loop control pictured on Figure VII-3. The pole configuration appears to lie somewhere between the high degree of control of the second weight set and the relatively mild pole adjustments of the first weight wet. The advantage of this approach is it requires no analysis experience with the plant, one merely specifies the degree of each state that is allowed and also, each control, enters OPTSYS obtaining the appropriate control law. Occasionally though the results aren't as acceptable as are these, leaving the engineer with the issue of weight iterations described in Section 7.2.

Each of the optimal solutions have reasonable responses. The second weight set provides the most stable response which might indicate its control would be large. On the other hand, the first case with its mild solution would be expected to require the least control application. The truth of this expectation is obvious from the control laws for each case (Table VII-1).

The control laws show the three cases to be quite different than the relative pole configurations would lead one to expect. The relative gains in each channel are indicative of the control output for a state disturbance input. The first case is most different from the last two, having the least amount of thrust feedback with much greater elevator and aft flap control. The last two cases are much milder controls. In fact the last two cases are much the same with differences of an order of magnitude on, only, the speed (u), altitude (h) and pitch rate (q)

channels. The largest difference between these last two examples is the feedback of pitch rate (q) to thrust. The second case has a great deal of this control, whereas the last one has practically none (a difference of two orders of magnitude between the two cases). The result is surprising, as it is not apparent from the dynamical equations that the thrust would play a significant role in pitch rate control (i.e. pitch damping).

7.5 COMMENTS ON MODERN CONTROL SOLUTIONS

Three different approaches provide three different control solutions. Each one optimal for the cost function applied. The application of modern control theory is demonstrated in these examples. Automated control analysis relieves the computational drudgery of hand solutions (which classical and approximate analyses tend to be) but does not relieve the control engineer. The focus of modern control theory is upon the definition or appropriate cost functions that provide controls that respond to specifications. The classical engineer must learn new terms and may approach problems from a point of view that is initially divorced from the classical pole location root locus concepts. That is, until a solution is attempted without success; whereupon a correlation between cost function and the classical pole location must be developed to change the solution. Although this seems like a great deal of trouble, two advantages are derived from its use. First, complex systems are directly analyzed without eliminating significant interactions from the analysis.

These interactions may be beneficial for example: the pitch rate feedback to thrust of case two which provides the highly stable response without large control gains. Second, the control engineer can relate control to minimizing functions of state variables with the cost function architecture, and as such can cast the control problem in terms of system performance, a form which management understands. The approach also has one drawback, it defines control as full state feedback. The full state vector is not measurable in most real systems. However, modern control theory provides a solution, the state estimator. The engineer, not wishing to add complex compensation, such as an estimator, may investigate whether an acceptable control results from dropping the feedback terms of the unmeasured states in the control law. One may expect that this approach will work if the unmeasured states do not require dominant feedback terms to provide the desired pole locations. This latter approach is investigated for this control study as it is attractive from an economy of parameters standpoint.

7.6 ELIMINATING FEEDBACK PATHS FROM OPTIMAL CONTROL

The optimal solutions are evaluated with particular feedback gains eliminated to evaluate the need of an estimator. The approach is to first determine the optimal feedback gains with the cost term on the unmeasured state set to zero; then to drop the resulting feedback gains from the unmeasured states without changing the remaining gains and evaluating the resulting pole locations. The last two optimal solutions (case 2 and 3 of the previous section) are used. The states that are

readily measured are the angle of attack state (w) and the altitude state (h). Altitude is commonly available as a measurement, on complex transport aircraft, however, it usually entails additional equipment beyond that needed for stability augmentation. The elimination of altitude feedback is attractive. The angle of attack, on the other hand, is not commonly provided as a measurement. Angle of attack metering systems are found on experimental and high performance aircraft with special needs. Inclusion of angle of attack (e.g. w) requires an estimator in the context of this study, so it is desirable to eliminate from the control law. The angle of attack (w) feedback is addressed first.

Before dropping the feedback gains; optimal control solutions are generated for the two cases of interest with the (w) weight set to zero. This is done to minimize the effect of making the w feedback gain zero. The characteristic response is then determined with the w feedback gains set to zero.

The pole configurations, using the modified approximate weights, (case 2 of Section 7.3) show a dependence of the phugoid mode on angle of attack feedback (Figure VII-4). The real phugoid poles (determined with the w weight included) become damped oscillatory poles with the w cost reduced to zero. These poles move closer to the $j\omega$ axis when the w feedback gains are set to zero. The short period and altitude poles are only slightly changed. The eigenvectors of these poles have a significant w contribution substantiating the hypothesis:

Phugoid Poles ($A_w \neq 0$)

Eigenvalue (sec^{-1})	Eigenvector (units in ft, sec, and rad consistent with the states vector $\underline{x}$)
-1.645	0.144
	-0.744
	-0.003
	-0.002
	0.652
-0.350	-0.116
	0.276
	0.0001
	0.0004
	-0.954

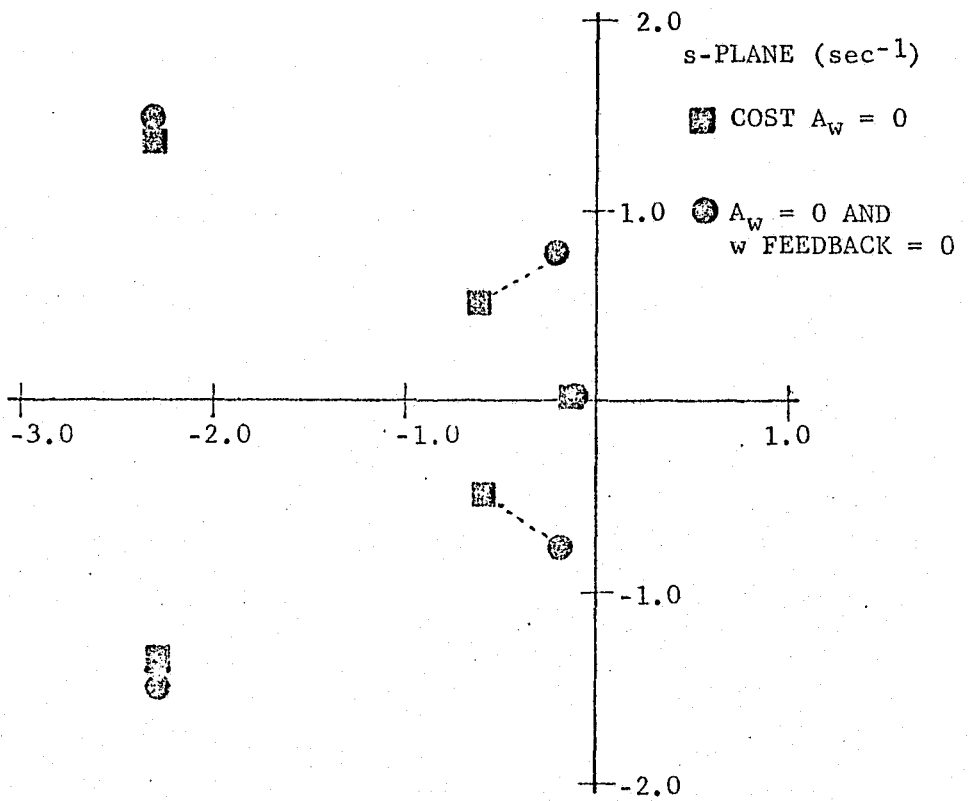

FIGURE VII-4 ELIMINATION OF w FEEDBACK FROM THE APPROXIMATE WEIGHTS SOLUTION

Phugoid Poles ($A_w = 0$)

Eigenvalue (sec^{-1})	Eigenvector	Units in ft, sec, and rad consistent with the states vector $\underline{x}$
$0.603 \pm j\ 0.517$	$0.088 \mp j\ 0.039$	
	$-0.606 \pm j\ 0.503$	
	$0.00007 \pm j\ 0.00005$	
	$0.00002 \pm j\ 0.0001$	
	$1.000 \mp j\ 0.000$	

The cost function chosen for this case (case 2 of Section 7.3) causes the rotation of the eigenvectors such that the traditionally separated mode states are mixed. The control law, in this case, suffers from the loss of angle of attack feedback causing a poorly damped oscillatory slow mode; that is not a traditional phugoid, but a heaving motion much like a ship at sea encounters.

The response with the control laws determined with a cost function defined by Bryson's rule show a more traditional result. Removing the weight from the w state results in real short period mode poles and a slight increase in phugoid stability (Figure VII-5). The subsequent setting of the w feedback gains to zero cause the short period poles to return to being oscillatory with less damping than they were initially. The phugoid poles move closer to the $j\omega$ axis decreasing their damping slightly. This choice of cost function weights maintains the standard aircraft modestate relations, and suffers very little in removing the angle of attack feedback. The main result is a loss of short period damping from a factor of 0.94 to 0.7 damping factor and increase in frequency by a factor of 2.

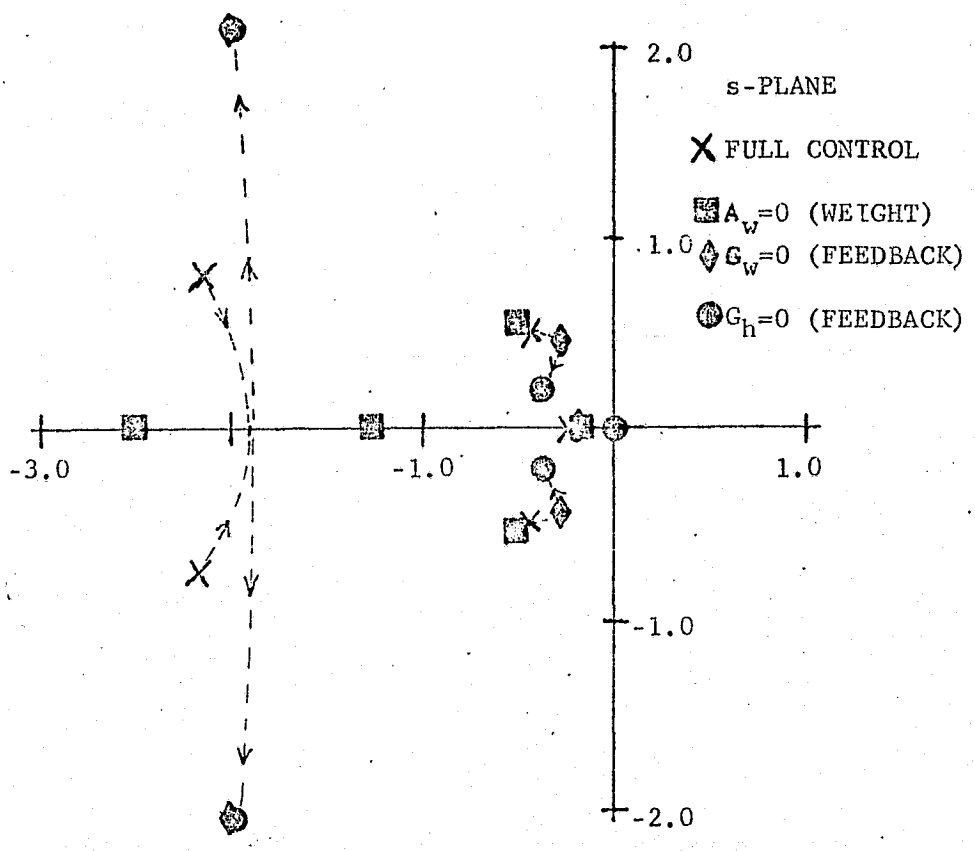

FIGURE VII-5 ELIMINATION OF FEEDBACK CHANNELS FROM THE BRYSON'S RULE WEIGHTS SOLUTION

The phugoid damping is reduced from 0.67 to 0.55.

This last case (case 3 Section 7.3) is investigated for sensitivity to eliminating the altitude feedback also. The altitude pole moves expectedly to the origin and the phugoid moves toward the real axis increasing its damping factor to 0.80 (Figure VII-5). These results indicate that this control law can be implemented, without angle of attack feedback, as a stability augmentation system (with speed control) which can be turned into an approach control sink rate alleviator by simply closing the altitude feedback loops when needed.

7.7 SPOILERS INCLUDED IN CONTROL

The spoiler control is a direct lift device which is apparent in its influence on the w state from the dynamical equations. The key to arresting sink rate growth is to be able to attain additional lift rapidly. The application of the only direct lift control may enhance the response to lift disturbances; such as the loss of thrust. Inclusions of this control is investigated to determine if it is effective in enhancing the closed loop response. The analysis is developed in the same manner as the three control investigation using the five state model and the OPTSYS optimal control computation.

The dynamic model and initial weights are taken from the previous analysis. The spoilers are assumed to be deployed thirty degrees nominally during approach. The equilibrium flight conditions were computed for this case in Section 5.2. A comparison of the equations of motion about the equilibrium flight conditions with the spoilers de-

flected is not significantly different from their undeflected (nominal configuration) case (cf. dynamics matrices Section 5.).
The dynamics matrices of the nominal case are chosen to be used for the spoiler control analysis to determine if their effectiveness is sufficient to warrant more careful investigation. Also, the initial cost function weights, as determined by Bryson's rule, for the nominal configuration are applied, as they appear to be a good compromise selection between plant response and control deflection. Additionally a small value control weight is defined for the spoiler to allow a full deflection of 30 deg (B_{dsp} = .001 deg^{-2}).

The spoiler does not appear to be a significant control contribution according to these results. The pole locations, for each of the conditions chosen, are virtually the same as the three control case (Figure VII-6). The response is not changed and the control gains are not significantly changed (Table VII-2). The thrust feedback gains are reduced an average of 25 percent. The other control gains are reduced somewhat also. The spoiler control inclusion takes some of the control burden without affecting the closed loop response. These results utilize the control in a linear fashion (the scope of this study). Perhaps a nonlinear control option is appropriate for spoiler control.

7.8 NON-LINEAR SPOILER CONTROL

The spoiler may be treated as a fast acting configuration device which may assist in alleviation of high sink rates. Plan a nominal

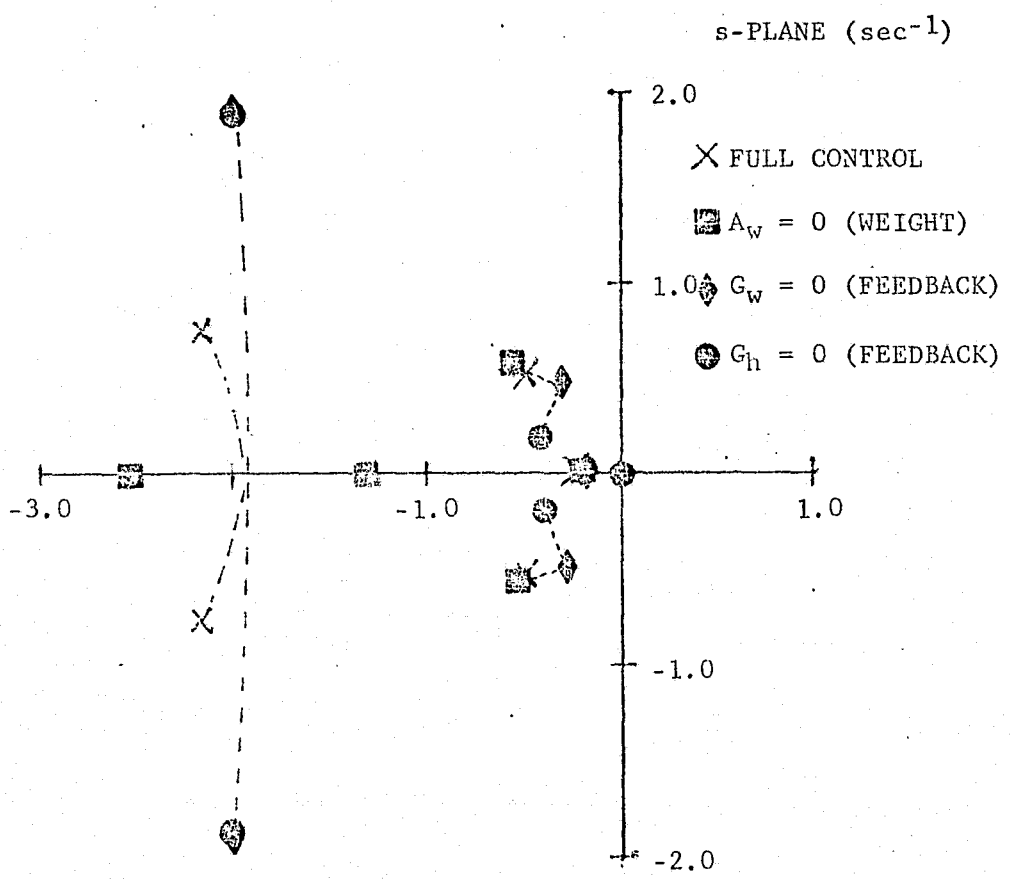

FIGURE VII-6 OPTIMAL CONTROL WITH SPOILERS INCLUDED USING BRYSON'S RULE WEIGHTS

TABLE VII-2

OPTIMAL CONTROL GAINS

(Bryson's Rule Cost Weights)

(Spoiler Control Included)

(In consistent units of ft, sec, rad and deg)

ALL STATES WEIGHTED

$$C = \begin{bmatrix} -0.028 & 0.021 & -0.041 & 3.145 & 0.013 \\ 0.738 & -0.342 & 108.27 & -190.07 & -0.386 \\ 1.388 & 0.335 & -54.91 & 119.37 & 0.308 \\ 3.334 & -2.861 & 13.83 & -433.88 & -1.792 \end{bmatrix}$$

ANGLE OF ATTACK (w) SET TO ZERO

$$C = \begin{bmatrix} -0.026 & 0.018 & -0.102 & 2.919 & 0.013 \\ 0.847 & -0.783 & 98.07 & -209.08 & -0.394 \\ 1.337 & 0.375 & -53.31 & 121.31 & 0.298 \\ 3.149 & -2.380 & 21.96 & -404.03 & -1.789 \end{bmatrix}$$

approach with partial spoiler deployment which is immediately retracted upon the loss of thrust. The equilibrium flight conditions for these two configurations indicates the strength of this concept (Figures V-1 and V-2). The approach condition for a 6 deg flight path with 30 deg of spoiler deployment is approximately 83 kt at 50,400 lb of thrust. Estimating the sink rate at the equilibrium flight condition with one engine failed results in a sink rate of 18.4 ft/sec with the spoiler retracted. The equilibrium sink rate at the nominal approach velocity is 19.7 ft/sec. The same comparison for 60 deg flap setting results in an estimated sink rate of 18.5 ft/sec (at about 90 kt). The initial deployment of the spoiler is worth about 1 ft/sec sink rate. This system also requires an engine thrust monitor to signal the spoiler retraction and as such it would not react to other disturbance inputs. The spoilers do not contribute a great deal to the direct control of sink rate. However, there may be a synergistic interaction with the other control capabilities due to the increased speed of approach with the spoilers deflected, which should be researched.

VIII. FOUR STATE MODEL ANALYSIS

8.1 SINK RATE ALLEVIATION THROUGH INCREASED DAMPING

The effectiveness on controlling sink rate without altitude feedback is investigated. The control concepts thus far have included altitude feedback providing integral control on sink rate and requiring altitude measurement or estimation. The elimination of altitude feedback is attractive if it can be accomplished without the need of angle of attack information since the resulting state feedback set as the standard stability augmentation measurement set of states. This approach was unsuccessfully researched by Messrs. Franklin and Koening in Reference N-2 stimulating its inclusion in this work, to determine if optimal control theory can identify harmonious interactions within the plant.

8.2 INITIAL COST WEIGHT SELECTION

The automated control computation (OPTSYS) is employed to the four state aircraft model to generate and analyze possible control laws. The four state model is generated by eliminating the altitude state from the nominal model. The initial weight selection is based upon Bryson's rule incorporating the state relationship to sink rate. The control set is the nominal three controls dcj, de, and df.

The initial weight selection includes the objective of minimizing sink rate. The optimal solution determines control that minimizes the cost functions:

$$J = \tfrac{1}{2}\int\left(x^{T}Ax + u^{T}Bu\right)dt.$$

Objective of the control is to minimize sink rate. The state weights are selected to reflect that objective. The sink rate perturbation in terms of the model states is given by:

$$\dot{h} = w + U_o \theta \ .$$

The cost function weights the square:

$$\dot{h}^2 = w^2 + 2\ U_o\ w\theta + U_o{}^2 \theta \quad .$$

Selecting weights in relation to allowable values of states according to this relationship may result in minimizing the sink rate response to disturbances. The state cost matrix is of the form:

$$A = \begin{matrix} Auu & 0 & 0 & 0 \\ 0 & Aww & 0 & Aw\theta \\ 0 & 0 & Aqq & 0 \\ 0 & A\theta w & 0 & A\theta\theta \end{matrix}$$

The weights Aww, $Aw\theta$, $A\theta w$, and $A\theta\theta$ are chosen in relation to the sink rate equation, arbitrarily letting the state values be unity:

$$Aww = \frac{1}{w^2} = 1. \quad ft^{-2}\ sec^2$$

$$A\theta w = Aw\theta = \frac{1.}{2U_o} = 0.0037 \quad ft^{-1}\ sec\ rad$$

$$A\theta\theta = \frac{1.}{U_o{}^2} = 0.0001 \quad rad^{-2}$$

Recalling that the equilibrium velocity is approximately 135 ft/sec. The control weights are chosen to be the same as those of the five state case

3; the application of Bryson's rule case (Section 7.3):

$$B_{cj} = 25.0$$

$$B_{de} = 0.01 \text{ deg}^{-2}$$

$$B_{df} = 0.01 \text{ deg}^{-2}.$$

8.3 OPTIMAL CONTROL RESULTS

The optimal control analysis is made using OPTSYS to obtain a well damped response and investigate the consequences of dropping the angle of attack feedback. The initial weights are applied to the optimal control problem with the resulting response pictured on Figure VIII-1. The short period is well damped at a frequency twice the magnitude of the earlier results. The phugoid response is nearly undamped. The eigenvectors associated with these poles identify the troublesome states:

Eigenvalue (sec^{-1})	Eigenvector Unnormalized (Units in ft sec rad)	Normalized Magnitude *100.
-4.88 ± 4.08	0.071 ± j 0.046	0.29
	1.000 ∓ j 0.000	3.39
	-0.023 ± j 0.035	93.4
	-0.006 ± j 0.002	2.9
-0.164 ± j 0.332	1.000 ∓ j 0.000	32.88
	0.007 ± j 0.008	0.36
	0.005 ± j 0.002	3.91
	0.002 ± j 0.014	62.84

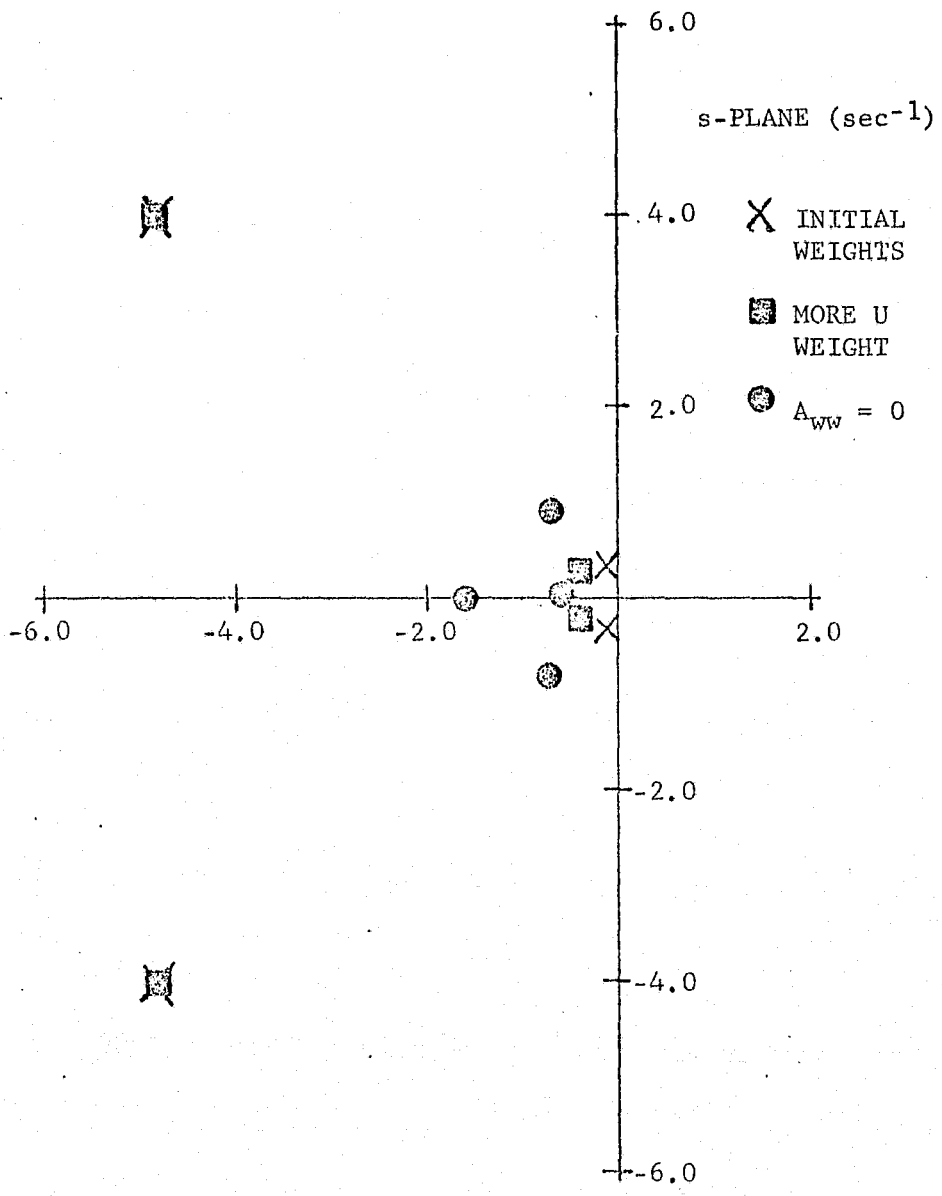

FIGURE VIII-1 POLE LOCATIONS RESULTING FROM FOUR STATE OPTIMAL FEEDBACK

The eigenvector components are normalized by non-dimensionalizing the state components with U_o and τ then computing the component magnitude for unit length of the vector. Clearly the major components of the phugoid mode are u and θ . The velocity state u does not appear in the $\dot{h}$ equation rendering it an independent phugoid state component of the cost function. Enlarging the cost weight on u by one order of magnitude induces more phugoid damping (Figure VIII-1). Previous experience with eliminating the angle of attack weight with the intention of eliminating w feedback has not affected the phugoid poles (Section VII). However this case is different from those previous cases. This difference is apparent from the closed loop eigenvector state makeup.

The enhanced phugoid mode control just determined has increased the interconnectivity between the modes. The eigenvectors are rotated in the states to increase the interaction of traditional slow and fast mode states. The eigenvectors are shown as before:

Eigenvalue (sec^{-1})	Eigenvector	Units in ft, sec & rad consistent with the state vector $[u, w, q, \theta]^T$
$-4.86 \pm j\ 4.07$	$0.071 \pm j\ 0.046$	
	$1.000 \pm j\ 0.000$	
	$-0.023 \pm j\ 0.035$	
	$-0.006 \pm j\ 0.002$	
$-0.453 \pm j\ 0.265$	$1.000 \pm j\ 0.000$	
	$0.049 \pm j\ 0.023$	
	$0.013 \pm j\ 0.005$	
	$0.017 \pm j\ 0.021$	

Compare the slow mode with the unnormalized eigenvectors of the previous case, the w state contribution is increased. One might conclude that the increased phugoid damping is obtained by increasing the state interaction between the two modes. The next step in attempting to eliminate w feedback is to reduce the w weight to zero to reduce the feedback gains.

The closed loop response of the system derived with the w weight set to zero is markedly different than the two previous cases. The short period roots move to the real axis and into the region of the all poles of the other solutions in this study (except of course the two initial cases of this section). The phugoid poles are significantly changed, too. Their frequency of response is increased with a slight loss of damping (0.68 damping factor). The optimal analysis the w state influence is dominant to the system response.

The elimination of w feedback must have a significant impact upon the pole locations since the system is sensitive to w control. The last step of eliminating w cost weight was taken to reduce the w feedback sensitivity, which is apparent from the resulting control law:

$$C = \begin{bmatrix} -0.003 & -0.000 & 0.017 & -0.034 \\ -0.794 & -0.194 & 52.41 & -68.86 \\ 2.872 & 0.206 & -39.11 & 86.40 \end{bmatrix}$$

(In consistent units of ft, sec, rad and deg)

The corresponding control law with the w cost weight included is:

$$C = \begin{bmatrix} -0.009 & 0.075 & 1.100 & 0.397 \\ -1.137 & 8.076 & 236.42 & -33.61 \\ 2.957 & 1.312 & -56.31 & 94.39 \end{bmatrix}$$

The w gains are reduced significantly, as are the dcj and de feedback gains in most channels.

The closed loop response changes significantly with the elimination of w feedback resulting in a well damped system and well mixed modes. The closed loop eigenvectors demonstrate that w is dominant in both modes:

Eigenvalue (sec^{-1})	Eigenvector (units in ft sec & rad consistent with the state vector $[u,w,q,\theta]^T$)
$-1.32 \pm j\ 1.29$	$0.030 \pm j\ 0.006$
	$1.000 \pm j\ 0.000$
	$-0.007 \pm j\ 0.009$
	$-0.006 \pm j\ 0.001$
$-0.541 \pm j\ 0.400$	$0.165 \pm j\ -0.079$
	$1.000 \pm j\ 0.000$
	$0.000 \pm j\ 0.003$
	$-0.002 \pm j\ 0.003$

The change in pole configuration from the previous case (with w feedback) is demonstrated on Figure VIII-2. The w sensitivity is apparent, the phugoid poles move a large amount as the short period is destabilized. The resulting system appears to be well behaved with approximately 0.7 damping factor on each mode. However as is apparent from the eigen-

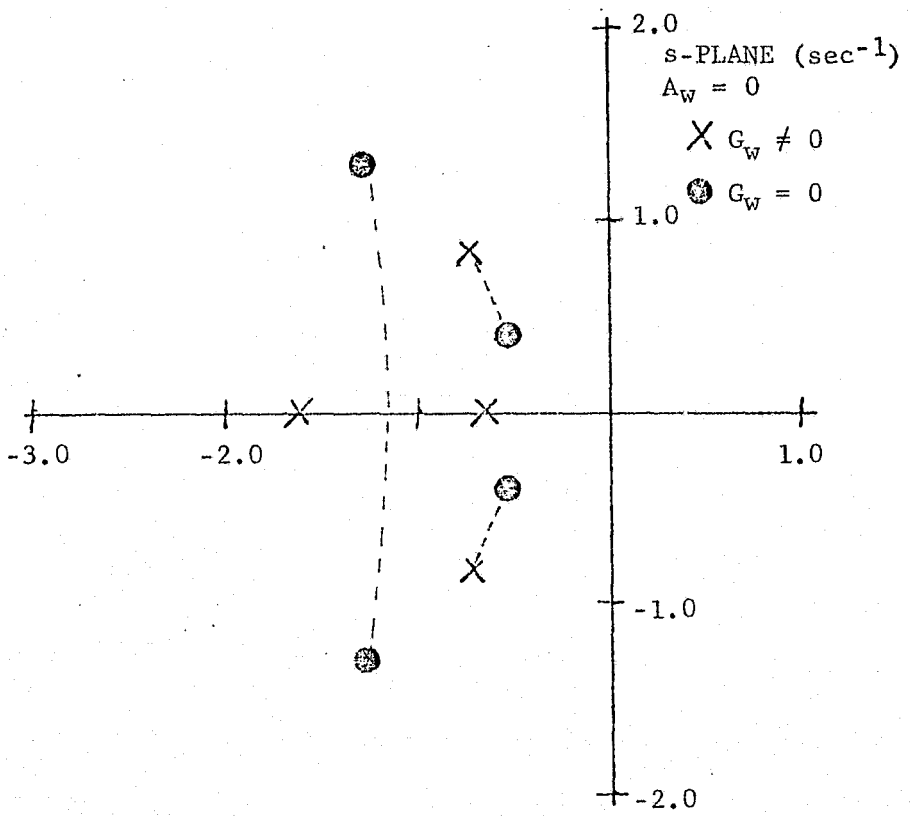

FIGURE VIII-2 ELIMINATION OF w FEEDBACK
FROM OPTIMAL CONTROL SOLUTION

vectors state makeup, these are not the traditional aircraft modes.

The vertical motion damping approach results in apparently well behaved systems. It is possible that these control laws may control the sink rate through damping. However the amount of damping required to eliminate major sink rate buildup is not yet determined. Testing these results by simulation is one way of evaluating their effectiveness with the additional feature of presenting control input histories for evaluation of their relative efficiencies.

IX. ENGINE MODEL

The engine model is provided by input-output thrust responses to step throttle changes. The data are provided in the form of the analog output of the NASA simulation (Reference N-1). A first order response model is defined for use with the control results in evaluating the thrust lag degradation of the system closed loop response. The raw form data are rescaled for presentation and future use. The thrust responses indicate that the engine is not accurately simulated as a first order system. Further work to incorporate these higher order responses is identified.

The engine model source is taken from the NASA analogue simulation output for several throttle setp inputs at initial thrust levels of: 50%, 70%, 80% and 100%. An example of this output form is provided on Figure IX-1, the time history responses overall of the data appear to be of high order (such as third order), but well damped with increased throttle command (+dcj). The engine failure problem is expected to require positive throttle commands, for the most part. The positive throttle direction is determined to be reasonably modelled by a first order response representing the thrust lag. The raw data form is used to determine an average first order model applicable to the thrust and throttle step ranges expected to alleviate sink rate growth due to loss of one engine (25 percent of the approach thrust). The approach thrust setting used in the current NASA simulation is approximately 60 percent

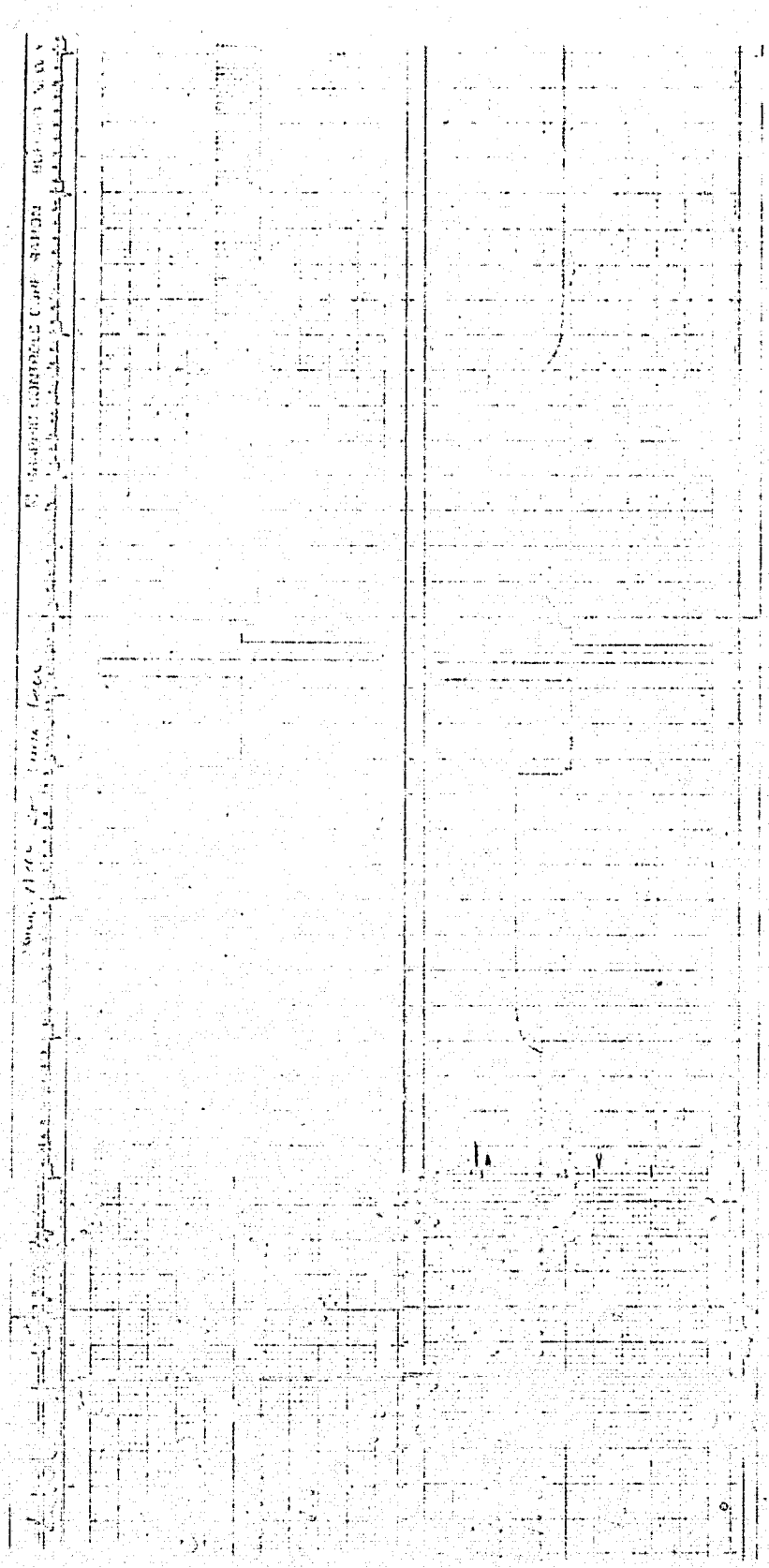

FIGURE IX-1 TYPICAL THROTTLE RESPONSE DATA (RAW FORM)

PRECEDING PAGE BLANK NOT FILMED

full thrust. Loss of one engine is a 15 percent total thrust level step decrease, which corresponds to a 5 percent thrust increase in the three remaining engines. 10 to 20 percent steps represent the range of expected control commands. The following responses are read from the raw thrust response data:

INITIAL THRUST (10^3 lb)	FINAL THRUST (10^3 lb)	TIME TO 95% OF FINAL THRUST (sec)
15.0	17.5	2.5
15.0	19.5	2.5
15.0	21.0	4.0
15.0	9.0	3.5
17.5	19.5	2.5
17.5	15.0	0.5
17.5	22.0	2.0
17.5	11.5	1.5
22.0	17.5	1.0
11.0	17.5	2.0
11.0	15.0	1.5
11.0	7.0	1.5
11.0	6.0	1.0

The full step change ($T_{95\%}$) is chosen to determine the time constant because the thrust histories due to a 10-20 percent positive step change appear to be nearly first order and the dominant control response is believed to be characterized by an equivalent lag over these command steps. The above data are averaged considering three partions of the data.

The first since the estimate is taken using the 50 percent initial thrust data, nominal approach thrust level is near 50 percent (between 50 and 70 in fact). The average of that response is determined; then the 70% range is included; and finally the full data set is averaged to determine how much difference exists (eg how special the subsets are). The time constants at $T_{95\%}$ are determined for the first order system.

$$\frac{T}{T_c}(s) = \frac{a}{s + a} \quad .$$

The three average time constants (in sec) and a (in sec^{-1}) are determined to be:

$$T_{low} : t_{95} = 1.5 \quad a \approx 2.1$$

$$T_{med} : t_{95} = 2.3 \quad a \approx 1.3$$

$$T_{all} : t_{95} = 2.0 \quad a \approx 1.5$$

The engine model is not a first order system as is apparent from a more close observation of the step histories. The initial approximation for positive thrust changes is approximately first order. However, the downward thrust steps are oscillatory indicating a second order component. A closer look at the upward data indicate additional order characteristics. To facilitate more careful studies of the engine model, the raw thrust response data is replotted on an enlarged grid to scale up the response curves (Figures IX-2 to IX-5).

The thrust history data is scaled up to make the unique response characteristics more apparent. An enlarged grid of the same structure of the raw data form is chosen. Data points are taken carefully from

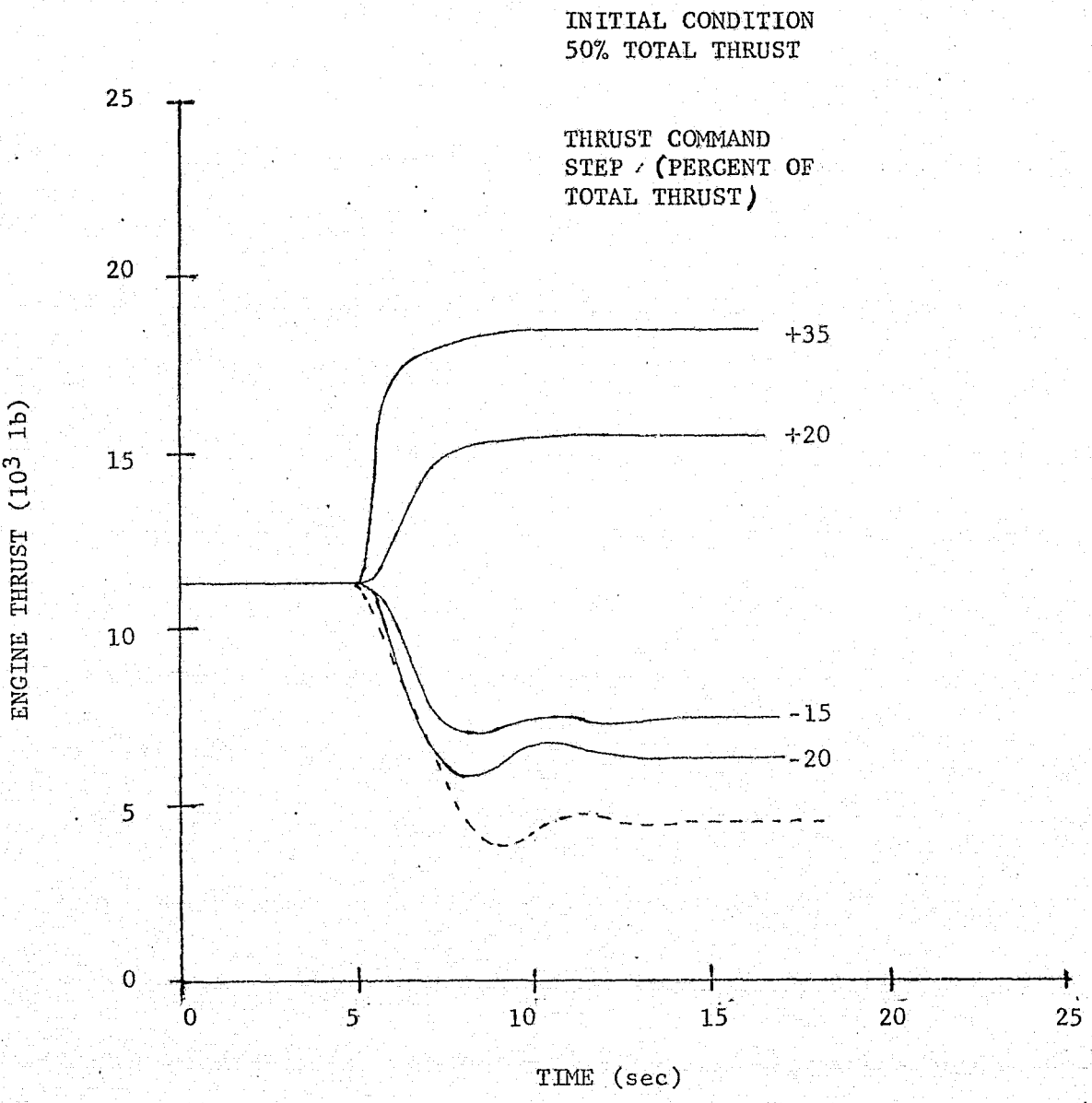

FIGURE IX-2 ENGINE THRUST
RESPONSE HISTORIES

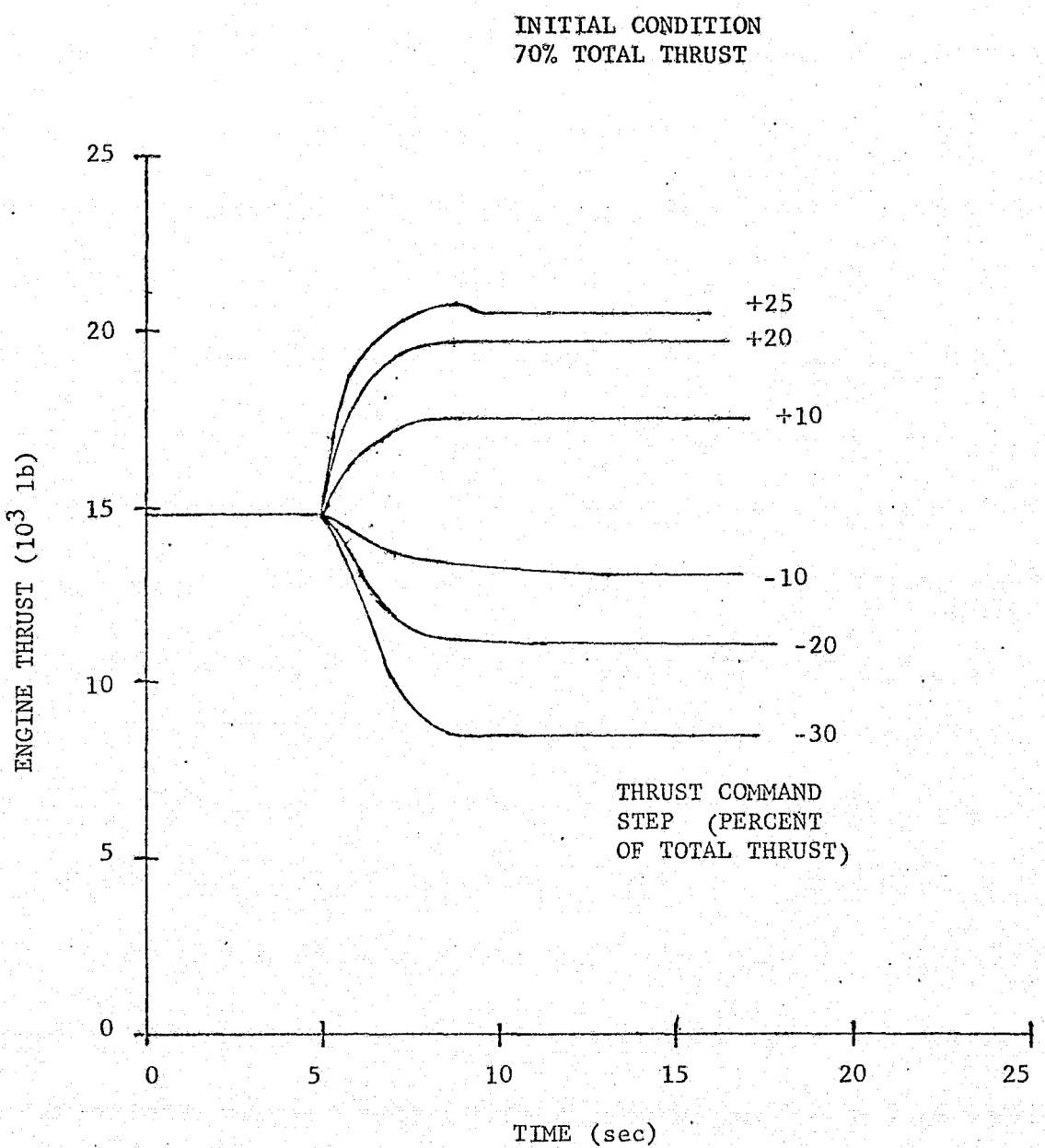

FIGURE IX-3 ENGINE THRUST
FEEDBACK HISTORIES

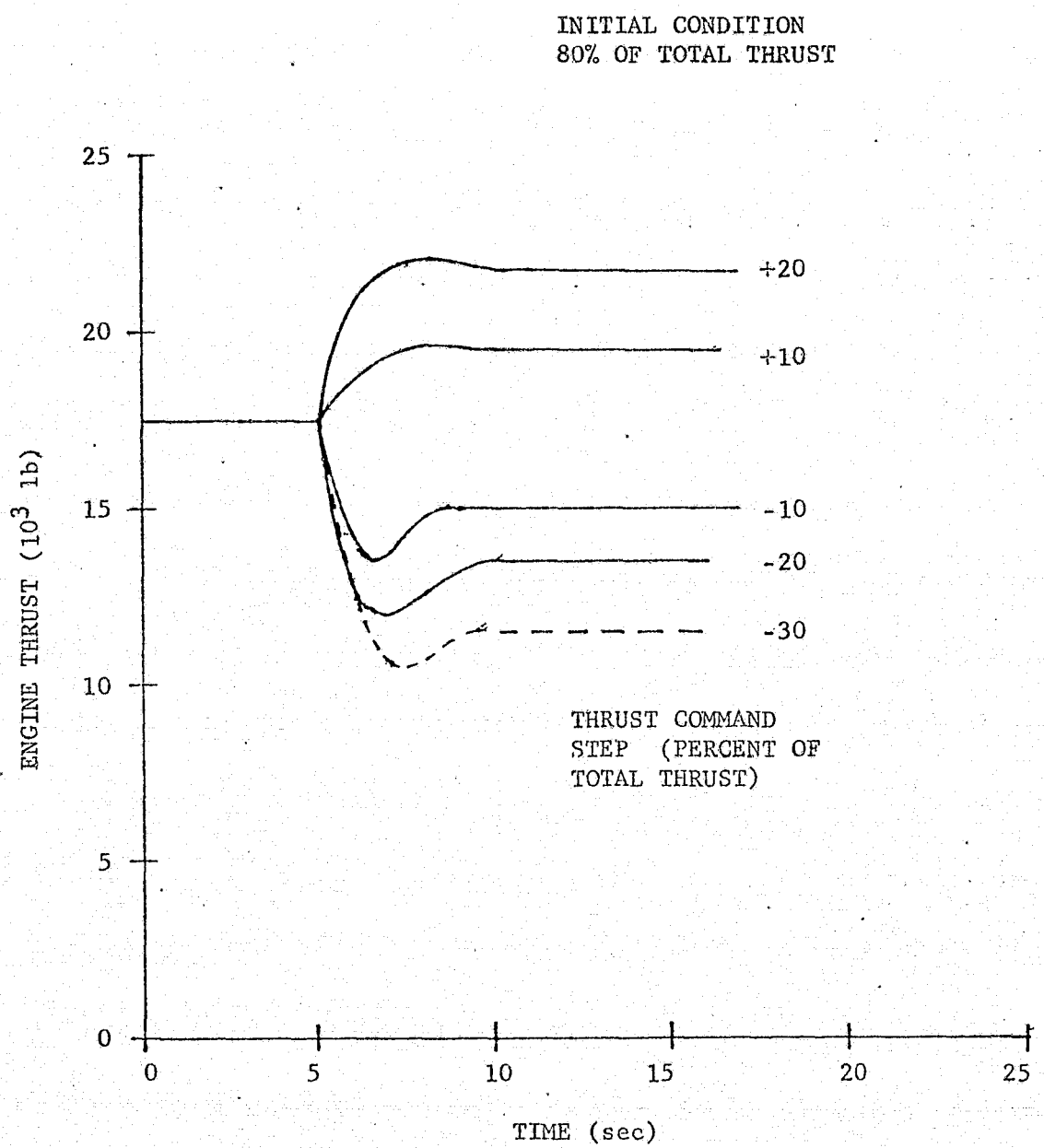

FIGURE IX-4 ENGINE THRUST
RESPONSE HISTORIES

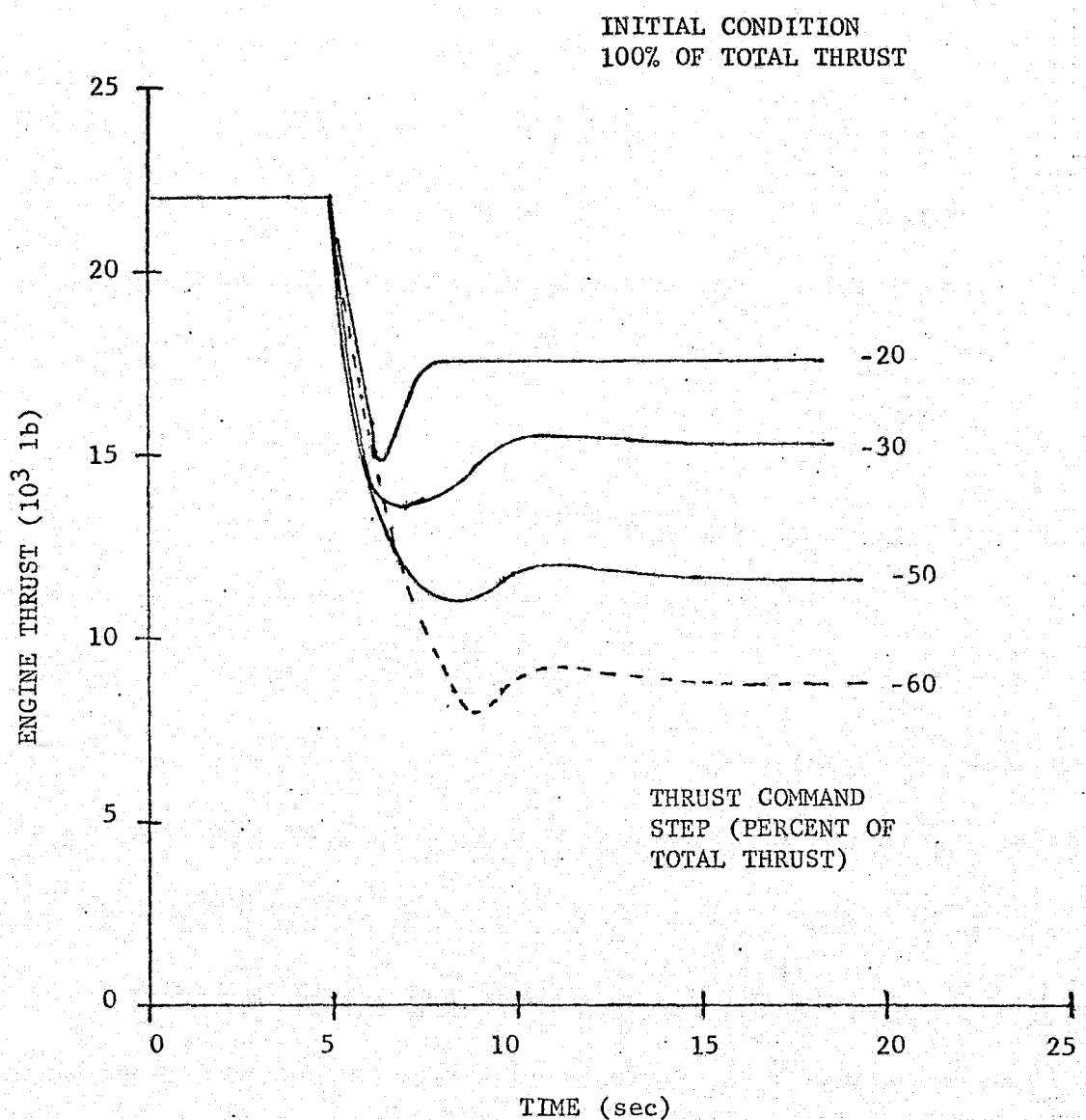

FIGURE IX-5 ENGINE THRUST
RESPONSE HISTORIES

easily identifiable points of the individual time histories and faired with the aid of a french curve. The resulting thrust time histories are presented on Figures IX-2, IX-3, IX-4 and IX-5 for initial thrust levels of 50, 70, 80 and 100 percent.

The engine thrust response is more complex than the initial first order approximation. The downward thrust steps are damped oscillatory responses. The upward steps demonstrate the influence of higher order poles, also. One particular observation of the low thrust (50 percent) condition is an apparent time lag in responding to step inputs; which increases as the step command is reduced (Figure IX-2). The low thrust upward steps also demonstrate a slow first order pole, other than the initial time lag, influencing the last portion of the rise to final thrust level. These effects change to an apparently well damped oscillatory influence at the 70 percent and 80 percent thrust levels where upon an oscillatory overshoot appears to increase with increased step input (Figures IV-3 and IX-4). The nature of the downward steps vary with initial thrust level, too; demonstrating more damping at the 70 percent thrust level than at either end of the thrust range. The engine plant appears to be a high order system of at least third order with poles sensitive to the initial thrust level and the input step command.

The influence of the engine model response variation with command inputs is an area of research not included in this work. The premise of designing the control without consideration of the unique engine thrust responses has been done with consideration of this model uncer-

tainty. The dominant first order response about the nominal approach conditions provides poles in the region of 2.1 to 1.5 on the s-plane real axis. The control analysis is done with this in mind by attempting to keep the closed loop response poles out of this region of influence, and by weighting engine control heavily so the closed loop response is not heavily dependent upon engine response. The success of this approach is evaluated against the first order engine model by simulation analysis.

The influence of additional slow engine response poles (not investigated in this research) is an interesting topic for further studies. The effects of the upward thrust response poles is not expected to be dominant under nominal approach conditions or conditions requiring higher thrust levels. Although the 60 percent thrust data is not available, it is expected that the lagging response is a low thrust phenomena since the 70 percent and higher thrust conditions do not exhibit any lag. However, the amount of lagging influence must yet be determined at the nominal approach condition. This lag was not considered in establishing the first order estimate of the engine model. Recomputing the first order time constant more carefully using the re-plotted thrust histories provides a value of 0.91 when averaging the rise times to 63 percent of the step command of the 50 and 70 percent initial thrust data (Figure IX-2 and IX-3). The following values are determined to compute the average first order coefficient value:

INITIAL THRUST LEVEL					
50%			70%		
STEP CHANGE OF TOTAL THRUST (percent)	RISE TIME $t_{63\%}$ (sec)	FIRST ORDER COEFFICIENT a (sec^{-1})	STEP CHANGE OF TOTAL THRUST (percent)	RISE TIME $t_{63\%}$ (sec)	FIRST ORDER COEFFICIENT a (sec^{-1})
+35	0.6	1.66	+25	0.6	1.66
+20	1.7	0.59	+20	0.8	1.25
-20	1.5	0.66	+10	1.0	1.0
-15	1.3	0.76	-10	1.75	0.57
-30	1.75	0.57	-20	1.5	0.66
			-30	1.7	0.58

The inclusion of the apparent lag slows the estimated engine response down into the airframe dynamic region on the s-plane. It is expected that the results would differ in view of the sensitivity of the airframe poles.

The control laws will generally command thrust decreases as well as increases in setting from a disturbance input. It is hoped (to be shown by simulation) the relaxation of control dependence upon thrust commands eliminates the overshoot of thrust command sufficiently to eliminate the oscillatory thrust response influence upon the system. It is possible that more efficient and fast responses could be obtained by including these effects into a control solution. Researching the control possibilities with a non-linear or more complex linear engine model including a detailed estimation of the engine's expected response is recommended for further development of a sink rate control system;

beginning with a third order identification study of the engine data and proceeding to control laws with an eight state dynamic model.

X. SIMULATION STUDY

10.1 INTRODUCTION

The premise of this control system analysis is tested by simulation with a linear model. The assumption was made at the outset of this study to ignore the engine interaction with the aircraft plant in developing control laws (as explained in Section 1.1). The dominant engine response, under nominal conditions, lies near the plant closed loop poles; and, as indicated in Chapter IX, may, in some cases, respond slightly slower than some of the fast short period closed loop responses. This assumption is tested by evaluating the performance of several of the control system candidates with the first order engine model developed in Section IX for this study. The simulation approach provides an additional result; in that the relative efficiency and actual sink rate performance is demonstrated so as to be compared with the s-plane analysis inferences. In this manner, the analyses performed to define the control laws are compared.

10.2 LINEAR SIMULATION MODEL

Linear model simulation is chosen to be adequate. The linear aircraft plant model is readily available as it is defined to perform the control law synthesis. The linear dynamic model is defined about the nominal approach path. Therefore, perturbations due to the response to an engine failure in the presence of a successful control law are expected to be within the linear approximate constraints (approximately 10 percent of the nominal conditions). Furthermore, the linear model is

readily available; ince it was defined for the control synthesis analysis; and its transformation to a time simulation is straightforward. The linear approach does not require the introduction of additional sophistication integration schemes.

The linear simulation model is produced by adjoining a first order engine model to the plant dynamics matrices and developing a state transition matrix solution for a fixted time step. The time step is chosen considering discrete information theory constraints upon sinusoidal time histories. The closed loop aircraft and engine dynamics have responses within approximately 5 rad/sec and for the most part within the engine response of 2 rad/sec (cf Chapters VI - IX). The selection of a time step of 0.1 sec results in 12 to 30 samples per cycle for frequencies of s to 2 rad/sec respectively. This is within the requirements of discrete systems theory (4-15 samples/cycle as discussed in reference F-1).

The linear transition matrices are defined from the state dynamics equations:

$$\dot{\underline{x}} = Fx + G_1\underline{u}_1 + G_2\underline{u}_2$$

where:

$\underline{u}_1$ = control input

$\underline{u}_2$ = disturbance input (engine thrust)

The engine failure dusturbance is modeled by superposition, applying a step input of negative thrust (cj) to simulate an engine failure. The plant

nominal approach model is applied since the nominal path is to be maintained and as such all deviations are perturbations. The transition matrix is defined by:

$$\underline{x}_{n+1} = \Phi \underline{x}_n + \Gamma_1 \underline{u}_{1n} = \Gamma_2 \underline{u}_{2n}$$

where:

$$\Phi = e^{-Ft}$$

$$\Gamma_i = \int_0^T e^{-F\gamma} d\gamma \quad G_i$$

T = time integration step (0.1 sec).

The transition matrices are defined by series approximation (as described in Reference F-1):

$$\Phi = I + FT + \frac{F^2T^2}{2!} + \frac{F^3T^3}{3!} + \ldots.$$

$$\Gamma_i = \left[IT + \frac{FT^2}{2!} + \frac{F^2T^3}{3!} + \ldots. \right] G_i .$$

An eleventh order series approximation is used. The simulation time histories are computed by a FORTRAN V computer program (a listing is included in Appendix D).

10.3 SELECTED CONTROL LAW CASES FOR SIMULATION

The control laws that are selected for computer simulation include: the approximate analyses results; the full state optimal solutions; an optimal solution, with $A_{ww} = 0$; and the four state control solutions (summarized on Table IX-1). The particular cases are numbered in associa-

TABLE X-1

CONTROL LAW SUMMARY

(Units are consistent ratios of the state vector $\underline{x}$ in ft, sec, and rad and the control vector $\underline{u}$ in deg)

Approximate Analyses (VI)

(VI-1) "Optimal" Case:

$$C = \begin{bmatrix} 0.175 & 0.000 & 0.000 & 13.762 & 0.013 \\ 0.000 & 0.000 & 40.000 & 0.000 & 0.000 \\ 3.186 & 0.000 & 0.000 & 105.260 & 0.000 \end{bmatrix}$$

(VI-2) Revised Phugoid Damping Case:

$$C = \begin{bmatrix} -0.058 & 0.000 & 0.000 & 3.895 & 0.0173 \\ 0.000 & 0.000 & 40.000 & 0.000 & 0.000 \\ 0.4946 & 0.000 & 0.000 & 119.900 & 0.000 \end{bmatrix}$$

Optimal Solutions (5 State Model) (VII)

(VII-1) Cost Weights Directly From Approximate Analysis:

$$C = \begin{bmatrix} -0.012 & 0.0079 & -0.0641 & 1.292 & -0.0068 \\ 4.523 & -3.244 & 85.241 & -581.320 & -2.100 \\ 3.262 & 1.262 & -45.091 & 203.350 & 1.385 \end{bmatrix}$$

(VII-2) Cost Weights Determined by Review of Approximate Analyses:

$$C = \begin{bmatrix} -0.058 & 0.210 & 8.479 & -1.384 & 0.063 \\ 0.062 & -0.178 & 106.584 & -205.563 & -0.083 \\ 0.225 & 0.167 & -50.252 & 115.130 & 0.057 \end{bmatrix}$$

(VII-3) Weights Determined by Bryson's Rule:

$$C = \begin{bmatrix} -0.039 & 0.024 & -0.080 & 4.128 & 0.017 \\ 1.093 & -0.519 & 109.510 & -218.710 & -0.483 \\ 1.607 & 0.272 & -54.470 & 109.770 & 0.274 \end{bmatrix}$$

(VII-4) Bryson's Rule Weights With $A_{ww} = 0$.

$$C = \begin{bmatrix} -0.035 & 0.022 & -0.142 & 3.689 & 0.016 \\ 1.212 & -0.979 & 99.784 & -241.749 & -0.520 \\ 1.501 & 0.331 & -53.003 & 114.765 & 0.273 \end{bmatrix}$$

Optimal Solutions (4 State Model) (VIII)

(VIII-1) h Damping Cost Weights With $A_{ww} = 0$.

$$C = \begin{bmatrix} -0.003 & -0.000 & 0.017 & -0.034 \\ -0.794 & -0.194 & 52.410 & -68.860 \\ 2.872 & 0.206 & -39.110 & 86.400 \end{bmatrix}$$

tion to their section reference on Table IX-1 and are referenced to in this section accordingly. The control laws use in the three standard controls dcj, de, and df. The spoiler control is not included; as the results of Section 7.7 indicate that the spoilers are not effective feedback controls in the nominal approach configuration. Each control law is discussed in the order of their development, beginning with the approximate analyses results.

10.4 SIMULATION PRESENTATION FORMAT

The significant simulation results are shown as time histories of the parameters of interest in a common format. This allows ready comparison of one case to another. The parameters are provided in standard aircraft terminology as follows:

AIRCRAFT MOTION	CONTROL INPUT
sink rate - $\dot{H}_o + \dot{h}$ (ft/sec)	thrust coefficient - $cj \equiv \frac{T}{\bar{q}S}$
forward speed - $U_o + u$ (ft/sec)	elevator deflection - $de_o + de$ (deg)
angle of attack - $\alpha \equiv \frac{w}{U_o}$ (deg)	aft flap deflection - df (deg)
pitch angle - θ (deg)	

Two figures are provided for each case; the first includes the aircraft motion history; the second provides the control history. The scales are identical where possible, to facilitate comparisons (scale changes are identified where they occur).

The time history results are output every second providing a summary of the motion. Fine oscillations may not be apparent in the results but none are expected either. This data rate facilitates hand plotting, the method employed in this work.

10.5 APPROXIMATE ANALYSES CONTROL LAWS

The approximate analyses defined two control laws of interest (Table IX-1). The initial analysis effort was an attempt to define an optimal control law using approximate dynamics equations. The result demonstrated that the special separation assumption had been violated. However, the result, though not appropriately predicted by the analysis, was stable with well damped slow mode poles. Since the validity was in doubt a second sub-optimal control law was defined by combining arbitrary pole placement with optimal (Root Square Locus) techniques that did not significantly violate the separation assumption. These two control laws are simulated, the results are shown on Figures X-1, X-2, X-3 and X-4. The two cases are remarkably similar. The first case (VI-1) shows the excellent damping that is identified on the s-plane pole plot (Figure X-1). The revised case (VI-2) is slower than its predesseor (VI-1), but allows a slightly lower peak sink rate, 17.8 as compared with 18.2 fps (Figure X-2). Their control responses are similar also, where the slowness of the second case (VI-2) is apparent from the thrust (cj) and aft flap histories (df) (Figures X-2 and X-4). The control histories show that the sink rate is controlled mainly by the thrust input with an initial aft flap transient motion assisting the response. This re-

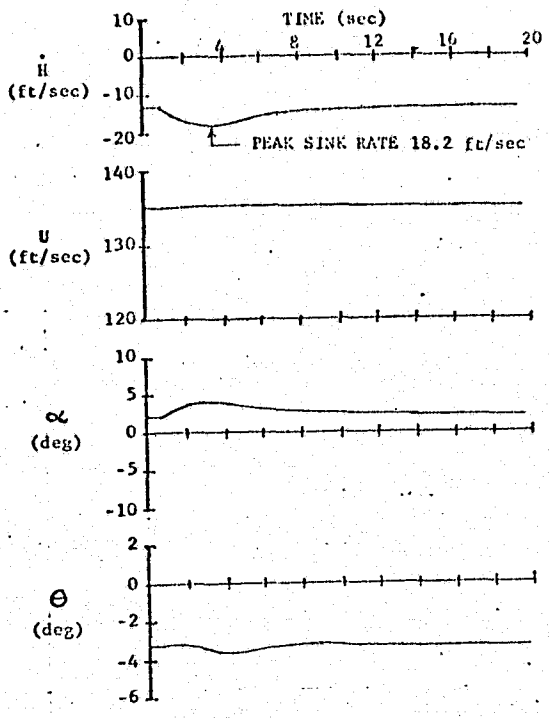

FIGURE X-1 CASE VI-1

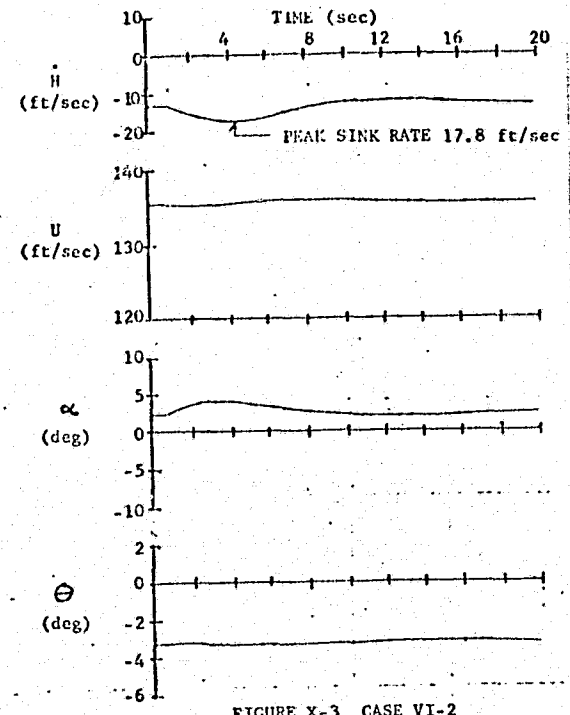

FIGURE X-3 CASE VI-2

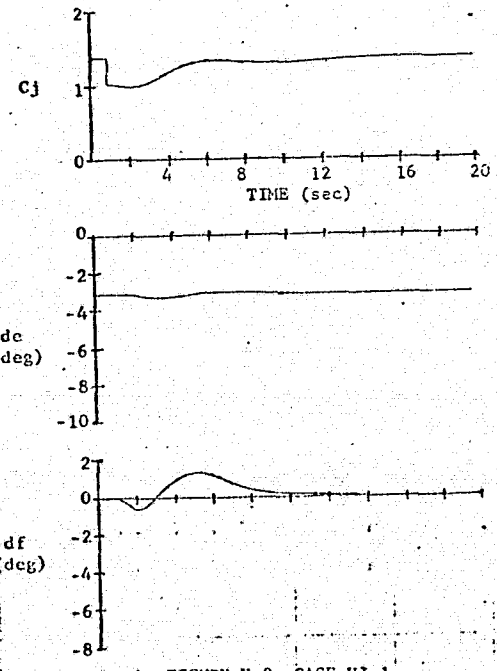

FIGURE X-2 CASE VI-1

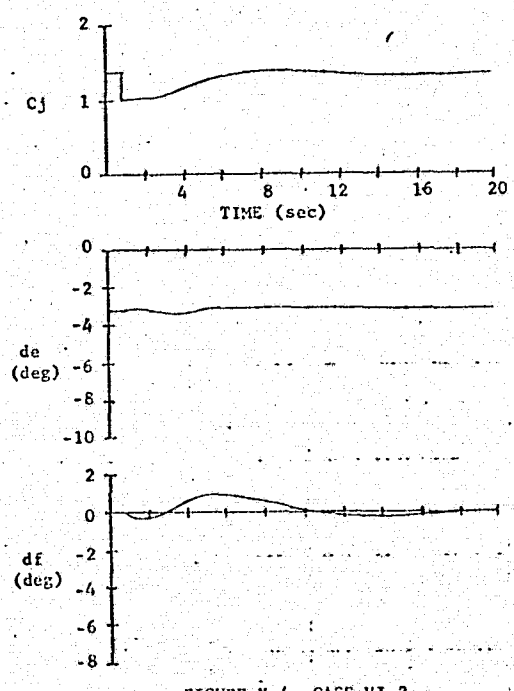

FIGURE X-4 CASE VI-2

sult indicates the response in alleviating sink rate is most likely sensitive to engine response. The engine model, included in this simulation (Chapter IX), reaches 90 percent of a step command in 1.1 sec. Whereas the thrust command asks that the loss in thrust be recovered in about 4 - 7 sec, for these two cases (Figure X-2 and X-4). The engine demands are not critical (which is consistent with the major premise of this study) and may tolerate the band of engine response variance (shown in Chapter IX). Also, the thrust history is, in the main, upward substantiating the engine model assumption of a first order model (Chapter IX). This last observation is true for all the cases presented in this section.

The approximate optimal solution, although it violates one major assumption, provides a more rapid control. This case (VI-1) uses faster control imputs (than the revised case VI-2) to bring the sink rate back to 90 percent of its initial condition in 6 sec; which is during a nominal altitude loss of 92 ft and incurring an additional loss of 22 ft. The sink rate increase is stopped in about 3 - 4 sec or in a vertical travel of about 50 ft. The optimal approach although not productive in identifying the response (cf Section 6.3) does maintain the nature of optimality by its slightly superior response without increased control inputs. These solutions, though approximate, have the advantage of specific feedback channels defined by the engineer resulting in an economy of feedback paths which eliminate (disregard?) unmeasured feedbacks that are not absolutely mandatory. There is no w

feedback, however h is required since it is controlled (Table X-1; cf Chapter VI).

10.6 OPTIMAL CONTROL USING THE FIVE STATE MODEL

The control solutions of Section VII are evaluated with the first order engine model of Section IX. The first two cases are the results of applying the weights derived from the approximate analyses studies. The last four cases are derived from the application of Bryson's rule without benefit of analysis and as such typify design by modern optimal control theory (as discussed in Section VII).

The first two cases, VII-1 and VII-2, are the result of applying, first, the particular cost weights that arise from defining the control case (VI-1) and, second by defining average cost weights with the benefit of the intuitive understanding of all the approximate analyses. Case VII-1 is compared directly with its approximate equivalent (case VI-1). The state time histories are very different (Figure X-5 compared with Figure X-1). The optimal solution has taken the cost definition with the system state information together to produce a control which epitomizes the apparent objective. The cost weights objective of the first analysis is to eliminate excessive thrust inputs, and the optimal solution does! The thrust is not applied in any significant amount, using large amounts of elevator (de) and aft flap (df) (Figure X-6). The result is large angles of attack (10 deg) and a likewise large pitch orientation (5 deg nose upwards). These responses are beyond the limits of the simulation linear model as evidenced by the equilibrium

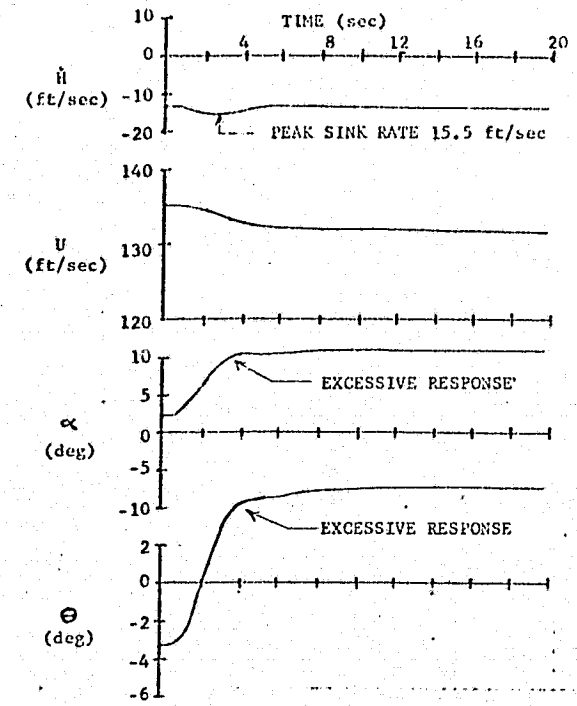

FIGURE X-5 CASE VII-1

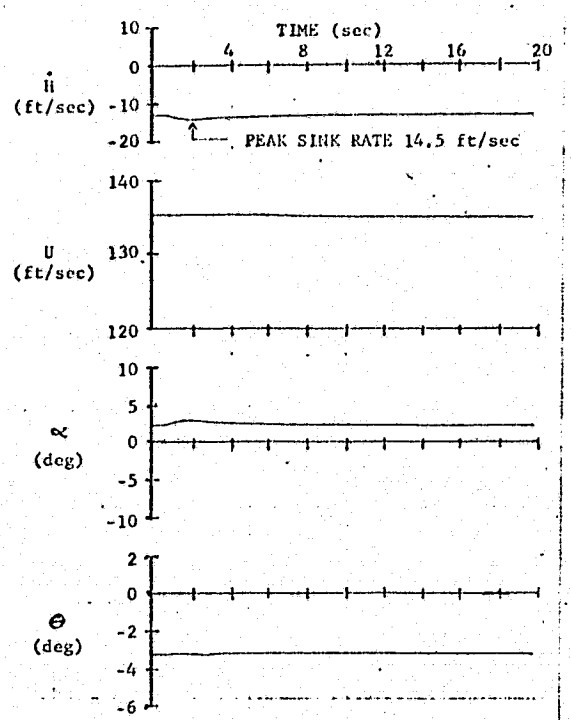

FIGURE X-7 CASE VII-2

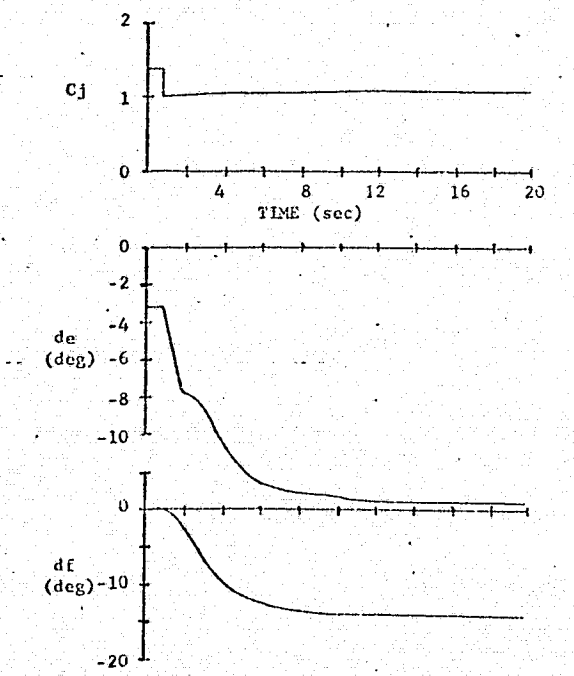

FIGURE X-6 CASE VII-1

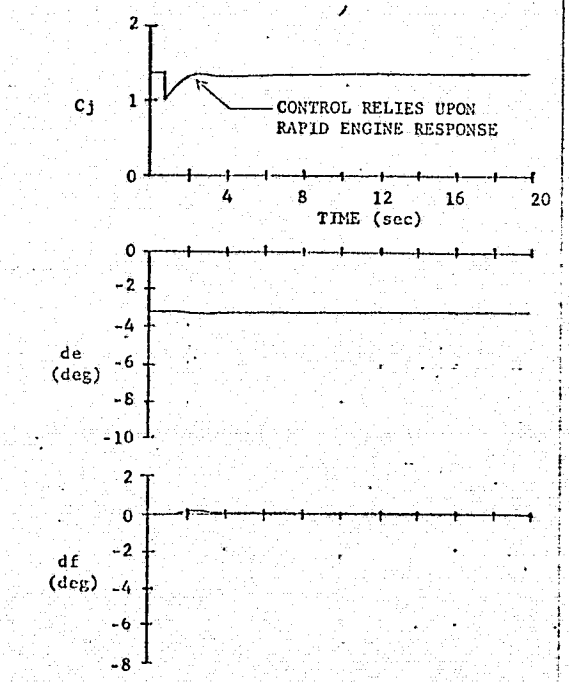

FIGURE X-8 CASE VII-2

performance map of Section 5.2; the condition of 132 ft/sec (78 kt) and 12 deg angle of attack has no equilibrium solution at the thrust level of one engine out (37800 lb). These results are not appropriate linear control solutions since their application violates the linear perturbation assumption of maintaining controls and states near their equilibrium values. However, the initial portion of the time histories remain valid, indicating a possible nonlinear approach to controlling these transients, since the sink rate builds to only 15.5 ft/sec in 2 sec with this saturating control. Immediate application of thrust may, in conjunction with this control law (acting in the presence of saturation), provide a nonlinear control that eliminates sink rate transients. Pursuance of this issue is beyond the scope of this study, instead the intuitively averaged cost function control law is offered.

The time history response to an engine failure using the control law of intuitive cost weights (Case VII-2) is shown to virtually eliminate sink rate transients on Figure X-7 without large control inputs (Figure X-8). The time histories demonstrate a mild transient; a peak sink rate of 14.5 ft/sec, and recovery in about 3 sec (less than 50 ft of altitude is travelled during the transients). This control law responds as the pilot should forcing the thrust back to its appropriate value in about 1.2 sec. These results are sensitive to engine response since the command asks essentially for full replacement of thrust as fast as the engine can provide it.

The results here in this case exemplify the premise that the engine response can be successfully ignored when it is slightly faster than the closed loop plant poles it affects. The pole plot (Figure VII-2) indicates poles on the real axis inside of 2 rad/sec from the origin, and short period poles at about 2.5 rad/sec. The engine response is at 2.1 rad/sec, providing the results on Figure X-7, indicating that the slow mode poles (although moved from their described locations) do not interact detrimentally to the system (i.e. the response does not become oscillatory or unacceptably slow). This case would be an interesting candidate for researching the effects of engine response and higher order modeling as described in Section IX. The next case considered, though, is the case of Bryson's rule optimal solution.

The control laws developed from applications of Bryson's rule (Case VII-3) are a compromise of sorts (the crux of optimal control is to compromise in a least square sense) between the two previous optimal cases (VII-1 and VII-2). The state histories show a mild transient response to the engine failure (Figure X-9) like the approximate solutions case (VI-1 and VI-2) applying thrust elevator and aft flap in quantities that appear to be an average of cases VII-1 and VII-2 control contributions (Figure X-10). The significance of this result is that it is obtained directly by using the expected control response in the cost function weights (Section 7.3), demonstrating that an efficient full state control can be defined from the designers performance requirements without explicit regard to the system characteristics. The optimal control solution utilizes the system characteristics in determining the specified solution.

The results of this case (VII-3) are better than the approximate case (VI-1) providing a peak sink rate of 16.5 ft/sec 2 sec after engine failure (Figure X-9). The recovery, however, is slower reaching 15 ft/sec in 3 sec and recovering to 13 ft/sec in about 9 sec. This is accomplished with 5 deg angle of attack and a pitch up to less than 1 deg nose down. The control demands are significant using 6 deg of elevator and 4 deg of aft flap extension (Figure X-10). This control law is the basis for further investigations concerning eliminating the feedback paths (discussed in Section 7.6). The cases leading to eliminating w feedback are discussed.

The analysis of Section 7.6 proceeds through three steps of state feedback elimination to remove first w feedback and then h feedback. The objective is to investigate control laws that do not require additional states beyond those provided to the standard stability augmentation system (eg u, g, and θ). The basis for these attempts is case VII-4 (Table X-1) developed in Section 7.6 by setting cost weight A_{ww} to zero. The resulting control law is applied to obtain the time histories on Figure X-11 and X-12. The results are similar to the earlier case but using slightly more control deflection (Figure X-12) to obtain slightly more angle of attack and pitch angle causing an improvement in sink rate response by recovering in 7 sec rather than 9 sec (Figure X-11); an improvement lost by removing the w feedback. The above control case is modified to eliminate w feedback, the results of which are shown on Figures X-13 and X-14. These results are similar to the two previous

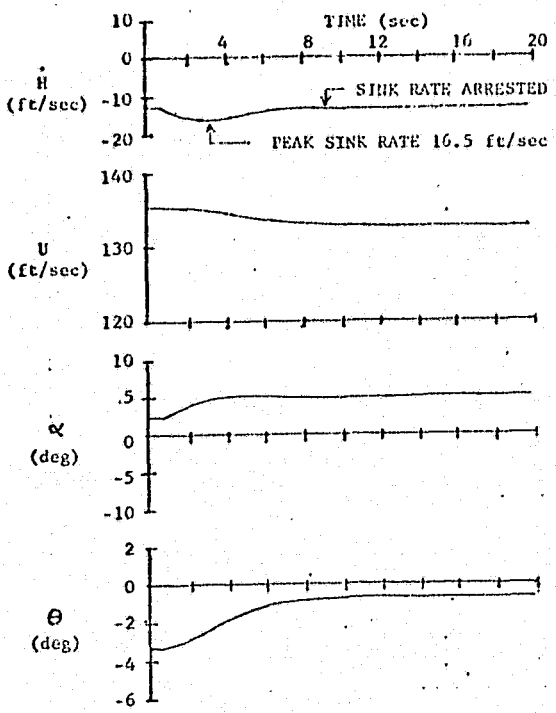

FIGURE X-9 CASE VII-3

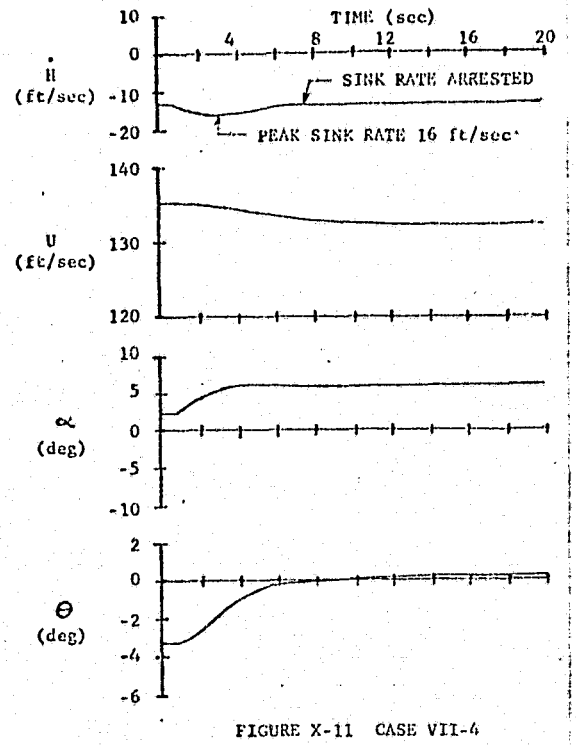

FIGURE X-11 CASE VII-4

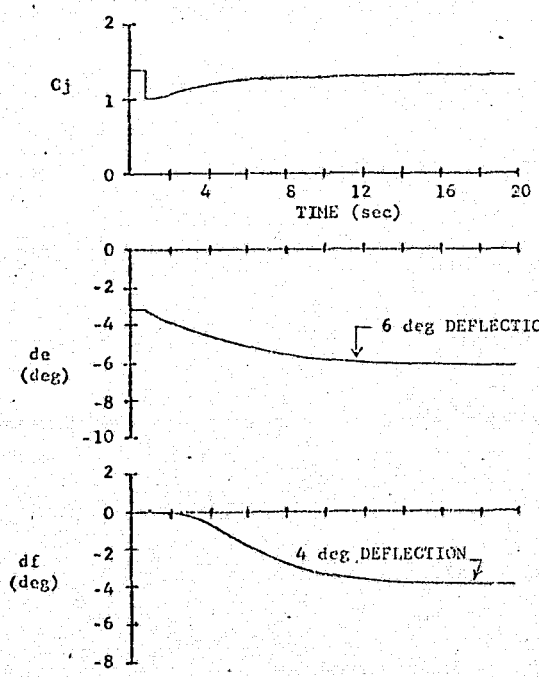

FIGURE X-10 CASE VII-3

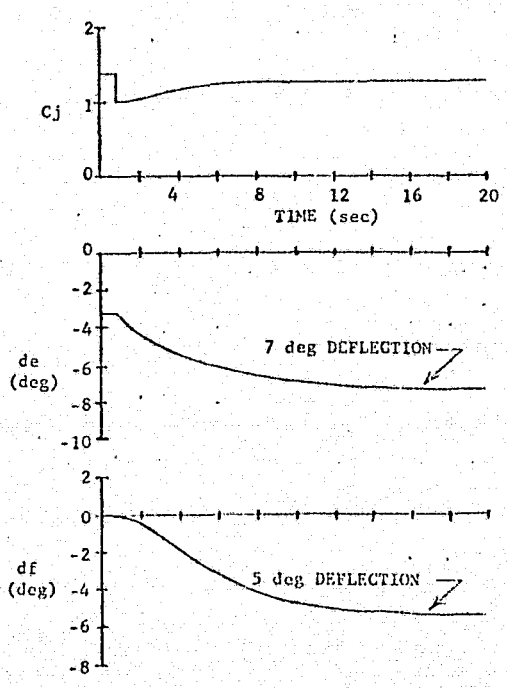

FIGURE X-12 CASE VII-4

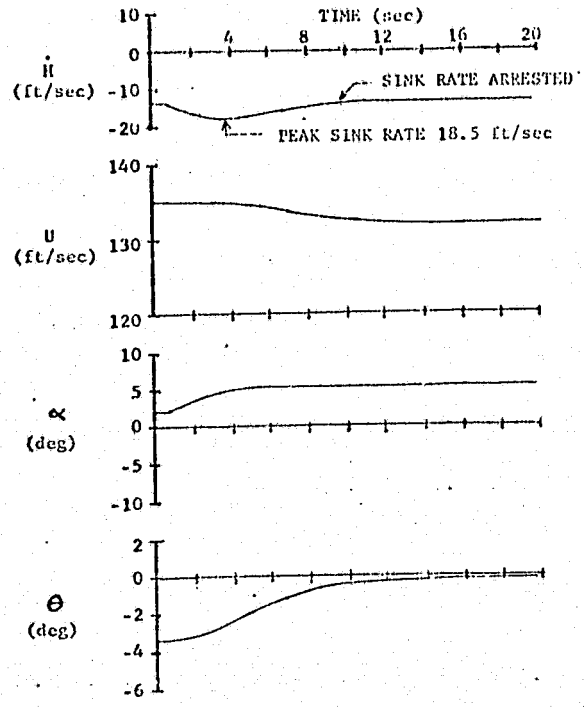

FIGURE X-13 MODIFIED, CASE VII-4
(G_W = 0)

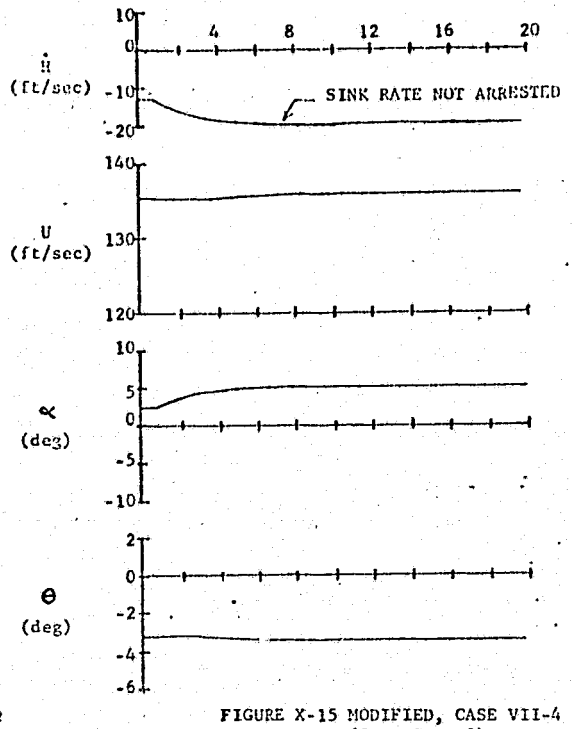

FIGURE X-15 MODIFIED, CASE VII-4
(G_W = G_h = 0)

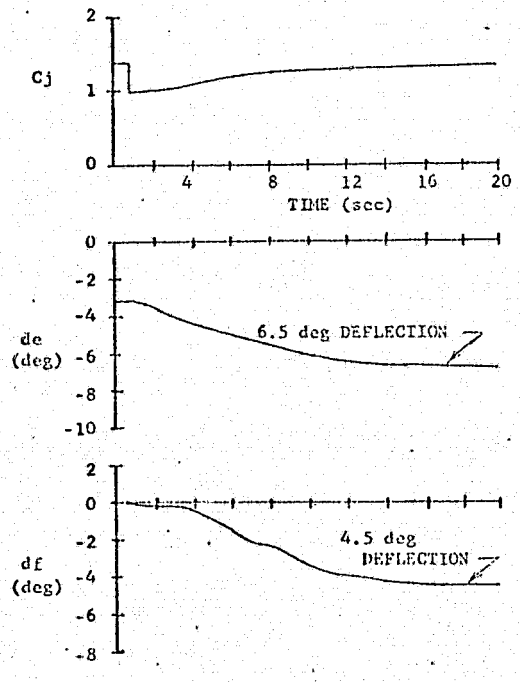

FIGURE X-14 MODIFIED, CASE VII-4
(G_W = 0)

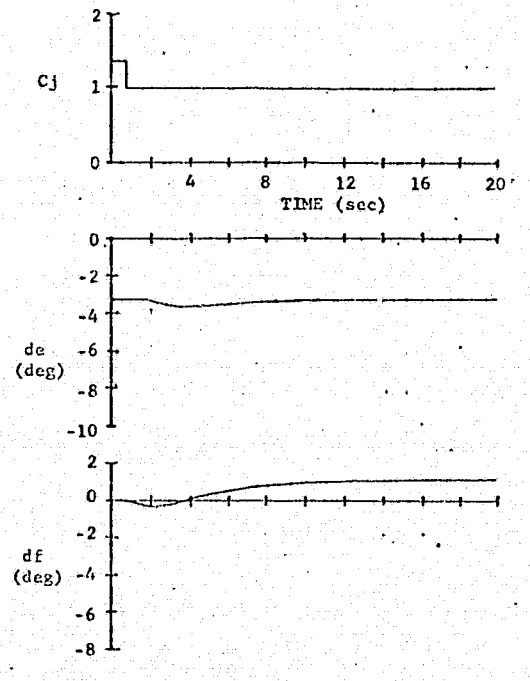

FIGURE X-16 MODIFIED, CASE VII-4
(G_W = G_h = 0)

cases with responses much as predicted in Section 7.6. The sink rate response is slower reaching a peak of 18.5 fps in 3 seconds and recovering to 90 percent in 8 seconds. These results are also much like the initial approximate cases in sink rate response but not in control response.

The suboptimal control case (with w feedback eliminated) provides a control that transitions to a new thrust trim condition whereas the approximate case maintains the initial condition. The attitude and control histories demonstrate this action (cf Figures X-1, X-2, X-13 and X-14). Case VII-4w (without w) trims up to 5 degrees angle of attack losing about 2 fps (Figure X-13). The initial approximate case (VI-1) drives the aircraft up to 3 degrees angle of attack in two seconds then returns to the initial attitude without changing speed (Figure X-1). The controls are different, too. Case VII-4w uses the moving surface controls to obtain a trim state with slow engine commands (Figure X-14). The approximate case on the other hand commands thrust relatively fast, supporting the transient alleviation with the movable surface (Figure X-2). The last case with its slow engine commands may be insensitive to slower engine response models, and may be the best solution to accommodate such cases. The loss of angle of attack feedback does not seriously degrade the control capability. Next, consider the loss of h feedback.

The consideration of eliminating h feedback is simulated and the resulting state histories are shown on Figures X-15 and X-16. The rationale for such a move is provided in Section 7.6. The objective to eliminate sink rate transients through the closed loop system damping provided by the control. It is apparent from the results that this

attempt at least is not successful. The equlibrium condition with one engine out at the nominal approach speed provide a sink rate of 18.8 fps (Figure 5-3). The steady state result from this case is 19 fps sink rate (Figure X-15)! The possibility that the control can provide damping without measuring h is discussed in Section VIII.

10.7 FOUR STATE VERTICAL DAMPING CONTROL

The results of Section VIII are simulated. The time histories demonstrate that the control provided is insufficient to restrain the aircraft (Figures X-17 and X-19). The problem with each of these cases is the engine is not commanded to increase thrust (a consideration that was overlooked in design due to the attention to transient behavior concepts yet ignoring the regulator nature of OPTSYS solutions!) A response which is obvious from the control law (VIII-1 on Table X-1). An example of how the solution should look is provided.

A four state damping control law was identified during the course of these simulation studies that successfully alleviated sink rate transients. The control law provides vertical damping with the inclusion of thrust response. The control law is similar to case VIII-1 (Table X-1) with larger feedback gains to thrust (cj) being the most significant difference, with corresponding decreases to the other channels:

$$C = \begin{bmatrix} -0.0005 & 0.0537 & 0.0118 & -0.0039 \\ -0.4420 & -0.4606 & 46.4900 & -48.5600 \\ 0.7303 & 0.0010 & -30.1850 & 44.9900 \end{bmatrix}$$

(where units are in ft, sec, rad, and deg).

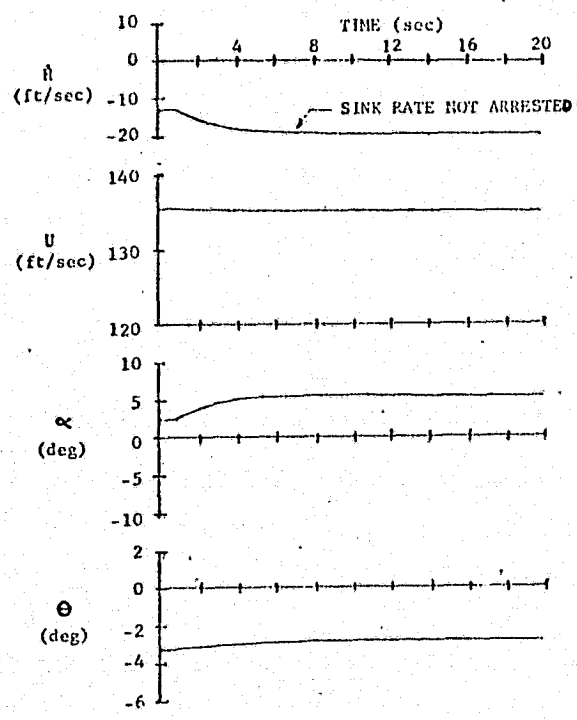

FIGURE X-17 CASE VIII-1

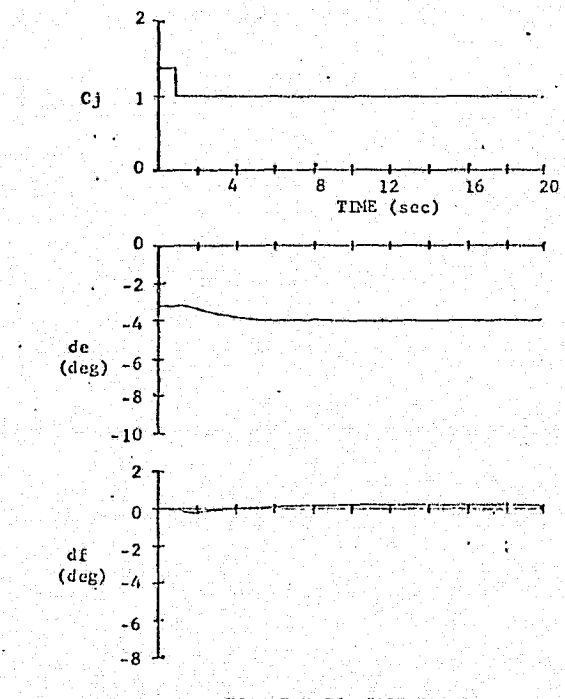

FIGURE X-18 CASE VII-1

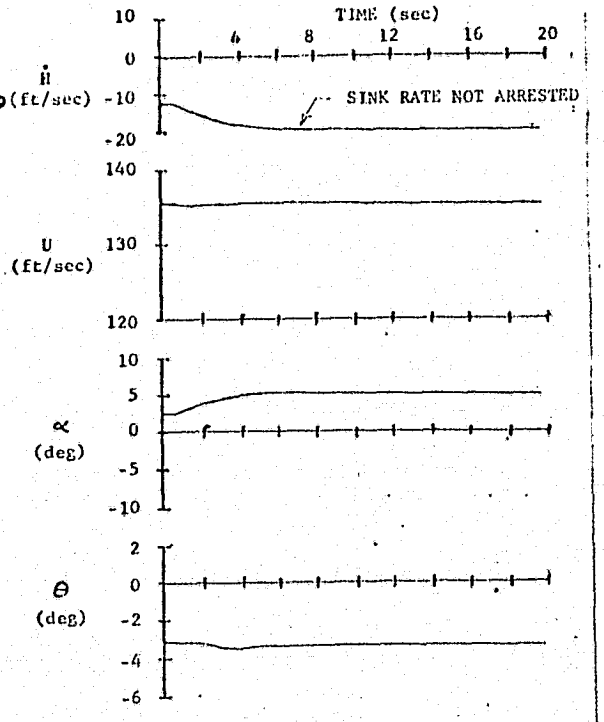

FIGURE X-19 MODIFIED CASE VIII-1 (C_w = 0)

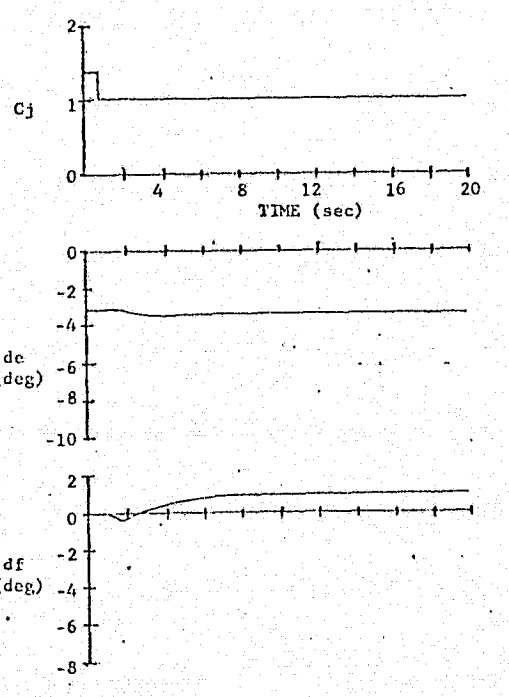

FIGURE X-20 MODIFIED, CASE VIII-1 (C_w = 0)

The aircraft response to an engine failure using this control law shows that sufficient control of the four body motion states (without h feedback) can arrest transient sink rates (Figure X-21). This task is accomplished with minor increases in angle of attack and pitch angle maintaining a nearly constant speed. The sink rate changes from the nominal approach condition of 13.1 ft/sec to a steady condition of approximately 15 ft/sec in 4 sec having passed through a peak of 16 ft/sec at 2 sec after engine failure (Figure X-21). This act is accomplished by commanding the controls as shown on Figure X-22. The elevator and aft flap are commanded with the engine thrust to minimize the sink rate transient.

10.8 SUMMARY

Several control laws are evaluated; their performance demonstrating the relationships of various states to the sink rate motion control problem. The approximate solutions have a common characteristic -- no w feedback. Another case (VII-4) is also evaluated without w feedback. These cases although different in detail provide nearly the same sink rate response, one that is slower than all the other cases that arrested sink rate. It is obvious then that w feedback is required to eliminate sink rate transients, thus requiring an estimator control system which is somewhat more complex (and requires an additional design task for the estimator gains). This analysis indicates the sink rates can be held to 17 ft/sec peaks at 2 - 3 sec after engine failure and recovering in less 10 sec of flight (which corresponds to 22-42 and 141 ft of altitude respectively) without providing w feedback, but including in

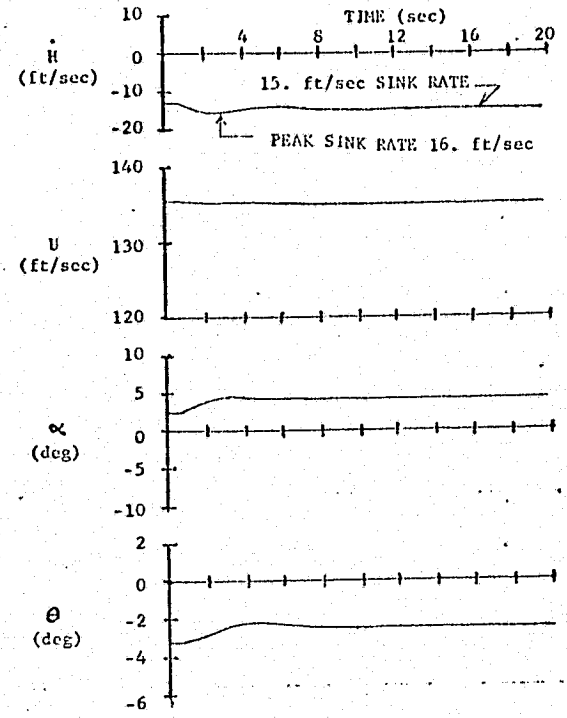

FIGURE X-21 4-STATE CONTROL CASE

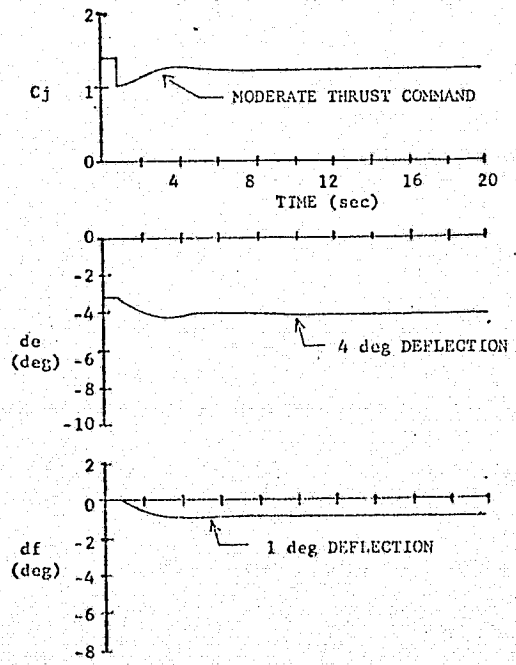

FIGURE X-22 4-STATE CONTROL CASE

every case altitude h state feedback. It is possible that these responses can be made more rapid with further work of the nature discussed in Section 7.6.

The optimal full state feedback cases provide the best responses demonstrating the capability to eliminate sink rate transients, but requiring state estimators or observers for implementation. The possibility exists that the excellent response of case VII-2 may be made poorer with the addition of an observer or estimator providing slower response. Such analysis is required to apply a full state control. The estimator work is left for future efforts, as the focus of this effort is upon control definition.

The issue of eliminating the altitude feedback, the only externally referenced measure considered (eg fixed to another axes system than the aircraft) is demonstrated to be possible, but with w feedback. Attempts to remove the critical w feedback did not result in successful actions (i.e. they did not eliminate sink transients). The vertical damping control is a desirable control approach which requires an angle of attack estimate in order to be applied to the study aircraft.

XI. CONTROL LAW APPLICATION TO AIRCRAFT

11.1 PERTURBATION CONTROL

The control laws developed in the course of this research are perturbation controls requiring care for their implementation to the study aircraft. The differences are apparent from the following two control implementation schematics, the perturbation mode on Figure XI-1, and the actual aircraft description on Figure XI-2. During the analytical analyses a perturbation model is employed which strips the nominal or steady state contributions from the parameters within the aircraft dynamics model. The control laws apply to the error (perturbation) from the nominal or desired conditions. When one seeks to use the resulting control laws, care must be taken to apply only the error portion of each feedback channel to the control law gains. The simplest approach to this problem is to analyze dynamical equations which have only zero steady states, which is impossible with moving aircraft. Furthermore, this study maximizes the non-zero steady state terms by using a nominal approach condition to define the dynamics equations providing V_o, W_o, Θ_o, and H_o states. Measuring devices provide the full values of the state parameters being measured.

The recommended application of the control laws resulting from this research is diagrammed on Figure XI-2. The diagram indicates the states that are provided by measurements already attributed to the study aircraft (see Chapter I). Angle of attack is not provided. The "estimator" provides the function of defining the control variables for the control

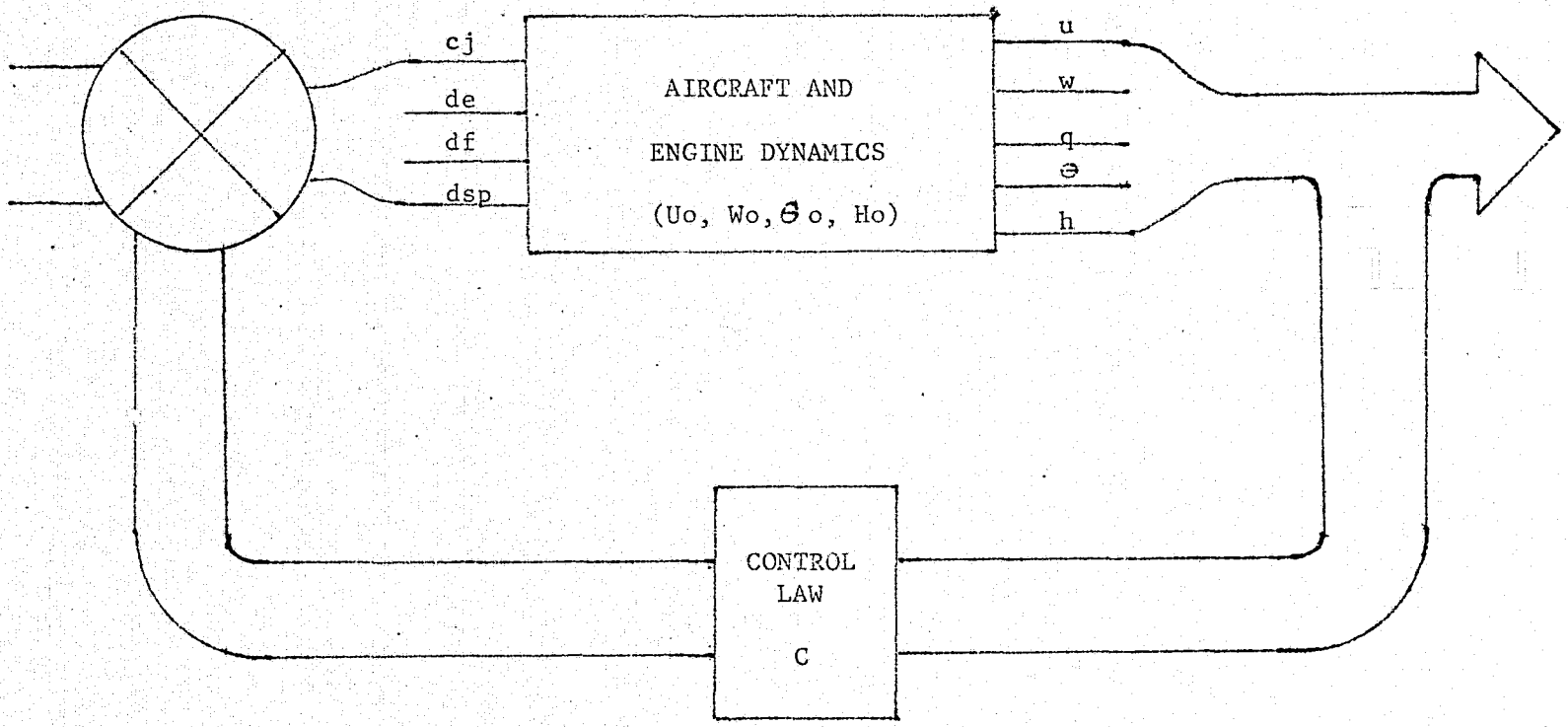

FIGURE XI-1 CONTROL DEVELOPMENT ANALYTICAL MODEL

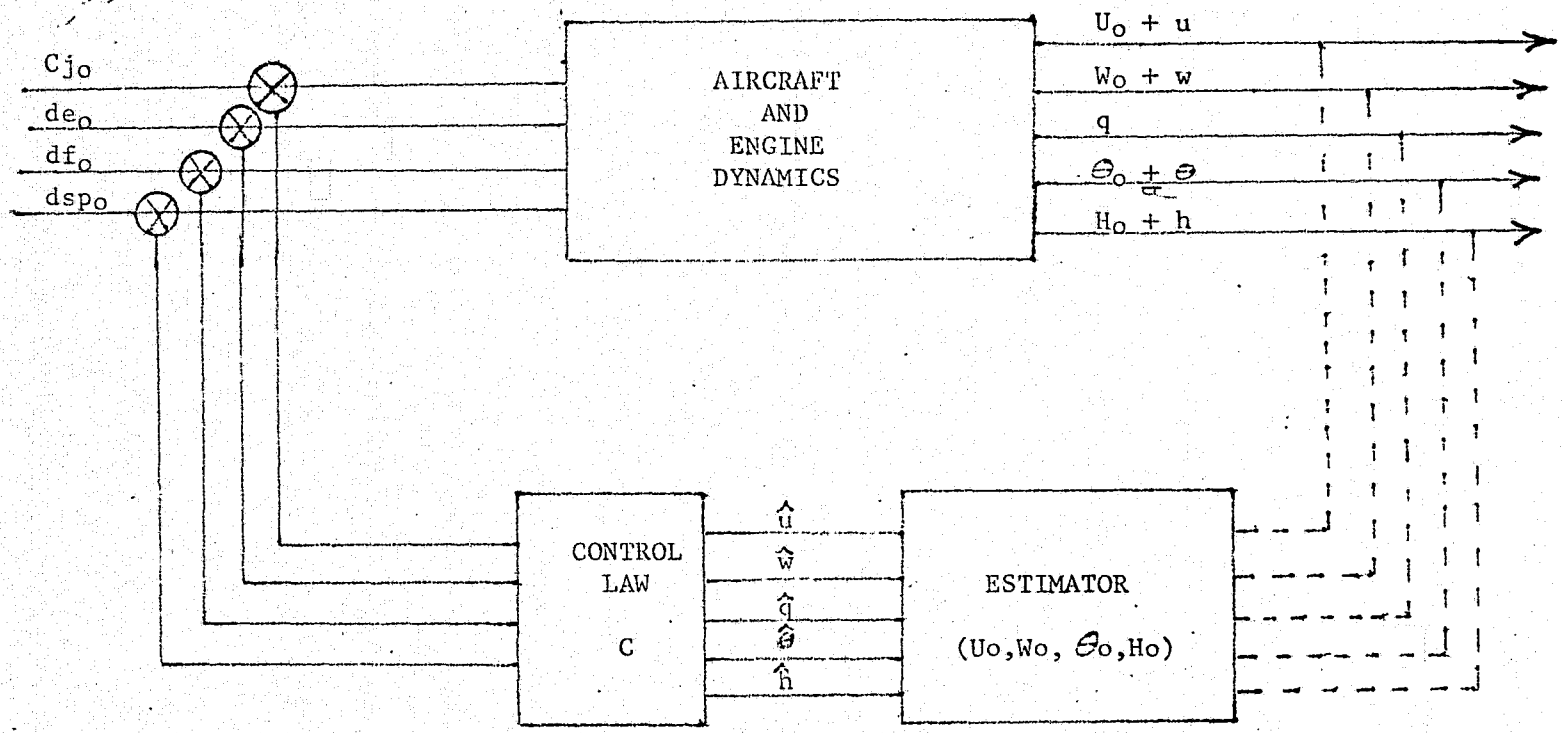

FIGURE XI-2 ACTUAL AIRCRAFT CONTROL LAW EMPLOYMENT

law. The estimator block may contain algorithms ranging from: (a) simply subtracting the measured state data from a preset reference to provide the perturbation state to the control law; to (b) full state estimators with control law feedback and manual input control feed forward paths that may bypass the control law.

The development of estimators for each candidate control law is not accomplished as part of this research. The complete task is left for future work (in addition to several more identified throughout the body of this report). However, one example is described to demonstrate the control application and bring out some of the issues involved.

11.2 EXAMPLE ESTIMATOR DEVELOPMENT

The example applies to the four state damping case discussed in Section 10.7. The four state dynamics matrix is applied so the inputs are in perturbation form requiring that each channel be stripped of the reference values (e.g. subtracted) for input. This is not a significant drawback because, of the measured states u, q and θ, only one has a significant steady component (e.g. u). The q state is zero in steady state. The Θ state is small, -3.2 deg (0.056 rad) and may not severely hamper the system if made zero. However, Θ_o is described here to be subtracted from the measured state. The ramifications of leaving it (Θ_o) zero are left for simulation studies not attempted here.

The estimator is a full steady state Kalman filter for which the OPTSYS computer program provides a stationary solution. The solution is developed and described in detail in Reference B-1. The form of the solution is as follows:

$$\dot{\underline{x}} = F\underline{x} + G_1\underline{u} + G_2\underline{w}$$

$$\underline{y} = H\underline{x} + \underline{v}$$

$$\hat{\underline{x}} = \bar{\underline{x}} + K\,(\underline{y} - H\bar{\underline{x}})$$

$$\underline{u} = C\,\hat{\underline{x}}$$

where:

$\underline{x}$ = the actual state vector

$\hat{\underline{x}}$ = estimated state vector

$\bar{\underline{x}}$ = an intermediate state vector

$\underline{y}$ = measurement vector

$\underline{v}$ = measurement noise (gaussian)

$\underline{w}$ = disturbance vector with gaussian noise

K = filter gain

The filter gain is described in terms of the error equation dynamics as a feedback term:

$$\dot{x} = (F - KH)\,x$$

The OPTSYS program solution utilizes the disturbance noise covariance and the measurement noise covariance in the same manner as the state

cost weights (A) and control cost weights (B) to determine the feedback matrix K in the above error equation. The concern with estimation is that the noise covariances are define terms unlike the designers choice of A's and B's and as such are not freely varied. Also problems exist such as including insufficient measures or defining disturbances that do not excites the plants modes leading to no solutions. These issues are discussed at length in references B-1, B-2 and F-1.

The disturbance covariance is treated in the same manner as the state cost matrix in Bryson's rule application to define an estimator (e.g. a diagonal matrix). Also, the measurement covariance matrix is described to include the measured variables u, q and θ and values chosen that typify their possible measurement precision. The measurement precision. The measurement covariance is chosen as the square of representative one sigma variances in the state measure. The resulting choices are as follows:

State	Disturbance Variance	Measurement	Measurement Variance
u (ft/sec)	100.0 ft^2/sec^2	u (ft/sec)	1.000 ft^2/sec^2
w (ft/sec)	100.0 ft^2/sec^2	q (rad/sec)	0.001 rad^2/sec^2
q (rad/sec)	0.01 rad^2/sec^2	(rad)	0.001 rad^2
θ (rad)	0.01 rad^2		

which provides the error equation response shown by the pole locations of the s-plane on Figure (XI-3). The associated eigenvectors are given

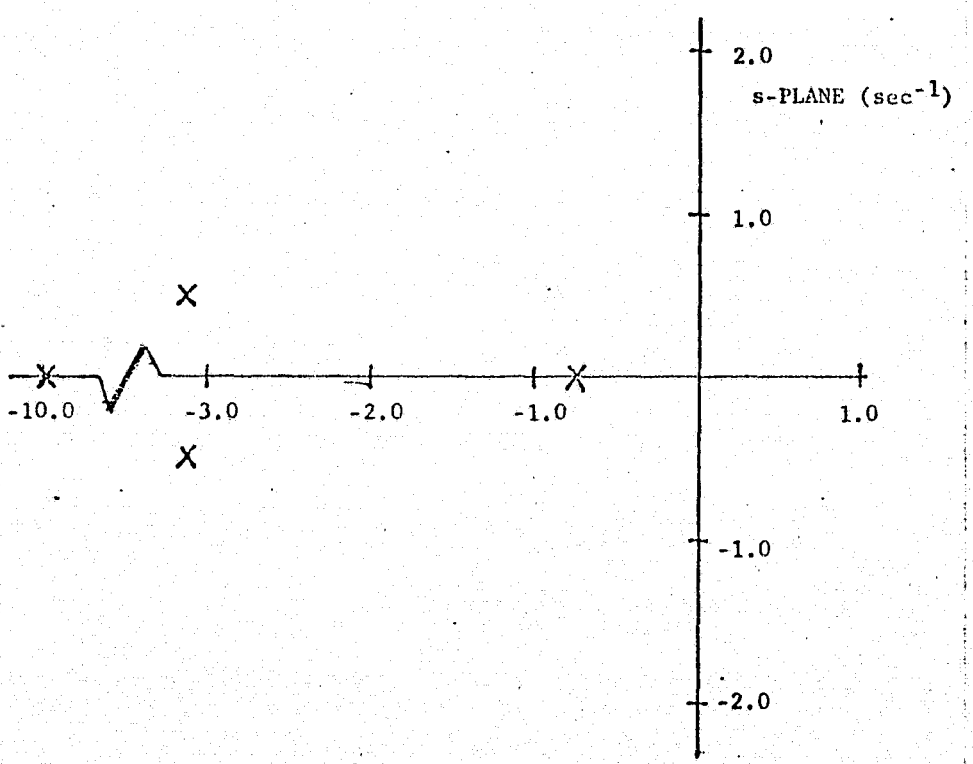

FIGURE XI-3 CLOSED LOOP POLES OF THE FILTER ERROR EQUATION

below:

Eigenvalue (sec^{-1})	Eigenvector (Units in ft, sec & rad consistent with the state vector $[u, w, q, \Theta]^T$)
-3.129 ± j 0.50	0.017 ± j 0.070
	1.000 ± j 0.000
	-0.016 ± j 0.004
	0.001 ± j 0.019
-9.99	-0.997
	-0.080
	0.003
	-0.001
-0.741	-0.010
	-1.000
	0.002
	-0.0004

Most of the poles are beyond the response region of aircraft plant sufficiently far so as not to interfere, except the last one above. It is an angle of attack pole that lies in the slow mode region which will interact with the system. The effects of this interaction may be tolerable. Therefore, it is recommended that such a test be performed in the context of further estimator studies. The filter gain provided from this solution is:

$$K = \begin{bmatrix} 9.988 & -1.967 & 8.064 \\ 0.249 & -33.722 & -9.770 \\ -0.002 & 2.528 & -0.383 \\ 0.008 & -0.378 & 3.250 \end{bmatrix}$$

(Where the units are ft, sec and rad consistent with the associated state vector $\underline{x}$.)

which may be implemented in a simulation.

XII. CONCLUSIONS

Several control laws to alleviate the transient sink rates during an engine failure during approach are defined with varying degrees of control in accordance with varying degrees of complexity. Comparison of analysis by approximate mode decomposition and by the full state variable optimal control, provides understanding of the dynamics and an indication of the limitation of the approximate analysis. These state variable control analysis solutions result in successful alleviation of sink rate transients whereas the classical autopilot did not. The classical autopilot allows peak sink rates up to 22 ft/sec within 4 sec after an engine failure, reaching a steady state sink rate of 18 ft/sec in 8 sec (corresponding to approximately 130 ft of altitude travel). The state variable solutions demonstrate an average response of 17 ft/sec peak sink rate in 2-4 sec, recovering to the initial sink rate in less than 9 sec, with an attendant smaller altitude loss, on the order of 120 ft.

The more complex feedback laws perform better. The approximate solutions and suboptimal solutions (without angle of attack feedback) provide less sink rate alleviation. However, the full state feedback control laws are yet to be analyzed with the limitations of an estimator providing the state feedback, so their performance quotes are tentative.

The full five state feedback cases using the average approximate solution derived weights and using Bryson's rule derived weights control

the sink rate transient to which a 15 ft/sec peak sink rate. The former solution provides the tightest control recovering in 4 sec after engine failure (about 80 ft of altitude) by depending heavily upon engine response. While the solution derived from application of Bryson's rule used slower engine commands to recover in 9 sec (about 100 ft of altitude).

The approximate solutions and the reduced feedback optimal solution (w feedback dropped) allow larger peak sink rates while recovering to the initial sink rate within 8 sec. A peak sink rate near 18 ft/sec occurs in each of these cases, which is less than that of the classical autopilot (22 ft/sec). These solutions are of particular interest because they use the same feedback channels as the classical autopilot with the one addition of altitude feedback.

The possibility of providing sufficient control (within h feedback) in the aircraft to eliminate sink rate transients is demonstrated. However, the successful solution does not develop from an optimal solution, but from an "intuitive gain changing happenstance result" solution! The optimal analysis is not a cure-all. The successful four state case provides good sink rate control without altitude feedback, but unfortunately requiring angle of attack (eg w) information. This case builds up to 16 ft/sec peak sink rate in 2 sec, recovering to a steady state 15 ft/sec sink rate in 4 sec (about 70 ft of altitude).

Throughout this research topics beyond the scope of this work are described for future work that may improve the performance of an actual aircraft control law. The results of this work demonstrate several successful

candidate control laws that may assist the pilot in arresting the engine failure sink rate transient. However, along the way several extensions of this work are identified ranging from; the basic issue of the cost function weight selection relationship to the modal eigenvectors; to, the addition of more complex analyses to test the assumptions and models used in this work. The dominant suggestions that may provide better control are summarized here:

- o Eigenvector constrained optimal control solutions.
- o Nonlinear control studies including verification of linear controls.
- o Engine model extension and integrated linear control analysis.
- o Estimator development to provide unmeasured states and possible engine thrust identification.
- o Integration of the longitudinal control with lateral control requirements.

The optimal control approach to developing control laws for complex systems does not provide a direct association of the modal states to the cost function. A first cut solution to a control problem may yield unacceptable response results; where the desired eigenvalues are determined, but where the desired fast and slow states are mixed in the modal eigenvectors. Additionally, if one could specify the state orientation of the closed loop modal response, then partial state feedback solutions could be more readily defined, without the trial and error methods demonstrated in this study. The need of an understanding of the relationship between the cost function, the closed loop poles, and their associated eigen-

vectors is suggested as fruitful research to reduce the art content of solution iteration.

The topic of nonlinear control schemes, although not included in this research, may provide a better solution. Two possible nonlinear control schemes for future investigation are identified in the course of this work; approach with spoilers; and saturating control. One possible control scheme is to fly the landing approach with the spoilers fully deployed, so they may be retracted upon failure. Linear control laws developed about nominally deployed spoilers did not show significant differences from the nonspoiler cases. However, there may be a synergistic interaction with the other control capabilities due to increased nominal speed of approach with the spoilers deflected, which should be researched. Control saturation is the deflection of the controls to their maximum extent, to arrest the transients. In this case, deflecting the aft flap and elevators so as to immediately arrest the sink rate, while simultaneously commanding an increase in thrust from the remaining engines, to hold the desired steady sink rate. One such possibility is identified within the body of this report, and should be analyzed further to prove its worth.

The engine; although represented in this work by its dominant positive thrust step response, as a first order system; appears to be more closely identified as a third order system with coefficients dependent upon the initial thrust, the size of thrust change command, and the direction of that command. The possibilities of better sink rate

control utilizing a nonlinear or more complex linear engine model integrated with the aircraft motion states should be researched as further development of a sink rate control system. It is recommended that such work begin with a third order identification study of the engine data, and proceeding to control law development with an eight-state dynamic model.

The optimal full state feedback cases provide the best responses to eliminating sink rate transients, but requiring state estimators to provide the unmeasured states for implementation. The possibility exists that their excellent responses may be constrained by slowly responding estimators. Additionally, estimators may provide an acceptable engine thrust failure identification, for nonlinear control application.

The scope of this study is limited to the longitudinal control problems associated with an engine failure. An engine failure requires asymetric laterial directional trim compensation that may detrimentally affect the sink rate problem. It is recognized that these aspects will be included in the future evaluation of an acceptable control solution. However, the possibilities of dominant interactions exhancing the control or estimator capabilities should also be researched.

APPENDIX A

DERIVATION OF THE PLANT EQUATION'S OF MOTION

The following is a derivation of equations of motion used in the S.T.O.L. engine failure during approach study in state variable form:

$$\dot{\underline{x}} = F\underline{x} + G\underline{u}$$

The study is limited to longitudinal flight (e.g. Translations in x and z body axes and rotation about the y body axes.).

From Newton's Law:

$$\underline{F} = m\underline{a} = m\dot{\underline{V}}$$

where

$$\underline{V} = \begin{bmatrix} U + u \\ W + w \end{bmatrix} = \begin{bmatrix} \dot{x} \\ \dot{z} \end{bmatrix}$$

differentiating

$$v = \begin{bmatrix} \dot{u} \\ \dot{w} \end{bmatrix} + \begin{bmatrix} q \end{bmatrix} \times \begin{bmatrix} U \\ W \end{bmatrix} = \begin{bmatrix} \dot{u} + qW \\ \dot{w} - qU \end{bmatrix}$$

where

$q =$, pitch rate.

The rotation is governed by

$$M = Iyy\ \dot{q}.$$

Expanding the forces and moments about a nominal approach condition in a Taylor's series provides the state variable form of the equation of motion:

$$m\,(\dot{u} + qw) = X = X_o + X_u\Big|_{uo} u + X_w\Big|_{wo} w + X_q\Big|_{qo} q + X_{controls}$$

$$m\,(\dot{w} - qu) = Z = Z_o + Z_u\Big|_{uo} u + Z_w\Big|_{wo} w + Z_q\Big|_{qo} q + Z_{controls}$$

$$Iyy\,\dot{q} = M = M_o + M_u\Big|_{uo} u + M_w\Big|_{wo} w + M_q\Big|_{qo} q + M_{controls}$$

Reorganizing the last equations so the derivatives appear on the left of the equation, alone and removing the equilibrium conditions results on the following perturbation equations:

$$\begin{bmatrix} \dot{u} \\ \dot{w} \\ \dot{q} \end{bmatrix} = \begin{bmatrix} X_u & X_w & X_q - W & 0 \\ Z_u & Z_w & Z_q - V & 0 \\ M_u & M_w & M_q & 0 \\ 0 & 0 & -1 & 0 \end{bmatrix} \begin{bmatrix} u \\ w \\ q \end{bmatrix} + \begin{bmatrix} X_{cj} & X_{de} & X_{df} & X_{dsp} \\ Z_{cj} & Z_{de} & Z_{df} & Z_{dsp} \\ M_{cj} & M_{de} & M_{df} & 0 \\ 0 & 0 & 0 & 0 \end{bmatrix} \begin{bmatrix} dcj \\ de \\ df \\ dsp \end{bmatrix}$$

where the mass and moment of inertial terms are incorporated into the dimensional derivatives.

The principal interest of this study is in the altitude loss due to major perturbations in engine thrust. The altitude relationship is defined in the study coordinates:

$$\dot{h} = W \cos\theta + V \sin\theta \ .$$

Expanding about perturbations

$$\dot{H}_o + \dot{h} = (W_o + w) \cos(\theta_o + \theta) + (U_o + u) \sin(\theta_o + \theta)$$

$$H_o + \dot{h} = (W_o + w)\ (\cos\theta_o \cos\theta - \sin\theta_o \sin\theta)$$
$$+ (U_o + u)\ (\sin\theta_o \cos\theta + \cos\theta_o \sin\theta)$$

since $\theta << 1$

$$H_o + \dot{h} = (W_o + w)\ (\cos\theta_o - \theta\sin\theta_o) + (U_o + u)\ (\sin\theta_o + \theta\cos\theta_o)$$

The aircraft attitude rarely exceeds 10 degrees during approach so $\theta_o < 1$ is also true

$$\dot{H}_o + \dot{h} = (W_o + w)\ (1 - \theta \cdot \theta_o) + (U_o + u)\ (\theta_o + \theta).$$

The perturbation equation is:

$$\dot{h} = w + U_o \theta$$

since, $u \cdot \theta_o$ is second order small like $\theta \cdot \theta_o$. This equation is adjoined with the above equations of motion to form the equations of motion for this study.

APPENDIX B

DIMENSIONAL AERODYNAMIC DERIVATIVES

The dimensional derivatives aerodynamic contributions are developed. The aerodynamic coefficients include the effects of thrust on lift, drag and moments:

$$cj \equiv \frac{T}{\bar{q}s}$$

$$F_a\ (\alpha,\ d_f,\ c_j)\ \bar{q}S$$

$$M_a\ (\alpha,\ d_f,\ c_j)\ \bar{q}S\bar{c}$$

$$\alpha \equiv \tan^{-1}\left(\frac{w}{u}\right)$$

The forces are to be expressed as a Taylor series approximately (1st order) in the variables of motion about the trim condition:

$$X = -\ D \cos\alpha + L \sin\alpha$$

$$Z = -\ L \cos\alpha - D \sin\alpha$$

$$M = M_y$$

First consider the prime aerodynamics (e.g. controls = 0):

$$D = C_D\ (\alpha,\ c_j,\ d_f)\ \tfrac{1}{2}\ \rho\ V^2\ S$$

$$L = C_L\ (\alpha,\ c_j,\ d_f)\ \tfrac{1}{2}\ \rho\ V^2\ S$$

$$M_y = C_m\ (\alpha,\ c_j,\ d_f)\ \tfrac{1}{2}\ \rho\ V^2\ S\bar{c}$$

where

$$V^2 = U^2 + W^2$$

$$= (U_o + u)^2 + w^2$$

$$= U_o^2 + 2U_o u + u^2 + w^2$$

$$= U_o^2 + 2U_o u \quad \text{(to first order with } W_o = 0)$$

Since the thrust is included in aero coefficients, the appropriate variables of expansion are:

$$u,\ w,\ c_j,\ q, \text{ and the controls (de, df, dsp).}$$

Expanding the axial motion equation (the first equation):

$$X = X_o + X_u\Big|_o u + X_w\Big|_o w + X_q\Big|_o q$$

$$X = D \cos \alpha + L \sin \alpha$$

The equilibrium conditions are:

$$X_o = - D_o \cos \alpha_o + L_o \sin \alpha_o$$

Determine the first perturbation derivative:

$$X_u = \frac{\partial}{\partial u}(- D \cos \quad + L \sin \ ) = \frac{-\partial D}{\partial u}(\cos\alpha) - \frac{\partial}{\partial u}(\cos \alpha) D$$

$$\frac{+\partial L}{\partial u}(\sin\alpha) + \frac{L \ \partial}{\partial u}(\sin \alpha)$$

is typically small ($\alpha < 1.$) so $\alpha = \left(\frac{w}{u}\right)$: Therefore $\cos\alpha = \cos\left(\frac{w}{u}\right)$; differentiating the cosine:

$$\frac{\partial}{\partial u}\cos\left(\frac{w}{u}\right) = -\sin\left(\frac{w}{u}\right)\frac{\partial}{\partial u}\left(\frac{w}{u}\right) = -w\sin\alpha\,\frac{\partial(u^{-1})}{\partial u}$$

$$= -w\sin\alpha\,(-1)u^{-2}$$

$$= \frac{w}{u^2}\sin\alpha = \frac{\alpha}{u}\sin\alpha$$

similarly the sine:

$$\frac{\partial}{\partial u}\sin\alpha = \cos\alpha\; w(-1)u^{-2} = -\frac{w}{u2}\cos\alpha = -\frac{\alpha}{u}\cos\alpha$$

The drag derivative is developed:

$$\frac{\partial D}{\partial u} = \frac{\partial}{\partial u} C_D \tfrac{1}{2} \rho V^2 S$$

since

$$V^2 = (U^2 + W^2)$$

$$\frac{\partial D}{\partial u} = C_{Du} \tfrac{1}{2} \rho V^2 S + C_D \tfrac{1}{2} \rho S\, 2\, U$$

The term C_{Du} is zero in subsonic flight, leaving:

$$\frac{\partial D}{\partial U} = C_D \rho S U$$

The lift perivative is identically developed; resulting in:

$$\frac{\partial L}{\partial u} = C_L \rho S U.$$

Substituting the derivatives into X_u provides:

$$X_u = - C_D \rho S U \cos\alpha - D \frac{\alpha}{u} \sin\alpha$$

$$+ C_L \rho S U \sin\alpha + L \frac{-\alpha}{u} \cos\alpha$$

For $\alpha << 1. \Rightarrow X_u = - \rho S U C_D$

The w axial perturbation is developed in the same manner:

$$X_w = \frac{-\partial D}{\partial w} \cos\alpha - D \frac{\partial}{\partial w} \cos\alpha$$

$$\frac{+\partial L}{\partial w} \sin\alpha + L \frac{\partial}{\partial w} \sin\alpha$$

The derivatives are determined:

$$\frac{\partial D}{\partial w} = \frac{\partial}{\partial w} C_D \tfrac{1}{2} \rho V^2 S = C_{D_w} \tfrac{1}{2} \rho V^2 S + C_D \tfrac{1}{2} \rho S 2 W$$

$$= C_D \rho S W + \tfrac{1}{2} \rho V^2 \frac{S}{U} C_{D_\alpha}$$

$$\frac{\partial L}{\partial w} = C_L \rho S W + C_{L_\alpha} \frac{1}{U} \tfrac{1}{2} \rho V^2 S$$

$$\frac{\partial}{\partial w} \cos\alpha = \frac{\partial}{\partial\alpha} \cos\left(\frac{w}{U}\right) = - \sin \frac{w}{U} \frac{1}{U} = - \frac{1}{U} \sin\left(\frac{w}{U}\right)$$

$$= - \frac{1}{U} \sin\alpha$$

$$\frac{\partial}{\partial w} \sin\alpha = \cos\alpha \frac{\partial\alpha}{\partial w} = \frac{1}{U} \cos\alpha$$

Substituting into Xw:

$$X_w = - C_D \rho S W + \tfrac{1}{2} \rho \frac{V^2}{U} S C_{D_\alpha} \cos\alpha - D \frac{-1}{U} \sin\frac{w}{U}$$

$$+ C_L \rho S W + \tfrac{1}{2} \rho \frac{V^1}{U} S C_{L_\alpha} \sin\alpha + L \frac{1}{U} \cos\alpha$$

Including the definitions for D and L:

$$X_w = -\left(C_D \rho S W + \tfrac{1}{2} \rho \frac{V^2}{U} S C_{D_\alpha}\right) \cos\alpha + \tfrac{1}{2} \rho V^2 S \frac{C_D}{U} \sin\alpha$$

$$+\left(C_L \rho S W + \tfrac{1}{2} \rho V^2 S \frac{C_{L_\alpha}}{U}\right) \sin\alpha + \tfrac{1}{2} \rho V^2 S \frac{C_L}{U} \cos\alpha$$

The conditions of zero α or $\alpha \ll 1$. imply $= \frac{w}{U} \ll 1$. ,also, which yields:

$$X_w = -\tfrac{1}{2} \rho V^2 S \frac{C_{D_\alpha}}{U} + \tfrac{1}{2} \rho V^2 S \frac{C_L}{U}$$

$$= -\tfrac{1}{2} \rho S U \; C_{D_\alpha} - C_L$$

The lift equation is determined in the same manner as above. The equations are:

$$Z = -L \cos\alpha - D \sin\alpha ,$$

differentiating:

$$Z_u = -\frac{\partial L}{\partial u} \cos\alpha - L \frac{\partial}{\partial u} \cos\alpha - \frac{\partial D}{\partial u} \sin\alpha - D \frac{\partial}{\partial w} \sin\alpha$$

$$Z_w = -\frac{\partial L}{\partial w} \cos\alpha - L \frac{\partial}{\partial w} \cos\alpha - \frac{\partial D}{\partial w} \sin\alpha - D \frac{\partial}{\partial w} \sin\alpha .$$

Computing the derivates in the expansion

$$Z_u = -C_L S \rho U \cos\alpha - C_L \bar{q} \frac{S}{U} \alpha \sin\alpha$$

$$- C_D S \rho U \sin\alpha + C_D \bar{q} \frac{S}{U} \alpha \cos\alpha$$

$$Z_w = -\left(C_L \rho S W + \frac{C_{L_\alpha}}{U} \tfrac{1}{2} \rho V^2 S\right) \cos\alpha + \tfrac{1}{2} \rho V^2 S \frac{C_L}{U} \sin\alpha$$

$$= -\left(C_D \rho S W + \tfrac{1}{2} V^2 \frac{S}{U} C_{D_\alpha}\right) \sin\alpha - \tfrac{1}{2} \rho V^2 S C_D \frac{1}{U} \cos\alpha$$

For $\alpha << 1$ approximation yields

$$Z_u = -\rho S U C_L$$

$$Z_w = -\tfrac{1}{2} \rho S U \left(C_{L_\alpha} + C_D\right)$$

The rotary force terms are negligible:

$$X_q = 0$$

$$Z_q = 0.$$

The moment equation, about the Y axis is:

$$M_y = -C_M \left(\alpha, c_j, d_{f_o}\right) \tfrac{1}{2} \rho V^2 S \bar{c}.$$

The expansion derivatives are:

$$M_u = +C_m \tfrac{1}{2} \rho S \bar{c} \, 2 U = +C_m \rho S \bar{c} U$$

$$M_w = +\frac{\partial C_m}{\partial w} \tfrac{1}{2} \rho V^2 S \bar{c} + C_m \tfrac{1}{2} \rho S \bar{c} \frac{\partial V^2}{w}$$

$$M_w = +\frac{\partial C_m}{\partial \alpha \cdot u} \tfrac{1}{2} \rho V^2 S \bar{c} + C_m \tfrac{1}{2} \rho S \bar{c} \, 2 w$$

$$M_w = +\frac{C_{m_\alpha}}{U} \tfrac{1}{2} \rho V^2 S \bar{c} + C_m \rho S \frac{\bar{c}}{C} w$$

Which for $\alpha << 1 \quad \Rightarrow \quad -C_{M_\alpha} \tfrac{1}{2} \rho U S \bar{c}$

The rotary damping derivative is significant:

$$M_q = \frac{\partial M}{\partial q}$$

$$= \frac{\partial}{\partial q} \left(\tfrac{1}{2} \rho V^2 S \bar{c} C_m \right) = \tfrac{1}{2} \rho V^2 S \bar{c} \frac{\partial C_m}{\partial q}$$

The aerodynamic derivative C_{m_q} is defined as:

$$C_{m_q} = \frac{\Delta C_m}{\Delta \left(\frac{q \bar{c}}{2U} \right)} .$$

$$M_q = \tfrac{1}{2} \rho V^2 S \bar{c} C_{m_q} \frac{\bar{c}}{2U}$$

Allowing that the velocities are:

$$V^2 \approx U^2$$

Results in the rotary damping dimensional derivative

$$M_q = \tfrac{1}{4} \rho U S \bar{c}^2 C_{m_q}$$

The control derivatives are straight forward aerodynamic coefficient applications. The non-dimensional derivative coefficients are provided in the aerodynamics data and are dimensionalized for the state equations as is shown for the thrust control (cj):

$$X_{cj} = \tfrac{1}{2} \rho V^2 S \left(- C_{D_{cj}} \cos \alpha + C_{L_{cj}} \sin \alpha \right)$$

$$Z_{cj} = \tfrac{1}{2} \rho V^2 S \left(- C_{L_{cj}} \cos \alpha - C_{D_{cj}} \sin \alpha \right)$$

$$M_{cj} = \tfrac{1}{2} \rho V^2 S \bar{c} \; C_{m_{cj}}$$

The derivatives of the elevator (de) aft flap (df) and spoiler (dsp) are determined by replacing the differential subscript (cj) with the appropriate variable. The aerodynamic coefficients are provided in APPENDIX C. Note that the coefficient $C_{m_{dsp}}$ is taken to be zero, since no data is provided for it in the aerodynamic data reference (N-1).

APPENDIX C

The digitized aerodynamic coefficients are presented on the tables in this Appendix. The coefficients are referenced, uniformly, to the wing area (AREF = 1667 ft^2) and the M.A.C. (CREF = 16.3 ft). The aerodynamic coefficients are presented for the range of angle of attack, alpha (α) and thrust coefficient (cj) over which the original data is plotted. The angle of attack extends from -10 deg to +28 deg. The thrust coefficient range is from 0 to 3.85. Alpha is in degrees, all other coefficients are nondimensional. The coefficients are arranged as follows:

Table C-1 Aerodynamic Coefficients (C_L, C_D, C_M)

Table C-2 Elevator Control Derivatives (C_{Lde}, C_{Dde}, C_{Mde})

Table C-3 Aft Flap Control Derivatives (C_{Ldf}, C_{Ddf}, C_{Mdf})

Table C-4 Spoiler Control and Pitch Damping Derivatives (C_{Ldsp}, C_{Ddsp}, C_{Mdsp}, C_{Mq})

TABLE C-1

AERODYNAMIC COEFFICIENTS

CL

ALPHA--- DJT=	0.0000	.3700	1.9300	2.9000	3.8500
-10.0000	-.1000	1.3000	3.0000	3.7000	4.2000
-2.0000	1.0000	3.2000	4.1500	4.9000	5.5000
6.0000	2.1000	4.1000	5.3200	6.2000	6.9000
12.0000	2.4000	4.5000	5.8000	6.8000	7.7000
18.0000	2.3000	4.5000	6.1000	7.3000	8.3000
24.0000	2.0000	3.6000	5.5000	7.0000	8.7000
28.0000	1.3000	3.2000	4.5000	6.3000	8.2000

CD

ALPHA--- DJT=	0.0000	.3700	1.9300	2.9000	3.8500
-10.0000	.2500	-.0400	-.5000	-.8000	-1.1000
-2.0000	.3000	.2500	.1000	-.5000	-.8000
6.0000	.5000	.5000	.6000	.5000	.2000
12.0000	.6000	.9500	1.1000	1.1000	.9500
18.0000	.8500	1.2000	1.5000	1.7000	1.9500
24.0000	1.0000	1.3000	1.6000	1.9500	2.4000
28.0000	1.1000	1.4000	1.7000	2.0500	2.6000

CM

ALPHA--- DJT=	0.0000	.3700	1.9300	2.9000	3.8500
-10.0000	.6500	.3300	.0900	-.2200	-.3500
-2.0000	.1500	-.0400	-.2400	-.4600	-.7000
6.0000	-.2500	-.4000	-.5200	-.7000	-.9000
12.0000	-.4000	-.5200	-.6300	-.8400	-1.1000
18.0000	-.3000	-.5200	-.7900	-.9300	-1.2000
24.0000	-.2500	-.4500	-.6300	-.9100	-1.2000
28.0000	-.2400	-.3500	-.5000	-.7000	-1.1000

TABLE C-2

ELEVATOR CONTROL DERIVATIVES

CLDE

ALPHA--- DJT=	0.0000	.9700	1.9300	2.9000	3.8500
-10.0000	.0154	.0017	.0017	.0085	.0130
-2.0000	.0068	.0082	.0111	.0130	.0137
6.0000	.0103	.0123	.0132	.0123	.0137
12.0000	.0085	.0116	.0128	.0133	.0103
18.0000	.0137	.0137	.0096	.0094	.0120
24.0000	-.0017	-.0051	.0017	.0068	.0120
28.0000	.0017	-.0034	-.0034	.0017	.0033

CDDE

ALPHA--- DJT=	0.0000	.9700	1.9300	2.9000	3.8500
-10.0000	.0031	-.0017	-.0027	-.0024	-.0014
-2.0000	.0024	.0024	.0043	.0051	.0055
6.0000	.0034	.0041	.0050	.0055	.0055
12.0000	.0062	.0055	.0075	.0075	.0065
18.0000	.0034	.0030	.0092	.0092	.0065
24.0000	.0034	.0051	.0073	.0075	.0065
28.0000	.0024	.0044	.0053	.0055	.0075

CMDE

ALPHA--- DJT=	0.0000	.9700	1.9300	2.9000	3.8500
-10.0000	-.0800	-.0520	-.0310	-.0330	-.0470
-2.0000	-.0670	-.0970	-.0860	-.0860	-.0860
6.0000	-.0540	-.0220	-.1050	-.1120	-.1050
12.0000	-.0250	-.0530	-.0930	-.1090	-.1050
18.0000	-.0100	-.0440	-.0520	-.0920	-.0960
24.0000	-.0050	-.0130	-.0350	-.0590	-.0720
28.0000	.0010	-.0200	-.0390	-.0590	-.0720

TABLE C-3

AFT FLAP CONTROL DERVIATIVES

CLDF

ALPHA--- DJT=	0.0000	.9700	1.9300	2.9000	3.8500
-10.0000	.0100	.0350	.0500	.0700	.0850
-2.0000	.0700	.0350	.0450	.0550	.0650
6.0000	.0100	.0250	.0400	.0500	.0550
12.0000	.0700	.0240	.0350	.0400	.0450
18.0000	.0200	.0250	.0300	.0350	.0400
24.0000	.0200	.0200	.0200	.0250	.0300
28.0000	.0300	.0300	.0300	.0250	.0200

CDDF

ALPHA--- DJT=	0.0000	.9700	1.9300	2.9000	3.8500
-10.0000	.0100	.0350	.0350	.0550	.0550
-2.0000	.0100	.0250	.0400	.0500	.0600
6.0000	.0100	.0230	.0350	.0500	.0650
12.0000	.0190	.0250	.0400	.0500	.0650
18.0000	.0100	.0250	.0400	.0600	.0750
24.0000	.0100	.0250	.0400	.0550	.0700
28.0000	.0100	.0250	.0350	.0550	.0700

CMDF

ALPHA--- DJT=	0.0000	.9700	1.9300	2.9000	3.8500
-10.0000	.1000	.1000	.1000	.1000	.1000
-2.0000	.0400	.0300	.0200	.0300	.0300
6.0000	.0600	.0700	.0600	.0500	.0900
12.0000	.0500	.0300	.0700	.0600	.0500
18.0000	.0600	.0400	.0300	.0400	.0400
24.0000	.0500	.0400	.0400	.0200	0.0000
28.0000	.0300	.0500	.0300	.0100	.0100

TABLE C-4

SPOILER CONTROL AND PITCH DAMPING DERIVATIVES

CLDSP

ALPHA--- DJT=	0.0000	.9700	1.9300	2.9000	3.8500
-10.0000	0.0000	-.0050	-.0100	-.0050	0.0000
-2.0000	-.0042	-.0054	-.0067	-.0046	-.0035
6.0000	-.0067	-.0075	-.0083	-.0063	-.0042
12.0000	-.0033	-.0108	-.0183	-.0092	-.0051
18.0000	-.0017	-.0075	-.0133	-.0107	-.0082
24.0000	-.0017	-.0075	-.0133	-.0144	-.0155
28.0000	-.0060	-.0013	-.0017	-.0180	-.0240

CDDSP

ALPHA--- DJT=	0.0000	.9700	1.9300	2.9000	3.8500
-10.0000	0.0000	0.0000	0.0000	0.0000	0.0000
-2.0000	0.0000	0.0000	0.0000	0.0000	0.0000
6.0000	0.0000	-.0004	-.0008	-.0008	-.0008
12.0000	0.0000	-.0009	-.0017	-.0017	-.0017
18.0000	0.0000	-.0021	-.0042	-.0017	-.0013
24.0000	0.0000	-.0021	-.0042	-.0057	-.0073
28.0000	0.0000	-.0009	-.0017	-.0053	-.0088

CMDSP

ALPHA--- DJT=	0.0000	.9700	1.9300	2.9000	3.8500
-10.0000	0.0000	0.0000	0.0000	0.0000	0.0000
-2.0000	0.0000	0.0000	0.0000	0.0000	0.0000
6.0000	0.0000	0.0000	0.0000	0.0000	0.0000
12.0000	0.0000	0.0000	0.0000	0.0000	0.0000
18.0000	0.0000	0.0000	0.0000	0.0000	0.0000
24.0000	0.0000	0.0000	0.0000	0.0000	0.0000
28.0000	0.0000	0.0000	0.0000	0.0000	0.0000

CMQ

ALPHA--- DJT=	0.0000	.9700	1.9300	2.9000	3.8500
-10.0000	-17.0000	-25.0000	-34.0000	-36.5000	-37.5000
-2.0000	-36.0000	-37.0000	-37.5000	-37.5000	-37.5000
6.0000	-37.0000	-48.0000	-54.0000	-53.5000	-53.0000
12.0000	-27.0000	-35.0000	-47.5000	-47.5000	-47.5000
18.0000	6.0000	-16.0000	-32.5000	-39.0000	-41.5000
24.0000	-6.0000	-25.0000	-42.5000	-40.0000	-38.0000
28.0000	-13.5000	-30.0000	-47.0000	-50.0000	-53.5000

APPENDIX D

COMPUTER PROGRAM LISTINGS

The computer programs developed for this work are included in this Appendix. They are as follows:

Equillibrium Performance Map	EQPERF
Calculate Dimensional Derivatives	EQNMOT
Linear Simulation Model	SIM

The subprograms required by each program are included following each main program listed above.

```
      SUBROUTINE EQPERF
      DIMENSION COEF(13,7,5),AT(7),CJT(5),AC(13)
      DIMENSION T(5),AL(10)
C AERO TABLE INPUT
      PRINT/,' INPUT AERO BY ADD DAERC'
      READ(5,/)(((COEF(IVAR,IA,IC),IA=1,7),IC=1,5),IVAR=1,13)
      READ(5,/)(AT(IA),IA=1,7)
      READ(5,/)(CJT(IC),IC=1,5)
      PRINT/,' QUICK SEE AT SEA LEVEL DATA AND 60 DEG FLAP'
      PRINT/,' INPUT CONDD RHO AREF WT'
      READ(5,/) RHO,AREF,W
      PRINT /,' DF  DSP'
      READ(5,/) DF,DSP
      IN=0.
      SHW=1.
      DMO=.88
      TO=21000.
      TN=4
      PRINT /,' INPUT 5 THRUST'
      READ(5,/)(T(I),I=1,5)
      PRINT /,' INPUT 10 ALPHA'
      READ(5,/)(AL(I),I=1,10)
      DO 10 IT=1,5
      PRINT/,
      PRINT /,' THRUST =',T(IT)
      PRINT/,' ALPHA      DE      CL      CD      CM      GAM'
      PRINT/,'   CJ       V(KTS)     V(FPS)'
      DO 11 IA=1,10
      AAL=AL(IA)
      CALL AERO(COEF,AT,CJT,AAL,1.5,AC)
      QB= W/(AREF*AC(1 ))
      IN=0
    9 IN=IN+1
      CJ=T(IT)/(QB*AREF)
      CALL AERO(COEF,AT,CJT,AAL,CJ,AC)
      V=SQRT(ABS(QB*2./RHO))
      CALL MDOT(V,T(IT),DMDT,DMO,TO,TN)
      DCD=DMDT*V*COS(GAM)/(QB*AREF)
      DE=-1.*(AC(3)+AC(9)*DF+AC(12)*DSP)/(AC(6)*SHW)
      CL=AC(1)+(AC(4)*SHW)*DE+AC(7)*DF+AC(19)*DSP
      CD=AC(2)+(AC(5)*SHW)*DE+AC(8)*DF+AC(11)*DSP+DCD
      CM=AC(3)+(AC(6)*SHW)*DE+AC(9)*DF+AC(12)*DSP
      GAM=-1.*CD/CL
      GAM=ATAN(GAM)
      QBN=W*COS(GAM)/(AREF*CL)
      IF(ABS(QBN-QB).GT. .01 .AND. IN.LT.10)QB=QBN:GOTO 9
      V=SQRT(ABS(QB*2./RHO))
      PRINT /,AL(IA),DE,CL,CD,CM,GAM*57.295
      PRINT/,'      ',CJ,V/1.69,V,IN
C     PRINT/,(AC(I),AC(I+3),AC(I+6),AC(I+9),I=1,3)
   11 CONTINUE
   10 CONTINUE
      RETURN
      END
```

```
      SUBROUTINE AERO(COEF,AT,CJT,AAL,CJ,AC)
      DIMENSION COEF(13,7,5),AT(7),CJT(5),AC(13)
      NCOEF=13
      NC=5
      NA=7
      ALI=AAL
      CJI=CJ
      IF(ALI.LT.AT(1))ALI=AT(1);PRINT/,' ALP LOW TABLE'
      IF(CJI.LT.CJT(1))CJI=CJT(1);PRINT/,' CJ LOW TABLE'
      IF(ALI.GT.AT(NA))ALI=AT(NA-1);PRINT/,' ALP HIGH TABLE'
      IF(CJI.GT.CJT(NC))CJI=CJT(NC-1);PRINT/,' CJ HIGH TABLE'
      DO 10 IA=1,NA
      IF(ALI.EQ.AT(IA))GOTO 11
      IF(ALI.LE.AT(IA)) IA=IA-1;GOTO 11
   10 CONTINUE
   11 CONTINUE
      DO 12 IC=1,NC
      IF(CJI.EQ.CJT(IC))GOTO 13
      IF(CJI.LE.CJT(IC))IC=IC-1;GOTO 13
   12 CONTINUE
   13 CONTINUE
C  IA IC AL LOWER EDGE OF VARIABLE SPACE
      RATA=(ALI-AT(IA))/(AT(IA+1)-AT(IA))
      RATC=(CJI-CJT(IC))/(CJT(IC+1)-CJT(IC))
      DO 20 ICF=1,NCOEF
      C1=(COEF(ICF,IA+1,IC)-COEF(ICF,IA,IC))*RATA+COEF(ICF,IA,IC)
      C2=(COEF(ICF,IA+1,IC+1)-COEF(ICF,IA,IC+1))*RATA+COEF(ICF,IA,IC+1
      AC(ICF)=(C2-C1)*RATC+C1
   20 CONTINUE
      RETURN
      END
```

```
      SUBROUTINE MDOT(V,T,DMDT,DMO,TO,TN)
      DIMENSION VT(5),AMT(5),ATT(5)
      DATA (VT(I),I=1,5)/0.,111.65,167.47,223.29,334.94
     & /(AMT(I),I=1,5)/1.0,1.01
     &,1.02,1.033,1.066
     &/(ATT(I),I=1,5)/1.0,1.037,1.07,1.115,1.227/
      DO 10 I=1,5
      IF(VT(I).GT.V)GOTO 11
10    CONTINUE
      I=5
11    IF(I.LE.1)GOTO12
      RAT=(V-VT(I-1))/(VT(I)-VT(I-1))
      AMR=(AMT(I)-AMT(I-1))*RAT+AMT(I-1)
      TGR=(ATT(I)-ATT(I-1))*RAT+ATT(I-1)
      DMDT=TN*DMO*AMR*T/(TO*TN*TGR)
      RETURN
12    DMDT=DMO*TN
      RETURN
      END
```

```
      SUBROUTINE EQNMOT
      DIMENSION COEF(13,7,5),AT(7),CJT(5),AC(13)
      COMMON /VARMOT/F(10,10),G(10,10),UO,WO,THETO,CJO,DEO
     & ,DFO,DSPO,VO,GAMO
C AERO TABLE INPUT
      PRINT /,' ADD AERO TABLE FROM ALD ELEMENT AERO'
      READ(5,/)(((COEF(IVAR,IA,IC),IA=1,7),IC=1,5),IVAR=1,13)
      READ(5,/)(AT(IA),IA=1,7)
      READ(5,/)(CJT(IC),IC=1,5)
C     WRITE(6,/)(AT(IA),IA=1,7)
C     WRITE(6,/)(CJT(IC),IC=1 ,5)
C     DO 12 IVAR=1,13
C     PRINT /,' IVAR =',IVAR,' IA 1 2 3 4 5 6 7'
C     DO 13 IC=1,5
C     PRINT/,IC,(COEF(IVAR,IA,IC),IA=1,7)
C 13   CONTINUE
C 12   CONTINUE
      RAD=57.295
      GE=32.2
      PRINT /,' INPUT COND  RHO AREF CREF W IYY'
      READ(5,/) RHO,AREF,CREF,W,AIY
      AM=W/GE
      SHW=1.
      DMO=.88
      TO=21000.
      TN=4
      PRINT/, ' DF  DSP'
      READ(5,/) DF,DSP
    1 PRINT /, ' INPUT FLIGHT COND THRUST V GAM'
      READ(5,/) T,V,GAM
      GAM=GAM/RAD
      AAL=0.
      QB=.5*RHO*V**2
      WS=W*SIN(GAM)
      WC=W*COS(GAM)
C FIND EQUILIBRIUM CONDITION
      IN=0
      IJ=0
      TG=TAN(GAM)
      PRINT /,' FIND EQUILIB CONDS'
      PRINT /,
    9 CJ=T/(QB*AREF)
      PRINT /, 'VAR AAL CJ'
      PRINT /,AAL,CJ
      CALL AERO(COEF,AT,CJT,AAL,CJ,AC)
      V=SQRT(QB*2/RHO)
      CALL MDOT(V,T,DMDT,DMO,TO,TN)
      DCD=DMDT*V*COS(GAM)/(QB*AREF)
      DE1=-1.*(AC(3)+AC(9)*DF+AC(12)*DSP)/(AC(6)*SHW)
      CL1=AC(1)+(AC(4)*SHW)*DE+AC(7)*DF+AC(10)*DSP
      CD1=AC(2)+(AC(5)*SHW)*DE+AC(8)*DF+AC(11)*DSP+DCD
      CALL AERO(COEF,AT,CJT,AAL-2.,CJ,AC)
      V=SQRT(QB*2/RHO)
      CALL MDOT(V,T,DMDT,DMO,TO,TN)
      DCD=DMDT*V*COS(GAM)/(QB*AREF)
      DE2=-1.*(AC(3)+AC(9)*DF+AC(12)*DSP)/(AC(6)*SHW)
      CL2=AC(1)+(AC(4)*SHW)*DF+AC(7)*DF+AC(10)*DSP
      CD2=AC(2)+(AC(5)*SHW)*DE+AC(8)*DF+AC(11)*DSP+DCD
```

```
      DCLA=(CL1-CL2)/2.
      DCDA=(CD1-CD2)/2.
      DAL=0.
      IF(ABS(DCDA) .GT. .001) DAL=(AS/(QB*AREF)-CD1)/DCDA
      IF(AAL+DAL .LT. -10. .OR. AAL+DAL .GT. 25.)
     &DAL=DAL*.1
      IF(ABS(DAL) .LT. .001 .AND. ABS(DCLA) .GT. .001) IN=10
      CALL AERO(COEF,AT,CJT,AAL+DAL,CJ,AC)
      V=SQRT(QB*2/RHO)
      CALL MDOT(V,T,DMDT,DMO,TO,TN)
      DCD=DMDT*V*COS(GAM)/(QB*AREF)
      DE =-1.*(AC(3)+AC(9)*DF+AC(12)*DSP)/(AC(6)*SHW)
      CL =AC(1)+(AC(4)*SHW)*DE+AC(7)*LF+AC(10)*DSP
      CD=AC(2)+(AC(5)*SHW)*DE+AC(8)*DF+AC(11)*DSP+DCD
      WRITE(6,/) ' VAR AAL DAL DCLA DCDA IN TC CD/CL CL CD'
      WRITE(6,/) AAL,DAL,DCLA,DCDA,IN,TC,CD/CL,CL,CD
      WRITE(6,/)' AC-S '
      DO 11 I=1,3
      WRITE(6,/) AC(I),AC(I+3),AC(I+6),AC(I+9)
11    CONTINUE
      IF(ABS(TC-CD/CL) .GT. .002 .AND. IN .LT. 10)
     & AAL=AAL+DAL;IN=IN+1;GOTO 9
      IF(ABS(DAL) .LT. .001 .AND. IJ.EQ.0)
     &GAM1=CD/CL;QB1=QB;QB=1.1*QB;IN=0;IJ=1;GOTO 9
      IF(IJ.EQ.1)DQDG=(QB-QB1)/(CD/CL-GAM1);QB=(TC-GAM1)*DQDG+QB1;
     &WRITE(6,/)' QBNEW=',QB;IJ=2;IN=0;GOTO9
      IF(IJ.EQ.2 .AND. ABS(TC-CD/CL) .GT. .002)
     &QB=(QB1+QB)/2.;WRITE(6,/)' QBNEW= ',QB;IJ=3;IN=0;GOTO 9
      IF(IN.LT.10) WRITE(6,/)' SOLUTION CONVERGED'
      AAL =AAL+DAL
      PRINT /,
C COMPUTE EQUILIB COND IN BODY AXES
      V=SQRT(QB*2./RHO)
      GAM=ATAN(CD/CL)
      PRINT /,' EQUILIB STAB AXES VO GAMO ALPO CJO TH DE'
      PRINT /,V,GAM*RAD,AAL,CJ,T,DE
C END STAB DERIVS
      PRINT /,' DEFINE F MATRIX AND G MATRIX'
C CALL AERO ETC.
      CALL AERO(COEF,AT,CJT,AAL-5.,CJ,AC)
      V=SQRT(QB*2/RHO)
      CALL MDOT(V,T,DMDT,DMO,TO,TN)
      DCD=DMDT*V*COS(GAM)/(QB*AREF)
      CL1=AC(1)+(AC(4)*SHW)*DE+AC(7)*DF+AC(10)*DSP
      CD1=AC(2)+(AC(5)*SHW)*DE+AC(8)*DF+AC(11)*DSP+DCD
      CM1=AC(3)+(AC(6)*SHW)*DE+AC(9)*DF+AC(12)*DSP
      CALL AERO(COEF,AT,CJT,AAL+5.,CJ,AC)
      V=SQRT(QB*2/RHO)
      CALL MDOT(V,T,DMDT,DMO,TO,TN)
      DCD=DMDT*V*COS(GAM)/(QB*AREF)
      CL2=AC(1)+(AC(4)*SHW)*DE+AC(7)*DF+AC(10)*DSP
      CD2=AC(2)+(AC(5)*SHW)*DE+AC(8)*DF+AC(11)*DSP+DCD
      CM2=AC(3)+(AC(6)*SHW)*DE+AC(9)*DF+AC(12)*DSP
C DERIV PER RADIAN
      CLA=RAD*(CL2-CL1)/(10.)
      CDA=RAD*(CD2-CD1)/10.
      CMA=RAD*(CM2-CM1)/10.
      CALL AERO(COEF,AT,CJT,AAL,CJ-.5,AC)
```

```
      V=SQRT(QB*2/RHO)
      CALL MDOT(V,T,DMDT,DMO,TO,TN)
      DCD=DMDT*V*COS(GAM)/(QB*AREF)
      CL1=AC(1)+(AC(4)*SHW)*DE+AC(7)*DF+AC(10)*DSP
      CD1=AC(2)+(AC(5)*SHW)*DE+AC(8)*DF+AC(11)*DSP+DCD
      CM1=AC(3)+(AC(6)*SHW)*DE+AC(9)*DF+AC(12)*DSP
      CALL AERO(COEF,AT,CJT,AAL,CJ+,5,AC)
      V=SQRT(QB*2/RHO)
      CALL MDOT(V,T,DMDT,DMO,TO,TN)
      DCD=DMDT*V*COS(GAM)/(QB*AREF)
      CL2=AC(1)+(AC(4)*SHW)*DE+AC(7)*DF+AC(10)*DSP
      CD2=AC(2)+(AC(5)*SHW)*DE+AC(8)*DF+AC(11)*DSP+DCD
      CM2=AC(3)+(AC(6)*SHW)*DE+AC(9)*DF+AC(12)*DSP
      CLCJ=CL2-CL1
      CDCJ=CD2-CD1
      CMCJ=CM2-CM1
      CALL AERO(COEF,AT,CJT,AAL ,CJ,AC)
      V=SQRT(QB*2/RHO)
      CALL MDOT(V,T,DMDT,DMO,TO,TN)
      DCD=DMDT*V*COS(GAM)/(QB*AREF)
      DE =-1.*(AC(3)+AC(9)*DF+AC(12)*DSP)/(AC(6)*SHW)
      CL =AC(1)+(AC(4)*SHW)*DE+AC(7)*DF+AC(10)*DSP
      CD =AC(2)+(AC(5)*SHW)*DE+AC(8)*DF+AC(11)*DSP+DCD
      CM =AC(3)+(AC(6)*SHW)*DE+AC(9)*DF+AC(12)*DSP
C OUTPUT AERO IN RAD CONTROL PER DEG
      PRINT /,' CL CLA CLCJ CLDE CLDF CLDSP'
      PRINT/,CL,CLA,CLCJ,(AC(4)*SHW),AC(7),AC(10)
      PRINT /,' CD CDA CDCJ CDDE CDDF CDDSP'
      PRINT /, CD,CDA,CDCJ,(AC(5)*SHW),AC(8),AC(11)
      PRINT /,' CM CMA CMCJ CMDE CMDF CMDDSP'
      PRINT /, CM,CMA,CMCJ,(AC(6)*SHW),AC(9),AC(12)
      PRINT /,' CMO =',AC(13)
C COMPUTE STAB DERIVS EQULIB IN BODY AXES
      CA=COS(AAL/RAD)
      SA=SIN(AAL/RAD)
      U=V*CA
      W=V*SA
      THET=GAM*RAD-AAL
      AL=AAL/RAD
C FORCE MATRIX
      F(1,1)=CL*AREF*(RHO*U*SA-QB*AL*CA/U)-CD*AREF*(RHO*U*CA+
     &QB*AL*SA/U)
      F(1,2)=CD*AREF*(QB*SA/U-RHO*W*CA)-CDA*AREF*QB*CA/U
     &+CL*AREF*(QB*CA/U+RHO*W*SA)+CLA*AREF*QB*SA/U
      F(1,3)=-1.*W
      F(2,1)=-1.*CL*AREF*(RHO*U*CA+QB*AL*SA/U)-CD*AREF*
     &(RHO*U*SA-QB*AL*CA/U)
      F(2,2)=CL*AREF*(QB*SA/U-RHO*W*CA)-CLA*AREF*QB*CA/U
     &-CD*AREF*(QB*CA/U+RHO*W*SA)-CDA*AREF*QB*SA/U
      F(2,3)=U
      F(3,1)=CM*RHO*AREF*CREF*U
      F(3,2)=CMA*QB*AREF*CREF/U+CM*RHO*AREF*CREF*W
      F(3,3)=AC(13)*QB*AREF*CREF**2/(2.*U)
C CONTROL MATRIX
      QBA=QB*AREF
      QBAC=QB*AREF*CREF
      G(1,1)=(CLCJ*SA-CDCJ*CA)*QBA
      G(2,1)=(-1.*CLCJ*CA-CDCJ*SA)*QBA
```

```
175             G(3,1)=CMCJ*QBAC
176             G(1,2)=((AC(4)*SHJ)*SA-(AC(5)*SHW)*CA)*QBA
177             G(2,2)=(-1.*(AC(4)*SHW)*CA-(AC(5)*SHW)*SA)*QBA
178             G(3,2)=(AC(6)*SHW)*QBAC
179             G(1,3)=(AC(7)*SA-AC(8)*CA)*QBA
180             G(2,3)=(-1.*AC(7)*CA-AC(8)*SA)*QBA
181             G(3,3)=AC(9)*QBAC
182             G(1,4)=(AC(10)*SA-AC(11)*CA)*QBA
183             G(2,4)=(-1.*AC(10)*CA-AC(11)*SA)*QBA
184             G(3,4)=AC(12)*QBAC
185             DO 111 I=1,2
186             DO 110 J=1,2
187             F(I,J)=F(I,J)/AM
188       110   CONTINUE
189       111   CONTINUE
190             DO 114 J=1,3
191             F(3,J)=F(3,J)/AIY
192       114   CONTINUE
193             DO 116 I=1,2
194             DO 117 J=1,4
195             G(I,J)=G(I,J)/AM
196       117   CONTINUE
197       116   CONTINUE
198             DO 118 J=1,4
199             G(3,J)=G(3,J)/AIY
200       118   CONTINUE
201             WRITE(6,/)' STATES ARE U W Q '
202             WRITE (6,/)'   F  MATRIX'
203             WRITE(6,/) (F(1,I),I=1,3)
204             WRITE(6,/) (F(2,I),I=1,3)
205             WRITE(6,/) (F(3,I),I=1,3)
206             WRITE(6,/) ' G MATRIX DCJ DE DF DSP'
207             WRITE(6,/) (G(1,I),I=1,4)
208             WRITE(6,/) (G(2,I),I=1,4)
209             WRITE(6,/) (G(3,I),I=1,4)
210       C NOW HAVE F G MATRICES FOR PASSING ON TO NEXT PROGRAM
211             UO=U
212             WO=W
213             THETO=THET
214             CJO=CJ
215             DEO=DE
216             DFO=60.+DF
217             DSPO=DSP
218             VO=V
219             GAMO=GAM*RAD
220             RETURN
221             END
```

```
      SUBROUTINE SIM
      DIMENSION X(6),U(6),UD(6),F(6,6),G(6,6),W(6,6),C(6,6)
      DIMENSION P(6,6),Q(6,6),WQ(6,6)
      COMMON /VARMOT/SF(10,10),SG(10,10),UO,WO,THETO,CJO,DEO
     &,DFO,DSPO,VO,GAMO
C INITIALIZE INPUTS
      GO=32.2
      RE=20900000.
      RAD=57.295
C STATES U W P THET H
C ZERO MATRICES
      DO 10 I=1,6
      DO 15 J=1,6
      F(I,J)=0.

      G(I,J)=0.
      W(I,J)=0.
      C(I,J)=0.
      P(I,J)=0.
      Q(I,J)=0.
      WQ(I,J)=0.
15    CONTINUE
      X(I)=0.
      U(I)=0.
      UD(I)=0.
10    CONTINUE
C ALL INPUTS ARE IN FEET DEGS SECS
C INPUTS OF F G UO WO THETO CJO DEO DFO DSPO VO GAMO
C ARE BY COMMON FROM EQNMOTDM
      DO 8 I=1,3
      DO 9 J=1,3
      F(I,J)=SF(I,J)
      G(I,J)=SG(I,J)
9     CONTINUE
8     CONTINUE
      G(1,4)=SG(1,4)
      G(2,4)=SG(2,4)
      G(3,4)=SG(3,4)
      F(1,4)=GO
      F(4,3)=-1.
      F(5,2)=1.
      F(5,4)=UO
C ENGINE THRUST DISTURBANCE MATRIX
C AND 1 STATE ENGINE RESPONSE MODEL
      DO 11 I=1,6
      W(I,1)=G(I,1)
      F(I,6)=G(I,1)
11    CONTINUE
      DO 12 I=1,6
      G(I,1)=0.
12    CONTINUE
      G(6,1)=2.1
      F(6,6)=-2.1
      DT=.1
C PRINTOUT MATRICES OF THE PROBLEM
      PRINT/,' '
      PRINT/,' F MATRIX'
      CALL PRN(F)
```

```
      SUBROUTINE SIM
      DIMENSION X(6),U(6),UD(6),F(6,6),G(6,6),W(6,6),C(6,6)
      DIMENSION P(6,6),Q(6,6),WQ(6,6)
      COMMON /VARMOT/SF(10,10),SG(10,10),UO,WO,THETO,CJO,DEO
     &,DFO,DSPO,VO,GAMO
C INITIALIZE INPUTS
      GO=32.2
      RE=20900000.
      RAD=57.295
C STATES U W P THET H
C ZERO MATRICES
      DO 10 I=1,6
      DO 15 J=1,6
      F(I,J)=0.

      G(I,J)=0.
      W(I,J)=0.
      C(I,J)=0.
      P(I,J)=0.
      Q(I,J)=0.
      WQ(I,J)=0.
15    CONTINUE
      X(I)=0.
      U(I)=0.
      UD(I)=0.
10    CONTINUE
C ALL INPUTS ARE IN FEET DEGS SECS
C INPUTS OF F G UO WO THETO CJO DEO DFO DSPO VO GAMO
C ARE BY COMMON FROM EQNMOTDM
      DO 8 I=1,3
      DO 9 J=1,3
      F(I,J)=SF(I,J)
      G(I,J)=SG(I,J)
9     CONTINUE
8     CONTINUE
      G(1,4)=SG(1,4)
      G(2,4)=SG(2,4)
      G(3,4)=SG(3,4)
      F(1,4)=GO
      F(4,3)=-1.
      F(5,2)=1.
      F(5,4)=UO
C ENGINE THRUST DISTURBANCE MATRIX
C AND 1 STATE ENGINE RESPONSE MODEL
      DO 11 I=1,6
      W(I,1)=G(I,1)
      F(I,6)=G(I,1)
11    CONTINUE
      DO 12 I=1,6
      G(I,1)=0.
12    CONTINUE
      G(6,1)=2.1
      F(6,6)=-2.1
      DT=.1
C PRINTOUT MATRICES OF THE PROBLEM
      PRINT/,' '
      PRINT/,' F MATRIX'
      CALL PRI(F)
```

```
      PRINT/,
      PRINT/,' G MATRIX'
      CALL PRM(G)
      PRINT /,
C FORM PHI GAM WGAM MATRICES
      CALL PHIGAM(F,G,W,P,Q,WQ,DT)
      PRINT /, ' PHI AND GAM MATRICES'
      CALL PRM(P)
      PRINT/,
      CALL PRM(Q)
      PRINT /,
      PRINT /,' ENGINE DISTRUBANCE MATRIX W AND WQ'
      DO 98 I=1,6
      WRITE(6,/) W(I,1),WQ(I,1)
98    CONTINUE
999   CONTINUE
      PRINT /,
      PRINT /,' INPUT CONTROL GAINS'
20    PRINT/,' I,J,COEF'
      READ(5,/) I,J,CT
      IF(I.EQ.0)GOTO 21
      C(I,J)=CT
      GOTO 20
21    CONTINUE
      PRINT/, ' C MATRIX'
      CALL PRM(C)
      PRINT/,' INITIAL CONDS TO RUN'
      PRINT/,' ALT HEOUT MAX TIME'
      READ(5,/) HO,HEOUT,TMAX
      RO=0.
      ALT=HO
      TOUT=-1.*DT
      DTOUT=1.
      T=0.
      ALP=WO/UO*RAD
      HDOT=WO*COS(THETO/RAD)+UO*SIN(THETO/RAD)
      WRITE(6,/)' OUTPUT'
      WRITE(6,/) '      T      RG      ALT      HO'
      WRITE(6,/) '      TOTU     ALP      THET      HDOT'
      WRITE(6,/)' U       W       Q       THET      H'
      WRITE(6,/)' DCJ    DE     DF      DSP'
50    CONTINUE
      IF(T.LT.TOUT)GOTO 997
      PRINT /,
      WRITE(6,101) T,RO,ALT,HO
101   FORMAT(5F10.4)
      WRITE(6,101) UO+X(1),ALP,THETO+X(4)*RAD,HDOT
      WRITE(6,101) X
      WRITE(6,101) U
      TOUT=TOUT+DTOUT
997   CONTINUE
      CALL VECM(U,X)
      CALL VXM(U,C)
      CALL DYN(P,Q,WQ,X,U,UD)
      T=T+DT
      HDOT=WO*COS(THETO/RAD)+UO*SIN(THETO/RAD)+X(2)+UO*X(4)
      ALP=(WO+X(2))/(UO+X(1))*RAD
      RO=RO+VG*COS(GAMO/RAD)*DT
```

```
117             HO=HO-VO*SIN(GAMO/RAD)*DT
118             ALT=HO-X(5)
119             IF(HO.LT.HEOUT .AND. UD(1).EQ.0.)UD(1)=-.25*CJO;TOUT=T-DT
120             IF(T.GT.TMAX)GOTO 998
121             IF(HO.GT.50)GOTO 50
122         998 CONTINUE
123             PRINT/,' ANOTHER CASE TYPE 1'
124             READ(5,/) IGAN
125             UD(1)=0.
126             DO 996 I=1,6
127             X(I)=0.
128             U(I)=0.
129         996 CONTINUE
130             IF(IGAN.NE.0)GOTO 999
131             END
```

```
      SUBROUTINE PHIGAM(F,G,M,P,Q,NQ,T)
      MONITOR
CF G FROM FX+GU  P AND Q ARE PHI AND GAM T IS SAMPLE DT
      DIMENSION F(6,6),G(6,6),P(6,6),Q(6,6),M(6,6),NQ(6,6)
      DIMENSION DI(6,6),ZER(6,6),E(6,6),D(6,6),C(6,6),TEMP(6,6)
      DO 10 I=1,6
      DO 10 J=1,6
      DI(I,J)=0.
      ZER(I,J)=0.
      D(I,J)=0.
      C(I,J)=0.
   10 CONTINUE
      DO 11 I=1,6
      DI(I,I)=1.
   11 CONTINUE
      CALL EQM(P,DI)
      DO 130 N=11,1,-1
      IF(N.GT.1)GOTO 100
      CALL EQM(TEMP,P)
      CALL SCM(TEMP,T)
      CALL EQM(E,TEMP)
  100 CONTINUE
      TN=N
      SC=T/TN
      CALL EQM(TEMP,E)
      CALL SCM(TEMP,SC)
      CALL XM(TEMP,P)
      CALL ADM(TEMP,DI)
      CALL EQM(P,TEMP)
  130 CONTINUE
      CALL EQM(TEMP,E)
      CALL XM(TEMP,G)
      CALL EQM(G,TEMP)
      CALL EQM(TEMP,E)
      CALL XM(TEMP,M)
      CALL EQM(NQ,TEMP)
      RETURN
      END
C  MATRIX OPERATIONS REQ'D
```

```
      SUBROUTINE DYN(P,Q,WQ,X,U,UD)
      DIMENSION U(6),UD(6)
      DIMENSION P(6,6),Q(6,6),WQ(6,6),X(6),TV(6),TV2(6),TEMP(6,6)
      CALL VEQM(TV,X)
      CALL VXM(TV,P)
      CALL EQM(TEMP,Q)
      CALL VEQM(TV2,U)
      CALL VXM(TV2,TEMP)
      CALL VADM(TV,TV2)
      CALL EQM(TEMP,WQ)
      CALL VEQM(TV2,UD)
      CALL VXM(TV2,TEMP)
      CALL VADM(TV,TV2)
      CALL VEQM(X,TV)
      RETURN
      END
```

```
      SUBROUTINE ADM(A,B)
      DIMENSION A(6,6),B(6,6)
      M=6
      DO 10 I=1,M
      DO 10 J=1,M
   10 A(I,J)=A(I,J)+B(I,J)
      RETURN
      END
```

** EQM **

```
      SUBROUTINE EQM(A,B)
      DIMENSION A(6,6),B(6,6)
      M=6
      DO 10 I=1,M
      DO 10 J=1,M
   10 A(I,J)=B(I,J)
      RETURN
      END
C     VECTOR MATRIX OPERATIONS REQ'D
```

** SCM **

```
      SUBROUTINE SCM(A,X)
      DIMENSION A(6,6)
      M=6
      DO 10 I=1,M
      DO 10 J=1,M
   10 A(I,J)=X*A(I,J)
      RETURN
      END
```

```
      SUBROUTINE AMULB(A,B)
      DIMENSION A(6,6),B(6,6),D(6,6)
      M=6
      DO 10 J=1,M
      DO 10 I=1,M
      D(I,J)=0.
      DO 9 N=1,M
    9 D(I,J)=D(I,J)+A(I,N)*B(N,J)
   10 CONTINUE
      DO 11 I=1,M
      DO 11 J=1,M
   11 A(I,J)=D(I,J)
      RETURN
      END
```

** TM **

```
      SUBROUTINE TM(A)
      DIMENSION A(6,6),D(6,6)
      M=6
      DO 10 I=1,M
      DO 10 J=1,M
   10 D(I,J)=A(J,I)
      DO 11 I=1,M
      DO 11 J=1,M
   11 A(I,J)=D(I,J)
      RETURN
      END
```

** PRN **

```
      SUBROUTINE PRN(A)
      DIMENSION A(6,6)
      DO 10 J=1,6
      WRITE(6,101) (A(J,I),I=1,6)
  101 FORMAT(6F10.4)
   10 CONTINUE
      RETURN
      END
```

```
      SUBROUTINE VADM(A,B)
      DIMENSION A(6),B(6)
      M=6
      DO 10 J=1,M
   10 A(J)=A(J)+B(J)
      RETURN
      END
```

** VEQM **

```
      SUBROUTINE VEQM(A,B)
      DIMENSION A(6),B(6)
      M=6
      DO 10 J=1,M
   10 A(J)=B(J)
      RETURN
      END
```

** VSCM **

```
      SUBROUTINE VSCM(A,X)
      DIMENSION A(6)
      M=6
      DO 10 J=1,M
   10 A(J)=X*A(J)
      RETURN
      END
```

** VXM **

```
      SUBROUTINE VXM(A,B)
      DIMENSION A(6),B(6,6),D(6)
      M=6
      DO 10 J=1,M
      D(J)=0.
      DO 9 N=1,M
    9 D(J)=D(J)+A(N)*B(J,N)
   10 CONTINUE
      DO 11 J=1,M
   11 A(J)=D(J)
      RETURN
      END
```

REFERENCES

B-1 Bryson, A. E. and Hall, E. W.
"Optimal Control and Filter Synthesis by Eigenvector Decomposition" SUDAAR No1 436, Stanford University Guidance and Control Laboratory, Stanford, Calif., November 1971

B-2 Bryson, A. E., and Ho. Y.
"Applied Optimal Control", Ginn and Co., Waltham, Mass., 1969

B-3 Bryson, A. E.
"Control Theory For Random Systems" Proceedings of Thirteenth International Congress of Theoretical and Applied Mechanics, Moscow USSR, August 1972

C-1 Chen, C. T.
"Introduction to Linear System Theory", Holt Rinehart and Winston, Inc., 1970

D-1 Domasch, D. O., Sherby, S. S., and Connolly, T. F.
"Airplane Aerodynamics", Third Edition, Pitman Publishing Corp., New York, 1961

D-2 Derusso, P. M., Roy, R. J., and Close, C. M.
"State Variables for Engineers", John Wiley and Sons, Inc., New York, 1965

E-1 Etkin, Bernard
"Dynamics of Flight Stability and Control", John Wiley and Sons, Inc., 1959

F-1 Franklin, G. F. and Powell, J. P.
"Digital Control Notes Prepared for E207", Stanford University, Stanford, Calif., 1975

N-1 Nieuwenhuijse, Albert W. and Franklin, James A.
"A Simulator Investigation of Engine Failure Compensation for Powered-lift STOL Aircraft", NASA Technical Memorandum, TMX-62, 363, Ames Research Center, Moffett Field, Calif., May 1974

N-2 Franklin, James A. and Koening, Robert W.
"A Simulator Investigation of the Influence of Engine Response Characteristics on the Approach and Landing for an Externally Blown Flap Aircraft", Part 1, Description of the Simulation and Discussion of Results

N-3 Ciffone, Donald L. and Robinson, Glenn H.
"A Simulator Investigation of the Influence of Engine Response Characteristics on the Approach and Landing for an Externally Blown Flap Aircraft", Part 2, Aerodynamic Model, NASA Technical Memorandum, TMX-62, 265, AMES Research Center, Moffett Field, Calif., May 1973

S-1 Seckel, Edward

"Stability and Control of Airplanes and Helicopters",

Academic Press, New York, 1964